CHAPTER I

I. INTRODUCTION

How do children learn curvilinear movements by imitating written letters? How do varying, error-prone movements during learning become correct, efficient movements after repeated trials? The principal goal of this research is to provide an answer to these questions by modelling the perception/action cycle of handwriting, which involves vision, attention, learning, and movement.

This work describes a new model, called Adaptive VITEWRITE (AVITEWRITE), which builds on two previous movement models. The first is the Vector Integration to Endpoint (VITE) model (Bullock & Grossberg, 1988a, 1988b, 1991) (Figure 1.1). The VITE model successfully explained psychophysical and neurobiological data about how synchronous multi-joint reaching trajectories could be generated at variable speeds. VITE was later expanded (Bullock, Cisek, & Grossberg, 1998) to explain how arm movements are influenced by proprioceptive feedback and external forces, among other related factors. The firing patterns of six distinct cell types in cortical areas 4 and 5 were also simulated during various movement tasks (Kalaska et al., 1990). In order to allow a greater focus on issues related to the learning of curved movements, the AVITEWRITE model avoids explicit descriptions of muscle dynamics, and therefore uses components of the earlier VITE models of Bullock & Grossberg (1988a, 1988b, 1991).

A second basis for the AVITEWRITE model is the VITEWRITE model of Bullock, Grossberg, & Mannes (1993) (Figure 1.2). The curved trajectories of handwriting require

more than simple point-to-point movements. Curved handwriting trajectories appear to be generated by component movement synergies (Bernstein, 1967; Kelso, 1982), or groups of muscles working together to drive the limb in prescribed directions, whose activities overlap in time (Morasso et al., 1983; Soechting &Terzuolo, 1987; Stelmach

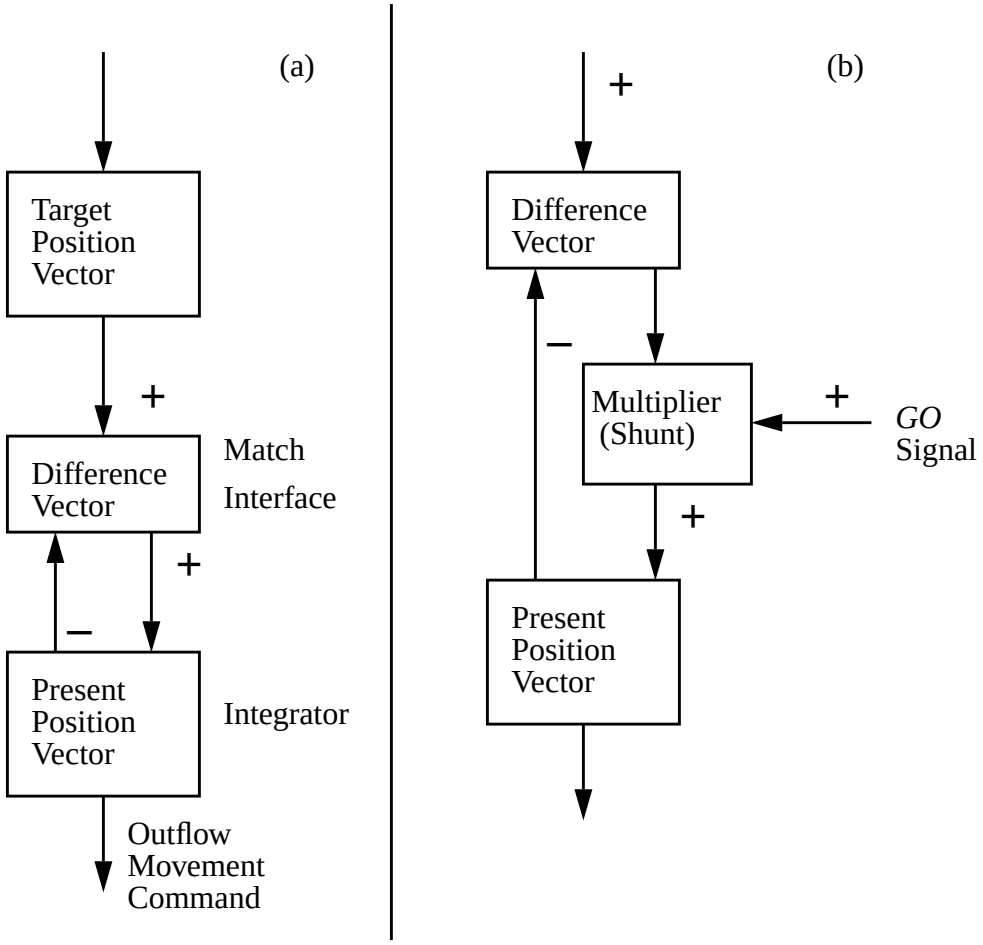

Figure 1.1. (a) A match interface within the VITE model continuously computes a difference vector (*DV*) between the target position vector (*TPV*) and a present position vector (*PPV*), and adds the difference vector to the present position vector. (b) A *GO* signal gates execution of a primed movement vector and regulates the rate at which the movement vector updates the present position command. (Adapted with permission from Bullock & Grossberg, 1988a.)

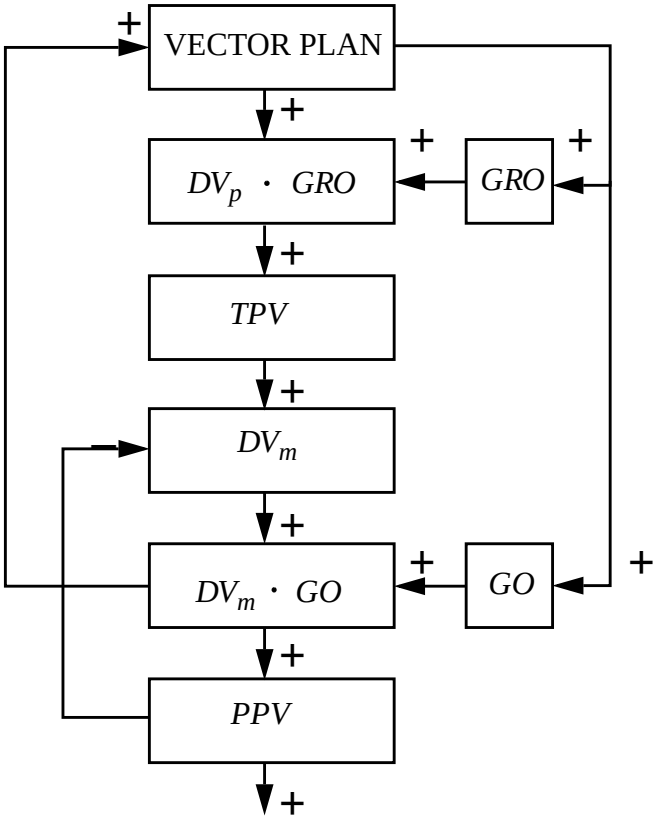

Figure 1.2. Schematic diagram of the VITEWRITE model of Bullock et al. (1993b): A Vector Plan functions as a motor program that stores discrete planning vectors DV_p in a working memory. A *GRO* signal determines the size of script and a *GO* signal its speed of execution. After the vector plan and these will-to-act signals are activated, the circuit generates script automatically. Size-scaled planning vectors $DV_p \cdot GRO$ are read into a target position vector (*TPV*). An outflow representation of present position, the present position vector (*PPV*), is subtracted from the *TPV* to define a movement difference vector (DV_m). The DV_m is multiplied by the *GO* signal. The net signal $DV_m \cdot GO$ is integrated by the *PPV* until it equals the *TPV.* The signal $DV_m \cdot GO$ is thus an outflow representation of movement speed. Maxima or zero values of its cell activations may automatically trigger read-out of the next planning vector DV_p. (Reproduced with permission from Bullock et al.,1993b.)

et al., 1984). VITEWRITE uses such a synergy-overlap strategy to generate curved movements from individual, target-driven strokes. A key issue faced by all models which

seek to generate curves by overlapping strokes is how to appropriately time the strokes to generate a particular curve. VITEWRITE avoids an explicit representation of time in the control of synergy activation by using a feature of the movement itself, the point of maximum velocity, to trigger activation of a subsequent synergy. However, movement in VITEWRITE is controlled by a predefined sequence of "planning vectors" which cause unimodal velocity profiles for the synergies that control each directional component of a curve. VITEWRITE does not address how these planning vectors may be discovered, learned, and stored in a self-organizing process which can generate unimodal velocity profiles for each directional component of a curved movement. This challenge is met by the *Adaptive* VITEWRITE model.

AVITEWRITE describes how the complex sequences of movements involved in handwriting can be learned through the imitation of previously drawn curves. Although the system described herein could be modified to learn from the actual movements of a teacher, the present model learns by imitating the product of that teacher's movements, the static image of a written letter. AVITEWRITE shows how initially segmented movements with multimodal velocity profiles during the early stages of learning, corresponding to early childhood, can become the smooth, continuous movements with the unimodal, bell-shaped velocity profiles observed in adult humans (Abend et al., 1982; Edelman & Flash, 1987; Morasso, 1981; Morasso et al., 1983) after multiple learning trials. Early, error-prone handwriting movements with many visually reactive, correctional components gradually improve over time and many learning trials, to become automatic, error-free movements which can even be performed without visual feedback.

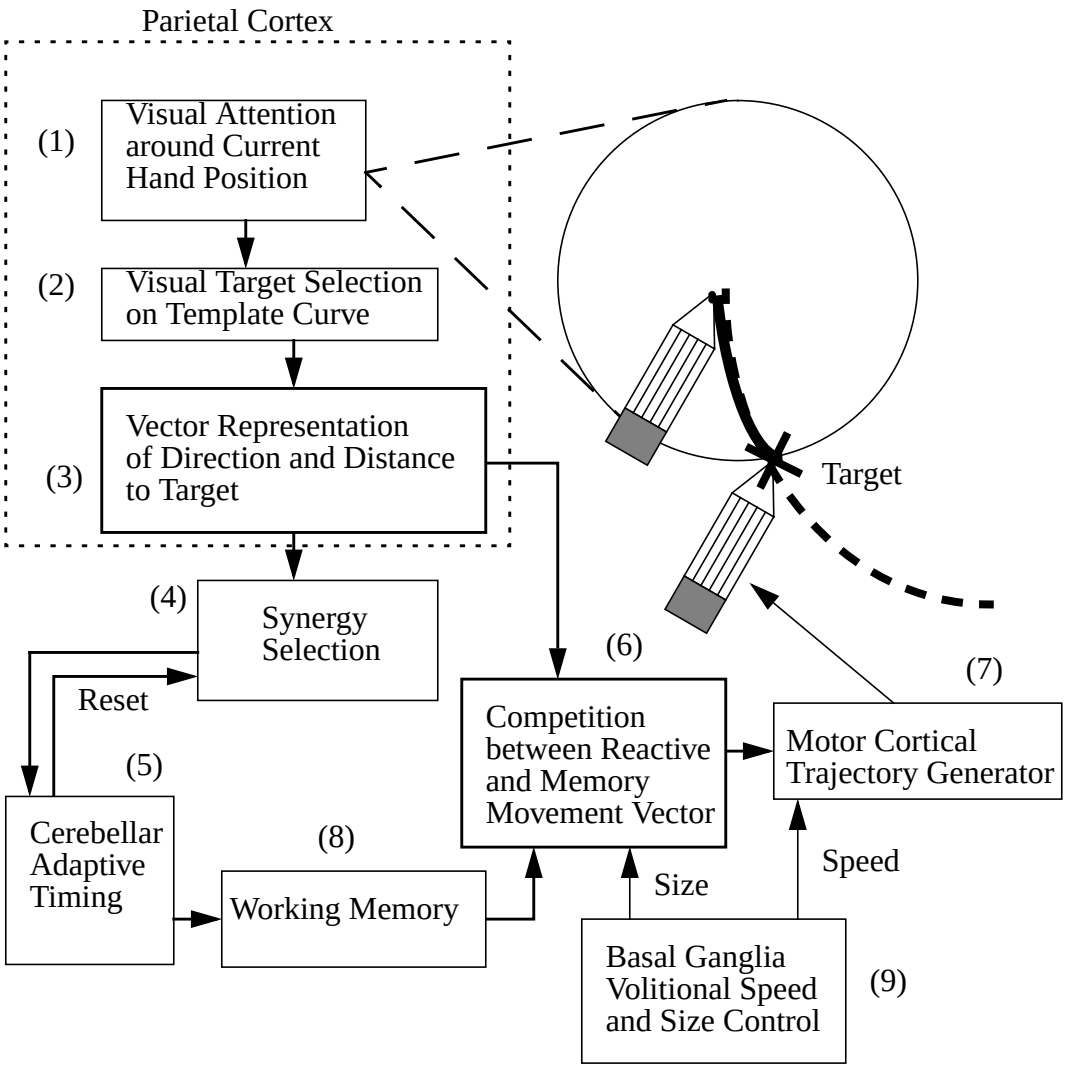

Figure 1.3. Conceptual diagram of the AVITEWRITE architecture. Numbers in parentheses indicate the order of discussion in the text.

The AVITEWRITE model architecture is schematized in Figure 1.3 and described later in detail in the Model Description (Figure 3.1). At the start of movement, visual attention (1) focuses on the current hand position and moves to select a target position (2) on the curve being traced. A Difference Vector representation (3) of the distance and direction to the target is formed between the current hand position (*PPV*) and the new target posi-

tion (*TPV*). This Difference Vector activates the appropriate muscle synergy (4) to drive a reactive movement to that target. At the same time, a cerebellar adaptive timing system (5) (Fiala et al., 1996) learns the activation pattern of the muscle synergy involved in the movement and begins to cooperate or compete (6) with reactive visual attention for control of the motor cortical trajectory generator (7). A working memory (8) transiently stores learned motor commands to allow them to be executed at decreased speeds as the speed and size of trajectory generation are volitionally controlled through the basal ganglia (9). Reactive visual control takes over when memory causes mistakes. Both the movement trajectory and the memory are then corrected, allowing memory to take over control again. As successive, visually reactive movements are made to a series of attentionally chosen targets on the curve, a memory is formed of the muscle synergy activations needed to draw that curve. After tracing the curve multiple times, memory alone can yield error-free movements.

Several properties of human handwriting movements emerge when AVITEWRITE learns to write a letter. Size and speed can be volitionally varied (Figure 1.3, stage 9) after learning while preserving letter shape and the shapes of the velocity profiles (Plamondon et al. 1997; Schillings et al., 1996; van Galen & Weber, 1998; Wann & Nimmo-Smith, 1990; Wright, 1993). Isochrony, the tendency for humans to write letters of different sizes in the same amount of time, is also demonstrated (Thomassen & Teulings, 1985; Wright, 1993). Speed can be varied during learning, and learning at slower speeds facilitates future learning at faster speeds (Alston & Taylor, 1987, p. 115; Burns, 1962, pp. 45-46; Freeman, 1914, pp. 83-84). Unimodal, bell-shaped velocity profiles for each move-

ment synergy emerge as a letter is learned, and they closely resemble the velocity profiles of adult humans writing those letters (Abend et al., 1982; Edelman & Flash, 1987; Morasso, 1981; Morasso et al., 1983). An inverse relation between curvature and tangential velocity is observed in the model's performance (Lacquaniti et al., 1983). It also yields a Two-Thirds Power Law relation between angular velocity and curvature, as seen in human writing under certain conditions (Lacquaniti et al., 1983; Thomassen & Teulings, 1985; Wann et al., 1988). Finally, context effects become apparent when AVITEWRITE generates multiple connected letters, reminiscent of carryover coarticulation in speech (Hertrich & Ackermann, 1995; Ostry et al., 1996), and similar to handwriting context effects reported by Greer & Green (1983) and Thomassen & Schomaker (1986).

CHAPTER II

BUILDING BLOCKS OF THE MODEL

2.1 Movement Synergies

As a starting point for the analysis and modelling of human handwriting, an understanding of the basic concept of movement synergies is necessary. Movement, or muscle, synergies are groups of muscles that work together in a common task. For example, groups of muscles are responsible for extending or flexing a leg in walking, or the arm,

wrist, and fingers in handwriting. The brain seems to control complex movement tasks, such as walking or handwriting, by issuing commands to a few muscle synergies, as opposed to specifying the movement parameters for scores of individual muscles separately (Bizzi et al., 1998; Buchanan et al., 1986; Kelso, 1982; Turvey, 1990). Using muscle synergies greatly simplifies the control and planning of movement by lessening the number of degrees of freedom requiring executive control (Bernstein, 1967; Turvey, 1990). Only at lower levels of the central nervous system, such as in the brainstem and spinal cord, would the motor synergy commands branch out to individual muscles. A key question is how these movement synergies are controlled.

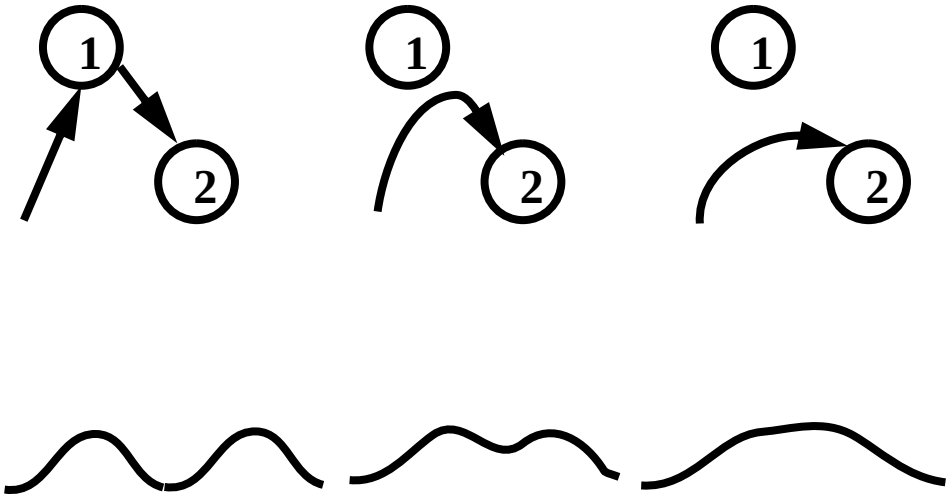

Figure 2.1. Velocity profiles become less segmented and more unimodal as the degree of superposition of consecutive strokes increases. (Adapted with permission from Plamondon & Guerfali, 1998.)

Human movements can be broken down into individual movement segments, or strokes. A stroke is usually defined by the zero crossings of the velocity profile for the corresponding synergy. The definition may become more complex in cases where strokes overlap. In the case of “via-point” movements (Figure 2.1), in which movement toward a

new target is begun before the movement to the prior target is complete, there may be no clear delineation of strokes reflected in the velocity profile (Georgopoulos et al., 1981; Plamondon & Guerfali, 1998).

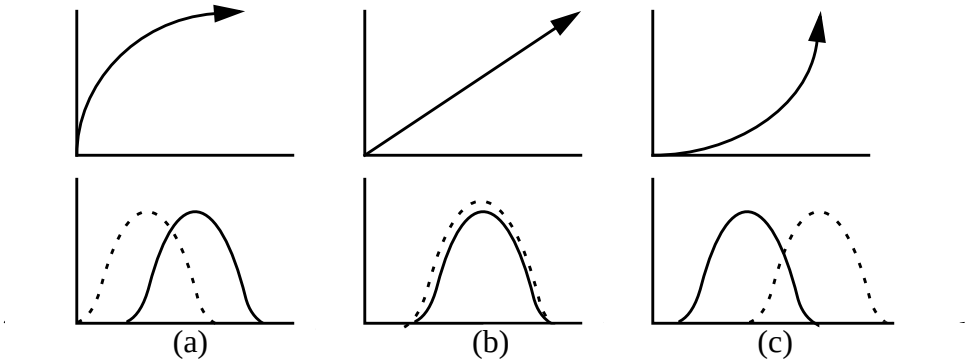

Figure 2.2. Varying the relative timing of synergy activation can yield different curved movements. For small segments of gradually curving arm movements, synchronous synergy activation yields approximately straight movements (b) while superposition of straight movement segments through asynchronous synergy activation yields short, highly curved movements in (a) and (c). The dotted and solid curves represent synergies that control movements in the orthogonal positive *y* and *x* directions, respectively.

Each stroke corresponds to the activities of particular muscle synergies. For simple, point-to-point horizontal planar arm trajectories, humans tend to generate straight movements with bell-shaped velocity profiles (Abend et al., 1982; Morasso, 1981; Morasso et al., 1983; Figure 2.2b). A key question is how the relative timing of muscle synergy activations is controlled to generate a desired trajectory. Recall that muscle synergies are groups of muscles working together in a common task. These muscle synergies may comprise the muscles used to move a single joint or even groups of muscles spanning several joints. When a given muscle synergy is activated, the contraction ratio of one muscle in that synergy to another in the same synergy remains relatively constant during the

movement. However, the activation timing of *separate* synergies may vary greatly from one movement to the next. It is the relative timing of the activation of these muscle synergies and the corresponding joint movements which determines the trajectory shape.

How are muscle synergy recruitment and subsequent hand movement controlled to generate arbitrary curves? Hollerbach and Atkeson (1987) showed that when a single synergy is activated across one joint in an arm movement, such as a simple elbow flexion, then a gentle arc-like curved hand trajectory is generated. This curved hand path is at a much larger scale than that of normal human handwriting. When one focuses on a small segment of this large curve, it appears locally straight. Thus, short duration activity of a single muscle synergy yields short, effectively straight segments. Similarly, if two approximately orthogonal muscle synergies are activated synchronously for a short duration, then short straight segments can be generated in arbitrary directions (Figure 2.2b).

This small scale behavior is in contrast with that observed at the larger scale of whole arm movements. Hollerbach and Atkeson (1987) reported that staggered, asynchronous muscle synergy activation is usually required in order to generate straight, large scale arm reaching movements. For such reaching movements, the active muscle synergies, which are not necessarily orthogonal to one another, must gradually change during the course of the movement as the body and arm posture change in order to yield an approximately straight hand trajectory. The manner in which the active arm synergies may change as a learned function of posture during a reaching movement has been studied in the DIRECT model of Bullock et al. (1993a).

In order to generate the smooth small scale and high curvature movements seen in

much human handwriting, how can the selection and timing of hand and arm muscle synergies be varied to generate a desired curve? If *synchronous* muscle synergies can generate straight, small scale movements, then one may hypothesize that sequential *asynchronous* activation of dissimilar synergies may yield the highly curved, small scale movements observed in handwriting (Figure 2.2a, c). In the AVITEWRITE model, the rapid direction changes needed for high curvature handwriting movements are generated by rapid switching of movement control among overlapping, orthogonal muscle synergies. The assumption of hand muscle synergy orthogonality is made for simplicity.

Thus, a main issue which must be addressed by AVITEWRITE is how the relative timing of muscle synergy activations in handwriting can be learned so as to generate a particular shape as the hand traverses the writing workspace. It will be shown how the relative timing of muscle synergy activations needed for a handwriting task can be learned through cycles of error-feedback driven learning in a modelled cortico-cerebellar system.

In curved movements, each synergy generates its own bell-shaped velocity profile. A simple example is a “U” curve (Figure 2.3), drawn as a combination of three strokes: one for a synergy in the negative, vertical direction; a second in the positive, horizontal direction; and a final stroke in the positive, vertical direction (Figures 2.3b and 2.3c). That the curved movements of handwriting obey an inverse relation between curvature and velocity (Lacquaniti et al., 1983) can be attributed to the direction reversal and synergy switching which occurs at points of high curvature, as at the bottom of a “U” curve (Figure 2.3d and 2.3e).

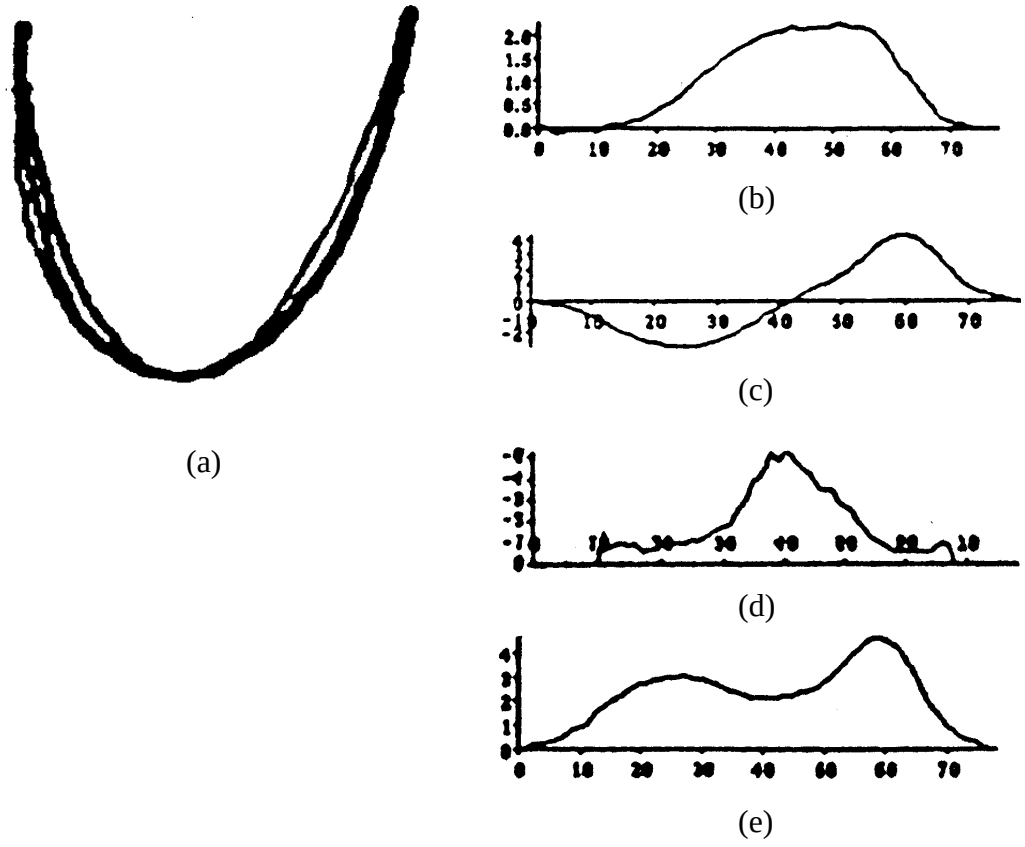

Figure 2.3. (a) A "U" curve written by a human; (b) and (c): x and y direction velocity profiles, respectively; (d) movement curvature; (e) tangential velocity. (Reproduced with permission from Edelman & Flash, 1987.)

2.2 The VITE Model of Reaching

How is movement direction represented in the brain? Much research, including that by Andersen et al. (1995), Georgopoulos et al. (1982, 1989, 1993), and Mussa-Ivaldi (1988), supports the idea that motor and parietal cortex compute a vectorial representation of movement direction in motor and/or spatial coordinates. This idea is known as the "population vector hypothesis," where a population vector is defined as a "weighted vector sum of contributions of directionally tuned neurons" (Georgopoulos et al., 1989, p. 234). The activity of one such directionally tuned neuron is illustrated in Figure 2.4.

The VITE, or Vector Integration to Endpoint, model (Bullock & Grossberg, 1988a, 1988b, 1991) uses a vectorial representation of movement direction and length to generate straight reaching movements with bell-shaped velocity profiles (Figure 1.1). "Trajectories are generated as the arm tracks the evolving state of a neural circuit" (Bullock & Grossberg, 1988a, p. 314). A Difference Vector (*DV*) is computed as the difference from an outflow representation of the current hand position, or Present Position Vector (*PPV*), to a target, or Target Position Vector (*TPV*) (Figure 2.5).

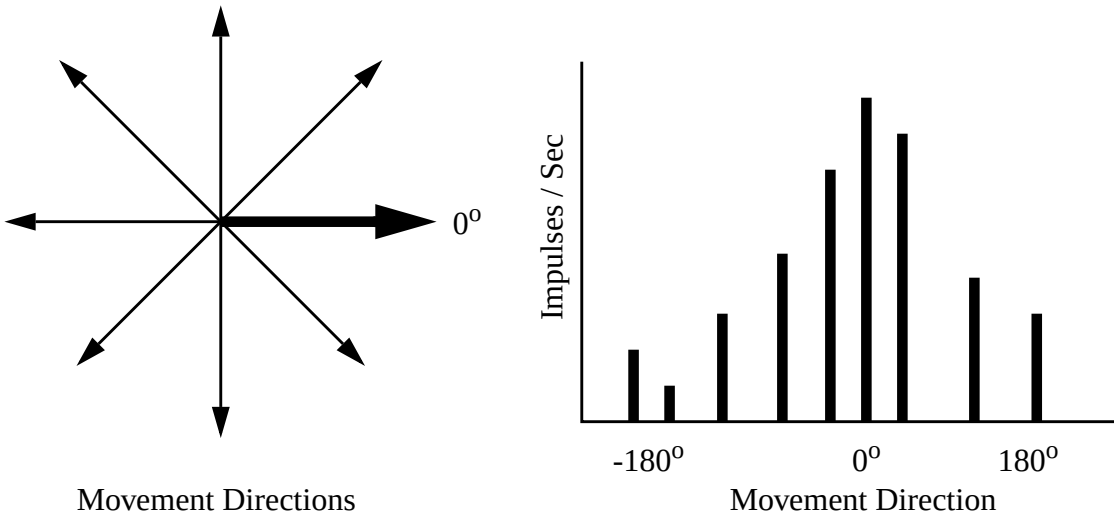

Figure 2.4. Illustration of neuronal directional tuning. The discharge frequency (b) of a motor cortical cell peaks for movement in a specific direction, 0^o in this case (a). (Adapted with permission from Georgopoulos et al., 1982.)

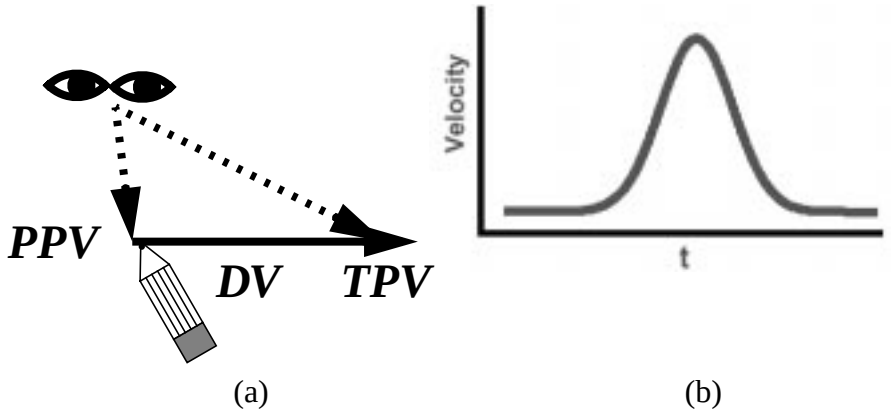

Figure 2.5. (a) Illustration of a Difference Vector (*DV*) formed from the current hand location, given by a Present Position Vector (*PPV*), to a Target Position Vector (*TPV*). The *DV* is integrated in a VITE circuit to generate a straight movement with a bell-shaped velocity profile (b).

The *DV* is multiplied by a gradually increasing *GO* signal, which is under volitional control, and whose growth rate can be changed to alter movement speed while preserving movement direction and length. The existence of a "*GO*" signal is supported by basal ganglia speed control studies, such as those of Horak & Anderson (1984a, 1984b), Turner et al. (1998), and others (Berardelli et al., 1996; Georgopoulos et al., 1983, Hallett & Khoshbin, 1980; Turner & Anderson, 1997). The *DV* times the *GO* signal is integrated at the *PPV* until the present position of the hand reaches the target.

The VITE model explains behavioral and neural data about how a motor synergy can be commanded to generate a synchronous, multi-joint reaching trajectory at various speeds. VITE describes how synchronous movements may be generated across synergistic muscles with automatic compensation for the different total contractions undergone by each muscle group. Many properties of human reaching movements emerge from VITE's performance, including the equifinality of movement synergies, a rate-dependence of velocity profile asymmetries, and variations in the ratio of maximum to average movement velocities (Bullock & Grossberg, 1988a, 1988b, 1991).

Although the earlier versions of the VITE model primarily addressed psychophysical data, the revised VITE model of Bullock, Cisek, & Grossberg (1998) assigned functional roles to six cell types in movement-related, primate cortical areas 4 and 5, and integrated them into a system which is capable of "continuous trajectory formation; priming, gating, and scaling of movement commands; static and inertial load compensation; and proprioception" (Bullock et al., 1998, p. 48). For example, model Difference Vector cells resemble the activity of posterior parietal area 5 phasic cells, while Present Position Vector cells

behave like anterior area 5 tonic cells (Figure 2.6). This expanded version of VITE described how cortical area 4 may assemble a "multicomponent motor command which simultaneously specifies desired position and load-compensating forces" (Bullock et al., 1998, p. 48). One limitation of the VITE model was that it did not explain how curved movements could be generated.

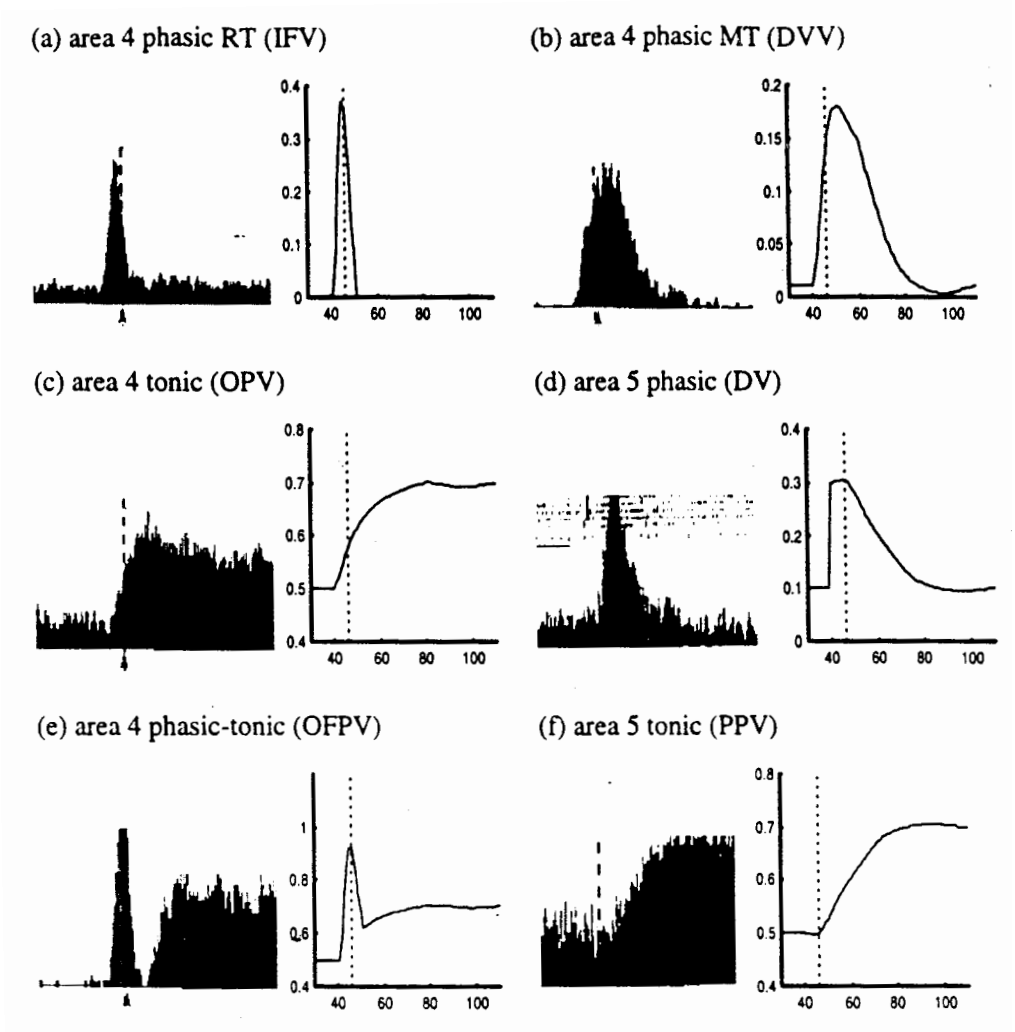

Figure 2.6. Comparison of six distinct cell types in cortical areas 4 and 5 (Kalaska et al., 1989, 1990) with model cell responses of the expanded VITE model of Bullock et al. (1998). (Reproduced with permission from Kalaska et al., 1989, 1990; and Bullock et al., 1998.)

2.3 The VITEWRITE Model of Handwriting Generation

The VITEWRITE model of Bullock, Grossberg, and Mannes (1993) (Figure 1.2) extended the VITE reaching model to explain handwriting data. In VITEWRITE, curved movements are generated using a velocity-dependent stroke-launching rule that allows *asynchronous* superposition of multiple muscle synergy activations with unimodal, bell-shaped velocity profiles for each synergy. Scaling the size of *DV*s by multiplication with a volitional *GRO* signal allows size scaling without significantly altering the trajectory shape or the shape of the velocity profile. Similarly, altering the size of the volitional *GO* signal alters trajectory speed without changing trajectory shape. The movements generated by VITEWRITE yield the inverse relation between curvature and tangential velocity observed in human performance, as well as the Two-Thirds Power law relation between angular velocity and curvature observed in humans under some writing conditions (Lacquaniti et al., 1983; Thomassen & Teulings, 1985; Wann et al., 1988). VITEWRITE also shows how size scaling of individual synergies via separate *GRO* signals can change the style of writing without altering velocity profile shape. Such independent scaling of muscle synergy commands is supported by the study of Wann & Nimmo-Smith (1990), which yielded data that "do not support common scaling for x and y dimensions" (p. 111).

The Adaptive VITEWRITE model captures key properties of VITEWRITE and yields performance which is equally consistent with available handwriting data. In addition, AVITEWRITE addresses the main limitation of VITEWRITE, which is its inability to learn and remember the motor plan that, once learned, yields such good performance. The original VITEWRITE model does not address "the self-organizing process that dis-

covers, learns, and stores representations of movement commands" (Bullock et al., 1993b, p. 22). The pattern of "planning vectors" which formed VITEWRITE's motor program, or plan, needed to be predefined in order for the system to generate a movement or write a particular letter. In contrast, AVITEWRITE learns how to generate letters by itself, and then remembers how to write them. It remains to be seen whether and how the synergy-launching rule that was used in VITEWRITE can be assimilated into this learning scheme.

2.4 Adaptive Timing in the Cerebellum

How are curved movements represented in the brain? Given that a particular curved movement may be generated by appropriately-timed activation of multiple muscle synergies, we need to understand how the time-varying activation of these muscle synergies, or strokes, is learned. Several mechanisms have been proposed to learn how to adaptively time responses to stimuli. Possible timing mechanisms include delay lines (Moore et al., 1989; Zipser, 1986), a spectrum of slow responses with different reaction rates in a population of neurons (Bartha et al., 1991; Bullock et al., 1994; Grossberg & Merrill, 1992, 1996; Grossberg & Schmajuk, 1989; Jaffe, 1992), and temporal evolution of the network activity pattern (Buonomano & Mauk, 1994; Chapeau-Blondeau & Chauvet, 1991). Given the need to learn time delays of up to four seconds in eye blink conditioning, delay lines of sufficient length do not appear to be present in the cerebellar cortex (Fiala et al., 1996; Freeman, 1969). Although Buonomano & Mauk (1994) showed that some sensitivity of a temporal network evolution model to network noise could yield the experimen-

tally observed decrease in conditioning as the interstimulus interval increases, they also found that their model was overly sensitive to noise, since noise caused the loss of the model's timing ability. Loss of timing due to network noise over a four second interval may therefore preclude temporal network evolution mechanisms.

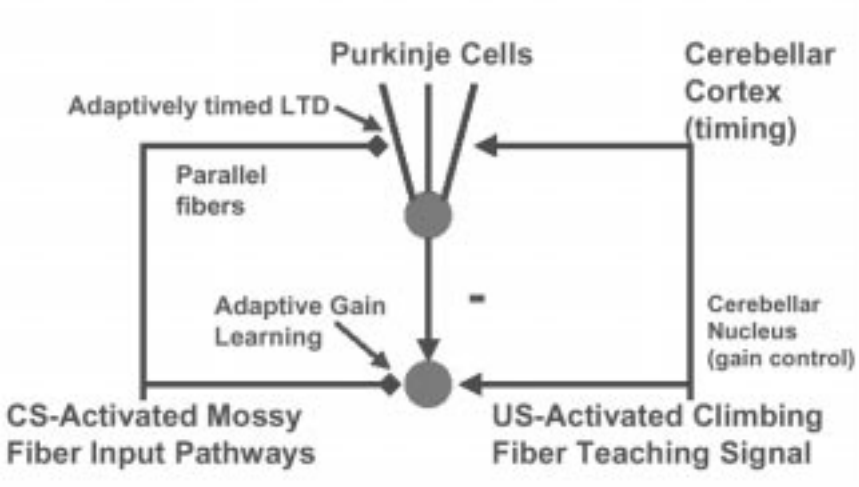

Figure 2.7. Overview of cerebellar spectral timing. Long term depression (LTD) occurs at the parallel fiber-Purkinje cell synapse when an unconditioned stimulus (US) is paired with a conditioned stimulus (CS) over multiple presentations. In the current discussion, the US is interpreted as an error signal, although in other contexts it may correspond to a reward signal. (Adapted with permission from Grossberg & Merrill, 1996.) See text for details.

Accumulating evidence suggests that adaptively timed learning of strokes may be achieved by *spectral timing* in the cerebellum. Ito (1984) and others (Fiala et al., 1996; Perrett et al., 1993) have suggested that the cerebellum may be involved in the opening of a timed gate to express a learned motor gain, as when a rabbit learns to blink after hearing a tone previously associated with an air puff. In this conception (Figure 2.7), a signal associated with a Conditioned Stimulus (CS) arrives via the cerebellar (mossy fiber)-to-

(parallel fiber) pathway at a population of Purkinje cells and triggers a series of phase-delayed activation profiles, or depolarizations, of the Purkinje cells, called a Purkinje cell "spectrum" (Figure 2.8b). When a signal associated with a subsequent Unconditioned Stimulus (US) arrives via climbing fibers at some fixed Interstimulus Interval (ISI) after the CS, then long term depression (LTD) of active Purkinje cells may occur at that time

(a)

(b)

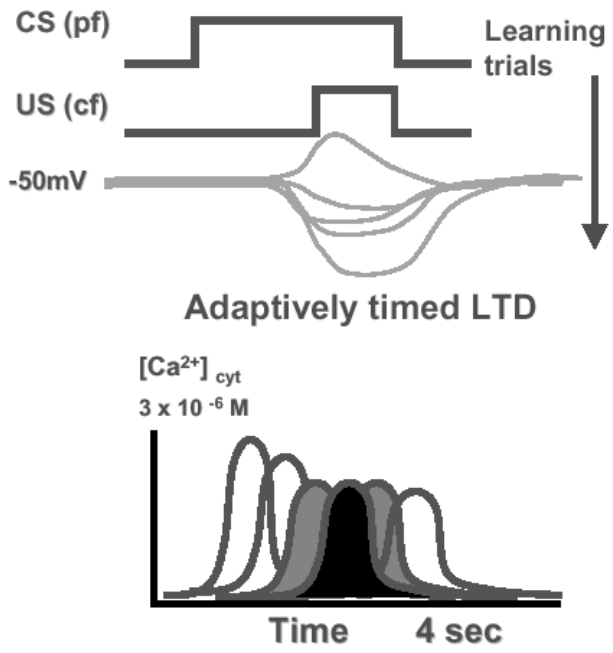

Figure 2.8. Conceptual diagram of a spectrum of calcium release in response to parallel fiber input to a population of Purkinje cells with different time constants due to varying concentrations of dendritic metabotropic glutamate receptor, mGluR (b); Adaptively timed long term depression (LTD) occurs over multiple CS-US pairings (a). As the unconditioned stimulus (US) arrives over multiple learning trials at a fixed interstimulus interval after the conditioned stimulus (CS), LTD occurs at those Purkinje cells which are active when the US arrives (shaded response curves in b). (Adapted with permission from Fiala et al., 1996.)

(Figure 2.8a), leading to disinhibition of the cerebellar nuclei at that time (Figure 2.7); hence the term "adaptive timing" (Fiala et al., 1996; Grossberg & Merrill, 1992, 1996;

Grossberg & Schmajuk, 1989). The staggered temporal pattern of Purkinje cell depolarizations following the initial CS ensures that some Purkinje cells will be active, and subject to long term depression, at the time that the US arrives via the climbing fibers (Figure 2.8a).

Fiala et al. (1996) utilized biochemical mechanisms of the metabotropic glutamate receptor (mGluR) system to simulate how learning of adaptively timed long term depression of Purkinje cells occurs and causes disinhibition of cerebellar nuclei during classical conditioning. The biochemical mechanism of spectral timing will be further summarized in the Discussion section. Fiala et al. (1996) also showed that a Purkinje cell spectrum could learn to respond to two conditioned stimuli with different interstimulus intervals (p. 3770). AVITEWRITE takes this approach one step further. Instead of learning one or two responses at discrete points in time, as in the conditioning task, it is hypothesized that the cerebellar adaptive timing mechanism can also learn a continuous response over time in more complex tasks like handwriting. For a continuous handwriting task, different Purkinje cell spectra are activated by the commands corresponding to different muscle synergies. The climbing fiber unconditioned stimuli act as error-based signals that train the Purkinje cells to become hyperpolarized in specific temporal patterns that lead to correctly shaped writing movements. The level of depression of a given Purkinje cell determines the extent of cerebellar nucleus disinhibition during that Purkinje cell's activation. Each Purkinje cell learns to control a particular muscle synergy during a brief time window of movement. When these brief, individual movement commands are summed over the entire Purkinje cell population with staggered, overlapping cell activations, a continu-

ously changing pattern of muscle synergy activations may be generated which can yield curved planned movements. Thus, a cerebellar adaptive timing system may learn to shape the time-varying activation pattern of asynchronous muscle synergies. Such an adaptive timing system forms part of an integrated handwriting learning and generation system (Figures 1.3, 3.1) that also uses elements of VITE trajectory formation for visually reactive movements to targets, as well as ideas from VITEWRITE about building curved movements from overlapping synergies in a way that preserves shape-invariant volitional speed and size scaling.

CHAPTER III

MODEL DESCRIPTION

3.1 Introduction to AVITEWRITE

The proposed AVITEWRITE model is a neural network handwriting learning and generation system that joins together mechanisms from the cortical VITE and VITEWRITE trajectory generation models (Bullock & Grossberg, 1988a, 1988b, 1991; Bullock et al., 1993b) and the cerebellar spectral timing model of Fiala et al. (1996). This synthesis creates a single system capable of both reactive movements (movements directly in response to stimuli without requiring learning in order to be made) as well as memory-based movements based on previous cerebellar movement learning and subse-

quent read-out from long-term memory (LTM). AVITEWRITE models curved movement trajectory generation by asynchronous, overlapping muscle synergy activations. It describes how spatial attention may be involved in the selection of targets on a curve that is to be traced. Reactive movements are made to these targets at the same time that adaptively timed learning of the muscle synergy activations involved in those movements occurs. The model explains how switching between reactive, visually-guided and memory-based control of movement generation may occur. Volitional control of movement speed and size may be achieved while preserving the key features of trajectory shape and velocity profiles over the wide range of speeds, with speed variation by a factor of 2.8 without significantly altering the trajectory, observed in humans (Wright, 1993). Further, the model describes how speed can be volitionally varied during learning without adversely affecting the learning process. Finally, AVITEWRITE describes a system of on-line movement error correction which automatically shuts off as learning succeeds and memory alone controls correct handwriting movement generation.

3.2 System Architecture

AVITEWRITE makes essential use of visual spatial attention to determine where the hand will move to imitate a curve. Attention is modelled algorithmically since it is not the main focus of the present study. The model assumes, for simplicity, that attention may be focused within a circular region around the present fixation point. In the model, visual spatial attention is initially focused around the current hand position on a template curve (Figure 3.1). The system begins with no prior memory of a given movement shape.

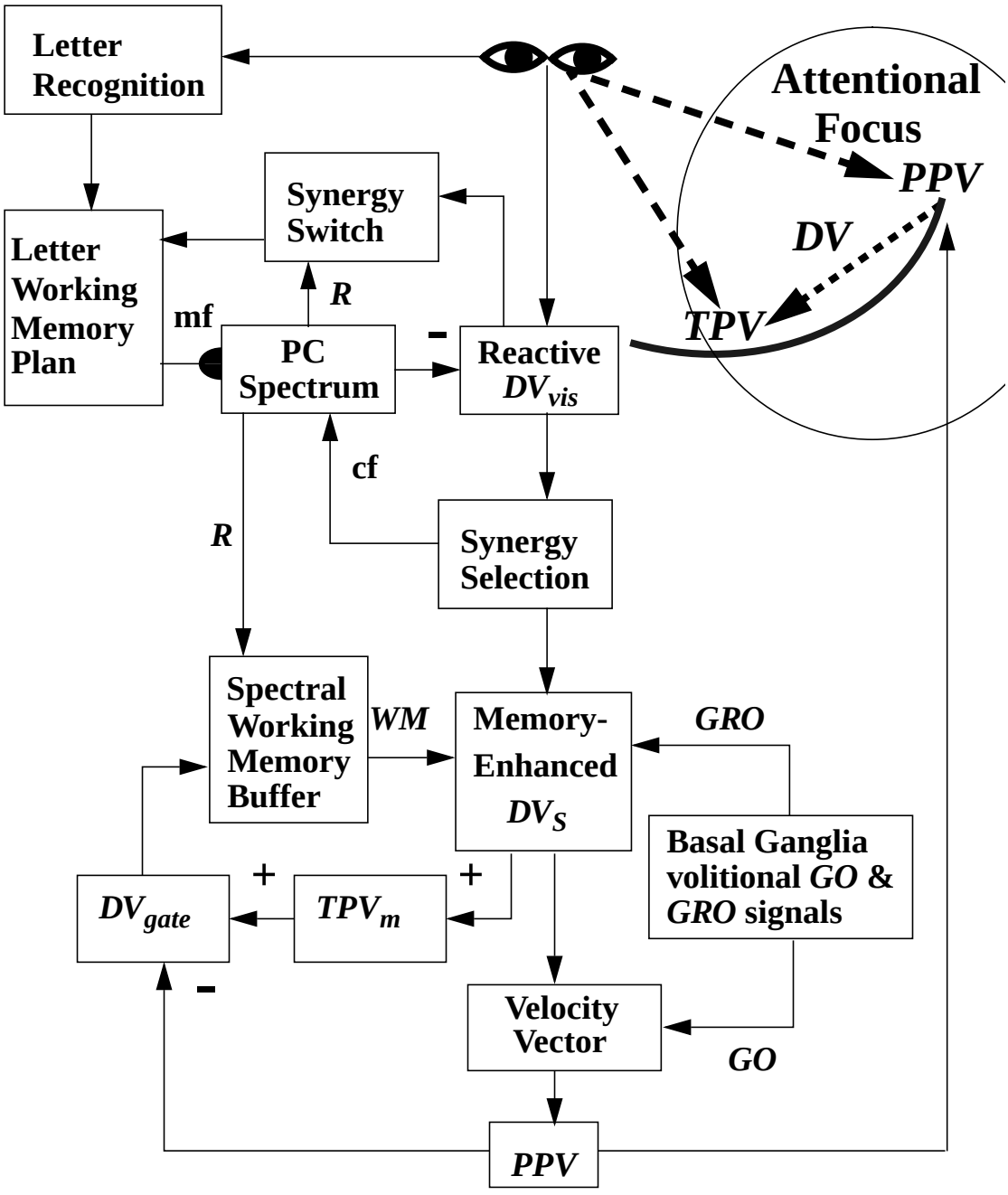

Figure 3.1. Diagram of the AVITEWRITE architecture: cf = climbing fiber; DV_{gate} = Gating Difference Vector; DV_S = Size-scaled, memory-enhanced Difference Vector; DV_{vis} = Visual Difference Vector; *GO* = Volitional speed control signal; *GRO* = Volitional size control signal; mf = mossy fiber; PC = Purkinje cell; *PPV* = Present Position Vector; *R* = Adaptively timed cerebellar output; *TPV* = Target Position Vector; TPV_m = Memory-modulated Target Position Vector; *WM* = Spectral Working Memory Buffer output.

From this predetermined starting point, attention shifts along the curve to another target (*TPV*: Target Position Vector) on the shape that lies within an attentional radius of the current hand position (*PPV*: Present Position Vector). How this is modelled will be more explicitly stated below.

In support of the model's use of spatial attention, experimental data suggest that superior frontal, inferior parietal, and superior temporal cortex are part of a network for voluntary attentional control (Hopfinger et al., 2000) which is critical for directing "unpracticed movements in man" (Richer et al., 1999, p. 1427). Jueptner et al. (1997a, 1997b) reported that the prefrontal cortex was activated in a finger movement-sequence learning task during new learning but not during automatic performance after learning. Further, the left dorsal prefrontal cortex was reactivated "when subjects paid attention to the performance of the prelearned sequence" (Jueptner et al., 1997b, p. 1313). Evidence for an interaction between parietal and frontal lobe activity and cerebellar activity was found by Arroyo-Anllo & Botez-Marquard (1998). The authors found that humans with olivopontocerebellar atrophy suffered deficits in copying a simple figure and in immediate visual spatial memory, "consistent with the hypothesis that the cerebellum is involved in visual spatial working memory... and that it modulates parietal lobe- and frontal lobe-mediated functions" (p. 52).

AVITEWRITE uses spatial attention to constrain the choice of the target positions that drive imitative tracing of a curve. The model assumes that these targets are selected within an attentional "tube" that is swept out by shifts in attention around the curve (Figure 3.2). If there is no memory, or if movement deviates from the attentional radius

around the curve being traced due to memory inaccuracy, then a new target is chosen on the curve.

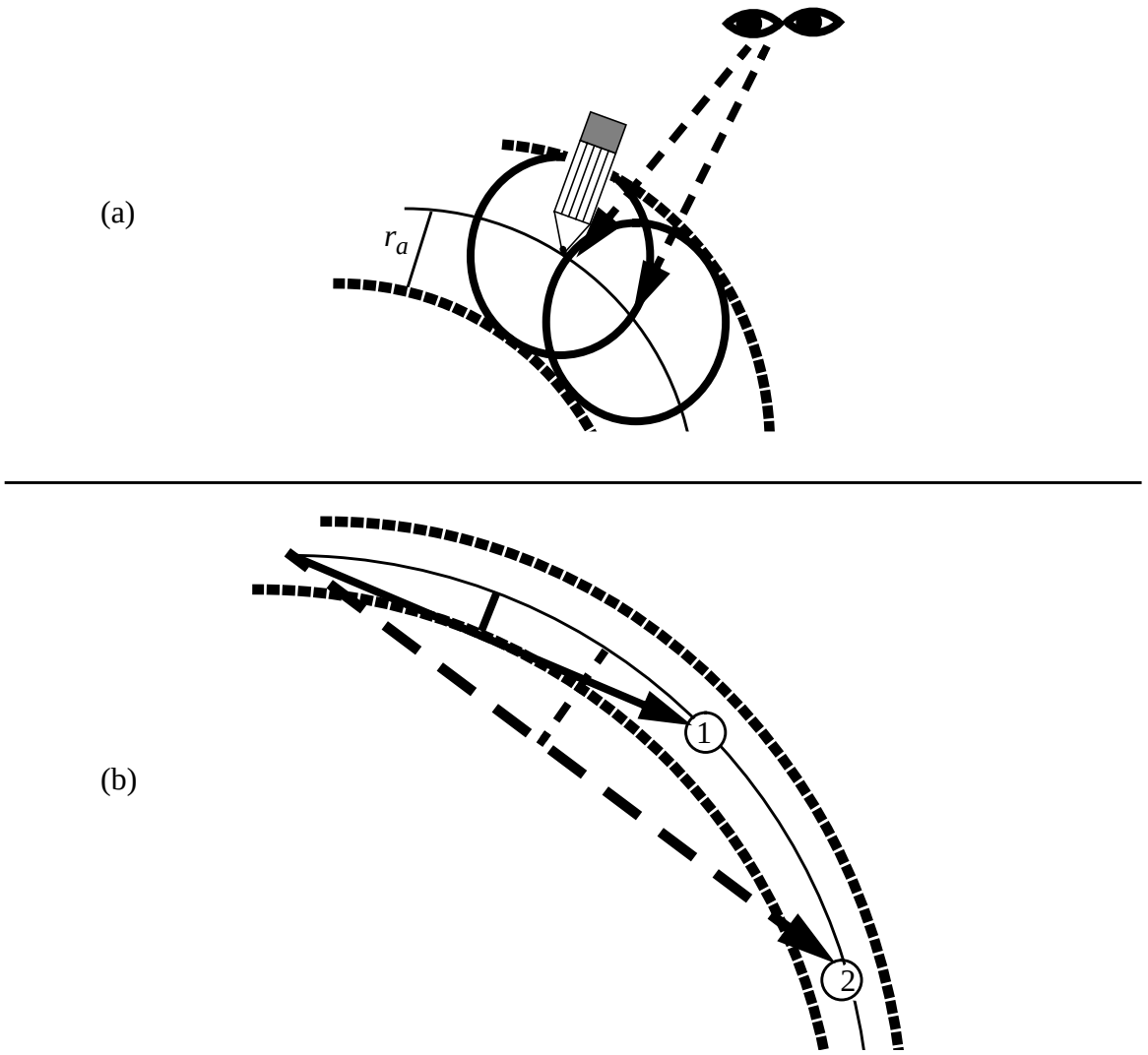

Figure 3.2. Illustrations of target selection. See Model Equations section for full description of the target selection algorithm. (a) Targets are chosen so as to keep the movement within an attentional radius, depicted as a circle around the current hand/pencil tip position, of the curve being traced. Superposition of these circular foci of attention as attention shifts across space generates an attentional "tube" around the template curve, shown as dotted lines. (b) Target 1 is possible because movement to it would not exceed the attentional radius, r_a, from the curve being traced, whereas Target 2 is invalid because r_a would be exceeded.

Each choice of a new *TPV* from the current *PPV* defines a visual Difference Vector, or DV_{vis}, that is constrained to point forward along the template curve (Figure 3.2) and remain within an attentional radius (r_a) of it, or else return the hand to within a distance r_a of the curve if it has exceeded it. The details of the target selection algorithm are described in the Model Equations section. The *TPV*s are used to form difference vectors, DV_{vis}, that both drive the movement and act as teaching signals to train a cerebellar spectral memory via climbing fiber inputs.

Once a target is chosen, vision provides direction and amplitude information, in the form of the difference vector, DV_{vis}, to a trajectory generator which can combine temporally overlapping muscle synergy activations to generate curved movements whose speed and size are volitionally controlled. Evidence that visual difference vectors may serve as triggers for movement error signals was found by Stuphorn et al. (2000). The authors found that gaze-related reach neurons in the superior colliculus could signal the motor error between the gaze axis and the reach target. Schwartz & Moran (1999) studied cell population vectors in motor and premotor cortex during drawing movements. They found that "population vectors predicted direction (vector angle) and speed (vector length) throughout the drawing task" and that the "2/3 power law described for human drawing was also evident in the neural correlate of the monkey hand trajectory" (p. 2705).

Once a visual difference vector is formed to a target on the template curve, AVITEWRITE assumes that a spatial to motor coordinate transformation occurs (see section 4.8) which allows activation of the appropriate muscle synergy to generate movement to that target. As described below and in Figure 3.3, the model also assumes that a letter

category representation of the letter being traced is formed which triggers a letter working memory plan to activate the appropriate muscle synergy-specific cerebellar spectra. The trajectory generator then starts to integrate the memory-enhanced difference vector, DV_S, generating a velocity vector that drives movement to the target (Figure 3.1). At the beginning of learning when there is not yet a memory contribution to movement control, DV_S equals DV_{vis} multiplied by a volitional size-scaling *GRO* factor. At the same time that movement towards the visual target is occurring, adaptively timed learning of the muscle synergy activations required to reach that target occurs. The cerebellum model stores movement commands for groups of muscles (muscle synergies) working together to drive the hand and arm in particular directions. The model uses separate spectral memories to learn and store the movement commands for different synergies. In the simulations (Figures 3.10, 3.14), four separate spectral memories are formed for positive and negative, horizontal and vertical movement synergies, respectively. The use of separate spectral memories allows muscle synergy-switching with independent control of each synergy. It also avoids the requirement that any one Purkinje cell spectrum be active for prolonged periods of time, allowing it to stay within the four second time limit for a spectrum of the Fiala et al. (1996) model.

A new synergy is activated in the model at the start of movement and whenever there is a reversal in movement direction, requiring activation of a different synergistic set of muscles. Prior to learning, the synergies needed to begin a movement are determined by the value of DV_{vis}. For example, when starting the letter “U” when there is no prior memory of this letter, a DV_{vis} is formed which initially points in the negative y and positive x-

directions. Purkinje cell spectra corresponding to the negative y and positive x-direction synergies therefore begin having their synaptic weights modified by the climbing fiber error/teaching signal. As memory starts to form, the model assumes that a visual representation of the letter is categorized by inferotemporal and prefrontal mechanisms in the "what" cortical processing stream, and that a visual cue is used to sample the appropriate synergies used to perform a given letter from memory (Figure 3.3). Although not modelled explicitly, AVITEWRITE assumes that a working memory, possibly in prefrontal cortex, forms a category representation of each letter which controls adaptive pathways to all the synergies. The letter category determines which cerebellar spectra, corresponding to the particular synergies needed to write that letter, are activated via mossy fiber inputs. Only those adaptive pathways that were modified due to prior learning will read-out non-zero values of the cerebellar spectral memory output, *R*. In order to initiate writing of a learned letter, the letter category triggers the initial spectra that control the synergies needed to start the movement. When writing the letter "U" for example, the letter category memory activates spectra corresponding to the negative y and positive x-direction synergies at the beginning of movement. The letter category representation also stores the identities of the other (the positive y) spectra involved in generating that particular letter. Their order of activation is determined automatically by the synergy switching rule described below. Note that it is *not* claimed that the cerebellum is the primary, or even sole, determinant of the serial order of movement. The letter working memory plan and synergy switch depicted in Figures 3.1 and 3.3 are assumed to be extracerebellar.

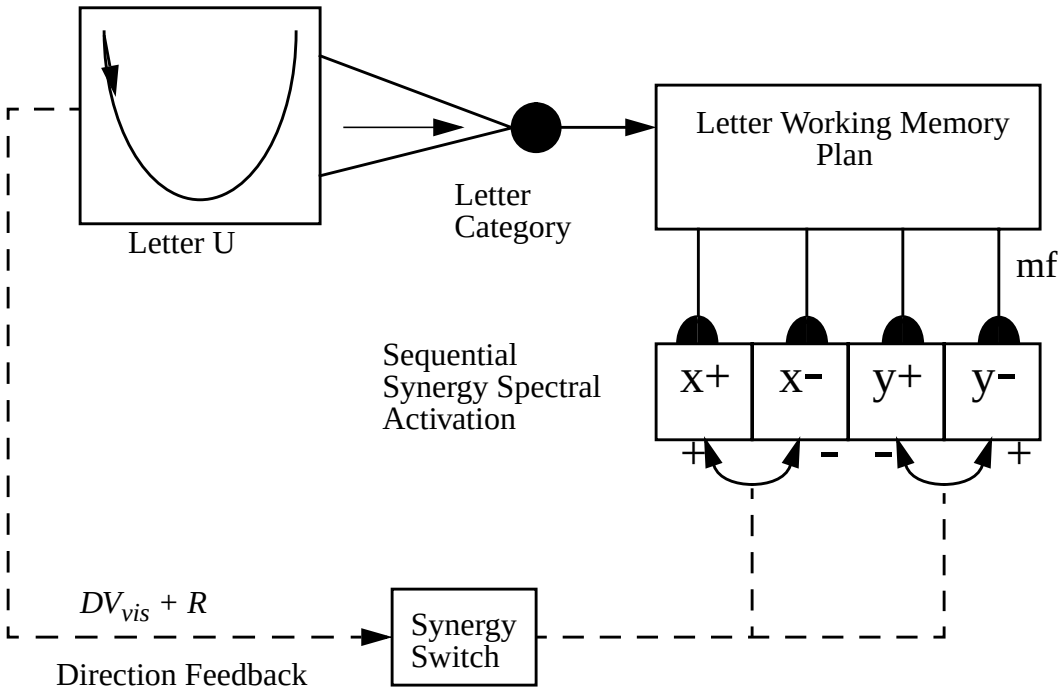

Figure 3.3. Blow-up of how a letter category controls read-out of learned performance via the sequential order of synergy-specific spectra for the positive and negative, x and y synergies, x+, x-, y+, and y-. Synergy switching is triggered by a change in sign of the total movement direction, DV_{vis} + R. mf = mossy fiber. See Figure 3.1 (upper left) for comparison.

Synergy switching is accomplished as follows in the model. If the total movement direction, determined by the sum of the reactive visual Difference Vector (DV_{vis}) and the cerebellar spectral memory (*R)* in Figure 3.1, changes sign, then a new synergy and Purkinje cell spectrum are activated. No new spectral components are activated in the spectrum from the prior synergy, although those components which are active at the time of the synergy switch continue to respond until they decay spontaneously. Such spectral behavior is supported by the responses of the biochemically-detailed Fiala et al. (1996) model to the sudden cessation of glutamate input to the Purkinje cells from the parallel fibers. In the Fiala et al. (1996) simulations, spectral components which are active at the

time of input cessation remain active for a time while decaying spontaneously, whereas no new spectral components respond once the glutamate input has been shut off (Figure 3.4).

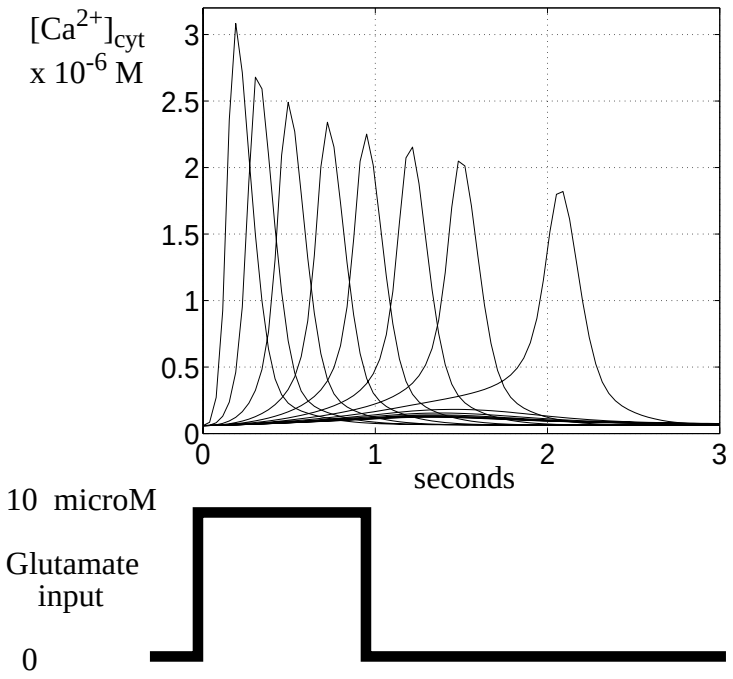

Figure 3.4. Fiala et al. (1996) spectra with glutamate input shut off after 1 second. Note that spectral components which are active—that is, with $[Ca^{2+}]_{cyt}$ greater than approximately 0.2 x 10^{-6}M—at time t = 1 remain active until the normal response is completed, whereas no large new spectral calcium responses occur once the glutamate input has been shut off.

The term spectral activity is here used to indicate the pattern of time-varying, intracellular Purkinje cell Ca^{2+} concentration changes with different latencies in response to parallel fiber inputs depicted in Figures 2.8 and 3.4. When writing a letter “U”, a negative y-direction muscle synergy starts the movement. One Purkinje cell spectrum would learn to correct all the negative y-synergy movement errors. At the bottom of the “U”, the y-synergy would reverse, triggering activation of a new spectrum to learn to correct the pos-

itive y-synergy errors. At this point, input to the negative y-synergy spectrum would be stopped; e.g., by shutting off the glutamate input released from parallel fibers in the Fiala et al. (1996) model equations, and the spectra active at the time of the direction reversal would decay.

Error-driven movement learning is mediated by climbing fiber error signals, based on the value of $TPV - PPV$, the difference between the target position and the current hand position. For a discussion of the coordinate systems assumed for these error signals and other components of the model, please refer to section 4.8. The climbing fiber signal modifies the parallel fiber/Purkinje cell synaptic efficacy by triggering patterns of long term depression across the Purkinje cell populations that control the respective muscle synergies. As the Purkinje cells' activity becomes more depressed, their target cerebellar nucleus becomes disinhibited (Figure 2.7), thereby enhancing muscle synergy activation over time according to the temporal pattern of Purkinje cell population activity.

The AVITEWRITE model incorporates competition between reactive movement and memory-based movement control systems. The model hypothesizes that the cerebellar motor memory competes for control of movement with prefrontal and premotor areas that guide reactive movements based on visual input (Caminiti et al., 1999; Dagher et al., 1999; Jueptner et al., 1997a, 1997b; Jueptner & Weiller, 1998; Kawashima et al., 2000; Sadato et al., 1996). In the model, the reactive visual difference vector (DV_{vis}) and the learned output from cerebellar memory (R), transiently stored in a working memory buffer (WM) described below, are combined to form the Memory-Enhanced Difference Vector, DV_S. The cerebellar spectral output is called R in keeping with the naming con-

vention of the spectral timing models of Grossberg & Schmajuk (1989) and Grossberg & Merrill (1992). *R* in AVITEWRITE should not be confused with the similarly named "reciprocal" (R) central movement command variable from the Equilibrium-Point model of Feldman & Levin (1995) and St.-Onge et al. (1997). Any similarity between AVITEWRITE's cerebellar output and the Equilibrium-Point command variable is unintentional.

The DV_S is, in turn, multiplied by a volitional size-scaling *GRO* signal to yield the size-scaled, memory-enhanced Difference Vector, DV_S. When the memory contribution to DV_S is strong enough, then the cerebellar memory determines DV_S, and DV_{vis} decays to zero (see Equation 1 below).

A visual difference vector (DV_{vis}) will be formed to a target if either of two conditions is met. First, if the memory is too small (below threshold ε in Equation 1), then the system waits for a brief period of time (parameter *Memlag* = 0.9) in case another memory is becoming active. If no memory grows beyond the threshold (ε) by the end of this time period, then a reactive visual DV_{vis} is formed in the manner described above. This DV_{vis} drives the reactive movement toward a target. Second, if an error is made due to a movement deviating from the attentional radius around the template curve, then a corrective visual DV_{vis} is formed which determines DV_S and drives a corrective movement. The difference between the target and present positions ($TPV - PPV$) generates a cerebellar teaching signal that updates the memory. Memory again takes over control once the trajectory re-enters the attentional focus around the template curve, at which time DV_{vis}

decays to zero. Thus, on-line error correction occurs which automatically shuts off as the system successfully learns to generate the desired curve. As learning proceeds, error-prone movements become successively more accurate until no errors are made and memory alone controls the movement. Once memory can control the movement without errors, the learned movement can be correctly executed without visual feedback.

As in the original VITEWRITE model (Bullock et al., 1993b), a volitional *GO* signal (Equations 8 and 9 below) scales movement speed in AVITEWRITE by altering the trajectory generator's rate of difference vector (DV_S) integration (Equation 7 below). However, the rate of predefined memory planning vector readout in VITEWRITE (see section 2.3) was a function of the movement's velocity. It is still unclear how such a rule can hold across learning trials during which a great variability in strokes and speeds eventually converges to a unimodal velocity profile.

When one turns to spectral learning to overcome this difficulty, one needs to face a different problem; namely, the rate with which cerebellar Purkinje cells can read out the synaptic weights that form their motor memory is limited. In other words, attempting to alter movement speed by changing the *GO* signal by a factor of 2.8 to match the range of human speeds (Wright, 1993) would not necessarily alter the rate at which the cerebellum reads out its stored motor commands by a comparable factor. AVITEWRITE hypothesizes that the rate at which the motor commands are retrieved from cerebellar long term memory defines the maximum possible rate at which error-free, memory-driven sequential handwriting movements can be made.

How can learned movements be made across a wide range of speeds while keeping tra-

jectory shape and velocity profiles relatively constant if the variability of the long term motor memory readout rate is limited? In his 1991 psychomotor theory of handwriting, Van Galen suggests that working memory buffers between handwriting "processing modules" may "accommodate for time frictions between information processing activities in different modules" (p. 182). AVITEWRITE hypothesizes that a working memory system helps to write at a wide range of speeds even if the read-out rate of cerebellar spectra does not change. This working memory system, with movement speed-dependent motor command readout, is not to be confused with the prefrontal working memory assumed to store letter category representations (discussed earlier but not explicitly modelled in AVITEWRITE). Experimental data support the idea that working memory function may influence movement speed. For example, several authors have found that lesions causing spatial working memory deficits also cause increased speed for learned patterns of limb movements. Ventral hippocampal lesions (Bannerman et al., 1999), cholinergic basal forebrain lesions (Waite et al., 1995), and NMDA receptor antagonism (Kretschmer & Fink, 1999) impair both spatial working memory and cause an increase in movement speed. Pleskacheva et al. (2000) found that voles with smaller hippocampal mossy fiber projections exhibited poorer spatial working memory and increased movement speed. Zhou et al. (1999) found that some neurons in the medial and lateral areas of the septal complex, which has close reciprocal connections with the hippocampus, display movement speed-related activity. Finally, Chieffi & Allport (1997) found support for the hypothesis that "short-term memory for a visually-presented location within reaching space" is represented in a "motoric code" (p. 244).

The AVITEWRITE model hypothesizes that the learned cerebellar movement commands are transiently stored in a working memory buffer (*WM* in Equation 5 below) which can read out those commands at a variable rate which is less than or equal to the rate at which motor commands are retrieved from the cerebellar spectral memory. The motor commands stored in the working memory are combined (Equation 6 below) with the reactive visual difference vector (DV_{vis}) and scaled by the volitional, size-controlling *GRO* signal to form the memory-enhanced, size-scaled difference vector (DV_S) discussed above. A *memory-modulated* movement target (TPV_m) is generated from the memory-enhanced difference vector by adding DV_S to the current value of TPV_m (Equation 10 below). At the beginning of movement, TPV_m is initialized to the starting position of the hand; that is, to the initial value of the Present Position Vector (*PPV*).

Some of the studies cited above seem to suggest a role for the hippocampal system in spatial working memory and the speed control of patterns of limb movements. Other experimental data suggest that the dorsolateral prefrontal cortex is involved in the working memory storage of targets (Goldman-Rakic, 1990, 1995; Wilson et al., 1993), although a role in the storage of motor commands with speed-regulated readout, as modelled by AVITEWRITE, is uncertain.

When an animal is making sequential movements to a series of targets, it must read out the next target from working memory as it reaches the current target in order to continue the sequence. In AVITEWRITE, a subsequent motor command is loaded from working memory and executed only when the previous memory-modulated target (TPV_m) is

reached. Specifically, when either the TPV_{mx} for the x synergy or the TPV_{my} for the y synergy is reached, then both x and y commands, WM_x and WM_y, are read from the spectral working memory buffer. A memory-derived target has been reached when the present hand position (*PPV*) equals the position of TPV_m. The difference vector from *PPV* to TPV_m is defined as DV_{gate} (Equation 11 below). Thus, when DV_{gate} reaches zero or becomes negative, TPV_m has been reached and the next command is loaded from the working memory buffer (*WM*) (Figure 3.1). (Alternatively, one could use a small, non-zero threshold value of DV_{gate} to trigger *WM* readout.) The working memory of AVITEWRITE allows the volitionally controlled *GO* signal to alter movement speeds of both reactive *and* learned movements, while preserving trajectory shape and the shapes of the velocity profiles, by altering the rate of memory readout relative to the speed of the movement. The maximum speed at which a learned movement can be executed without error is determined by the rate of long term memory readout from the cerebellar spectral memory. In the model, removal of the cortical working memory buffer impairs the system's ability to decrease the speed of learned movements while preserving their kinematic features, such as shape and velocity profile invariance. If the working memory buffer is damaged so that it can store only a few values of the cerebellar output, then AVITEWRITE must increase movement speed in order to keep up with the rate of cerebellar long term memory readout and execute learned movements correctly with trajectory shape and velocity profile invariance. The model offers one possible explanation for the experimentally observed movement speed increases following spatial working mem-

ory impairment. The spectral working memory would store commands in a motor coordinate system, but the aforementioned data concerning speed increases after working memory damage imply that working memory storage of targets is formed in spatial coordinates. However, the Chieffi & Allport (1997) data mentioned earlier support the idea that the working memory for visually-presented target locations is actually represented in a motor coordinate system.

One consequence of decreasing movement speed and the rate of motor command readout from the working memory buffer is that visual error feedback will be delayed. If the Purkinje cells responsible for triggering the erroneous movement have returned to their baseline activity by the time that the error feedback arrives via climbing fibers, then the parallel fiber/Purkinje cell synaptic weights will not be modified and the error will be repeated on the next learning trial. Further, the late error feedback may "correct" the wrong synaptic weights if other Purkinje cells in the population are active at the time that the climbing fiber signal arrives. A corrective movement could still be learned by modifying the weights of the Purkinje cells which are active when the error signal arrives, but it could be too late for it to significantly improve the movement trajectory. Further, it might even worsen performance if the curvature of the template curve near the current position of the moving hand has changed since the time the error occurred and the corrective movement points away from the curve at the time it is made. In summary, delayed error feedback due to volitional movement slowing could negatively affect the model's ability to learn to write a letter.

AVITEWRITE proposes the following solution to the problem of delayed error feedback to the cerebellar Purkinje cell spectrum. This solution is consistent with the fact that increasing the conditioned stimulus intensity can "speed up the clock" in the rabbit nictitating membrane paradigm which earlier versions of spectral learning were used to model (Grossberg & Schmajuk, 1989, p. 93). In the model, the density of the Purkinje cell responses over time varies during learning as a function of the volitionally controlled *GO* signal that controls movement speed. "Density" of the Purkinje cell spectrum refers to the relative time separation between adjacent calcium response profiles (Figure 3.5) for Purkinje cells which differ in their concentrations of dendritic metabotropic glutamate receptor. When the next Purkinje cell calcium response occurs at a relatively short time after the preceding response of another cell, then the spectrum is described as being of a higher density compared to a spectrum for which there is a greater time interval between Purkinje cell calcium responses. When AVITEWRITE learns at slower movement speeds, the density of Purkinje cell responses over time is decreased. This decreased density allows the activities of the Purkinje cells responsible for a given component of a movement synergy command to span a greater period of time so that more of them may be active at the time that the error feedback arrives. As speed increases, error feedback arrives sooner and Purkinje cell spectral density increases so that more cells are active sooner to sample the earlier error feedback. Simulations of the biochemically-predictive spectral timing model of Fiala et al. (1996) demonstrated that the rate of Purkinje cell response—that is, the spectral density—can be decreased by decreasing the amount of glutamate released at the parallel fiber/Purkinje cell synapse (Figure 3.5).

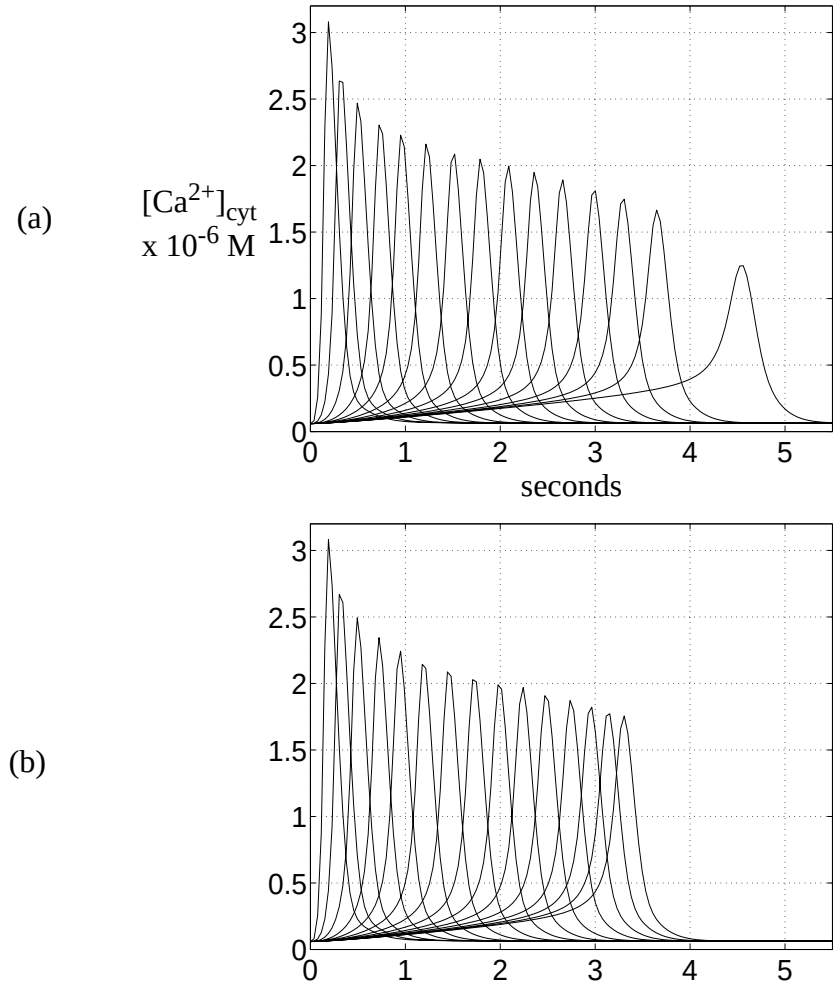

Figure 3.5. (a) Purkinje cell calcium release spectrum from the Fiala et al. (1996) equations. $[Ca^{2+}]_{cyt}$ is the cytosolic Purkinje cell calcium concentration. Continuous glutamate input = 5 microM. (b) Continuous glutamate input = 25 microM. Note that the spectrum is more dense and spans a shorter time than in (a).

By varying spectral density with speed in AVITEWRITE, successful learning may occur over a wider range of speeds. Although published data about the range of speeds in humans across multiple handwriting learning trials is lacking, preliminary analysis of data received from Dr. Arend Van Gemmert suggests that the range of speeds during

learning is comparable to that during the performance of learned letters reported by Wright (1993). Wright showed that the speed of learned letters can be varied by a factor of 2.8 without significantly altering the shape of the letter. AVITEWRITE is capable of learning a letter even when the movement duration varies by such a wide range, as illustrated in Figure 3.20 and Table 3.1.

3.3 Model Equations

The equations used to implement the AVITEWRITE model are now described. The reader can skip directly to the Simulations of Section 3.4 before reading the equations. Note that all integrations were carried out using the fourth order Runge-Kutta method with a step size of 0.05.

At the beginning of movement learning, a visual target position (*TPV*) is chosen in a predefined forward direction on the curve to be learned such that the line from the current hand position, *PPV,* to *TPV* never exceeds an attentional threshold distance, or radius, from the curve being traced (the template curve). How this is done is described more completely below. Errors occur when movement deviates from the attentional radius around the curve due to memory inaccuracy. As described later for Equation (1), when the spectral memory (R) grows beyond a threshold value ε, DV_{vis} decays to zero and memory alone forms DV_S and guides the movement trajectory. Since R forms an imprecise representation of the visual difference vector, the movement trajectory may surpass the original visual target and/or form a curved path toward it which may deviate from the attentional radius around the curve. In the case where movement has deviated from the

attentional radius around the curve due to memory inaccuracy, the *TPV* is chosen so that movement toward it will return the trajectory to within the attentional radius around the template curve.

In the simulations, the attentional radius is chosen by trial and error for learning a given shape. For example, if the attentional radius is too big when learning a letter, then AVITEWRITE will quickly learn a coarse version of that letter with large discrepancies between the learned and actual letter shapes (Figure 3.6a). In contrast, as the attentional radius is decreased, AVITEWRITE learns to generate a more accurate version of the letter, but more learning trials are needed to learn it (Figures 3.6b and 3.6c). If the attentional radius is decreased too much, then AVITEWRITE may not be able to learn the shape at such a high level of accuracy within a limited number of trials. After trial and error, an attentional radius is found which allows AVITEWRITE to learn a trajectory that is a reasonably accurate copy of the original shape and which yields fast movements with unimodal velocity profiles for each synergy.

The target selection algorithm functions as follows. For a discussion of its experimental predictions and applicability to learning methods other than tracing, see section 4.3. The algorithm makes precise the idea that visual attention shifts to help select a new target along the curve in a given direction, or it returns the hand to within the attentional radius. The algorithm achieves this as follows. First, it sequentially forms line segments (L in Figure 3.7a) from the *PPV* to all the points on the template curve (defined by a finite number of points) ahead of the current hand position. The algorithm then sequentially evaluates each of those potential target points to determine if movement to it would keep

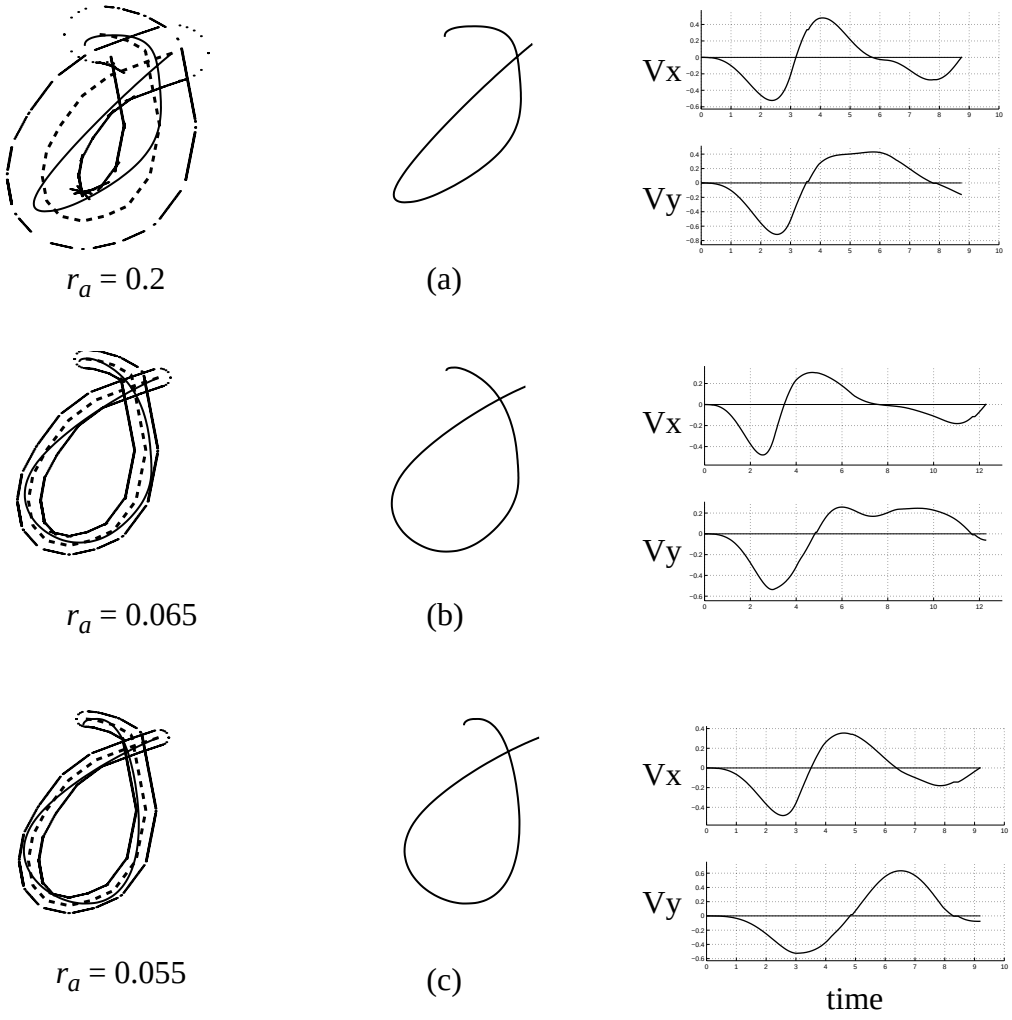

Figure 3.6. Simulation results demonstrating the effect on learning of using a large or small attentional radius, r_a. *Left:* Learned gamma curves with attentional focus illustrated by the tube around the dashed template curve. *Middle:* The learned gamma viewed in isolation. *Right:* x (top) and y (bottom) velocity profiles, Vx, Vy. (a) r_a = 0.2, Gamma learned in 6 trials; (b) r_a = 0.065, Gamma learned in 13 trials; (c) r_a= 0.055, Gamma learned in 49 trials. Note that as the attentional radius is decreased, the accuracy of the learned curve increases and the velocity profile appears less segmented, with a single bell-shaped profile for each synergy. However, the number of trials required to learn the curve increases as r_a is decreased. Also note that the final y velocities, Vy, are close to but not equal to zero. Movement is stopped by shutting off the *GO* signal when both x and y velocities are below some threshold value near the end of the curve or if the end of the curve has been reached and a direction reversal occurs, as when the y velocity becomes negative at the ends of the Vy profiles in (a)-(c) above. See the discussion of the *GO* reset rule in the Equations section.

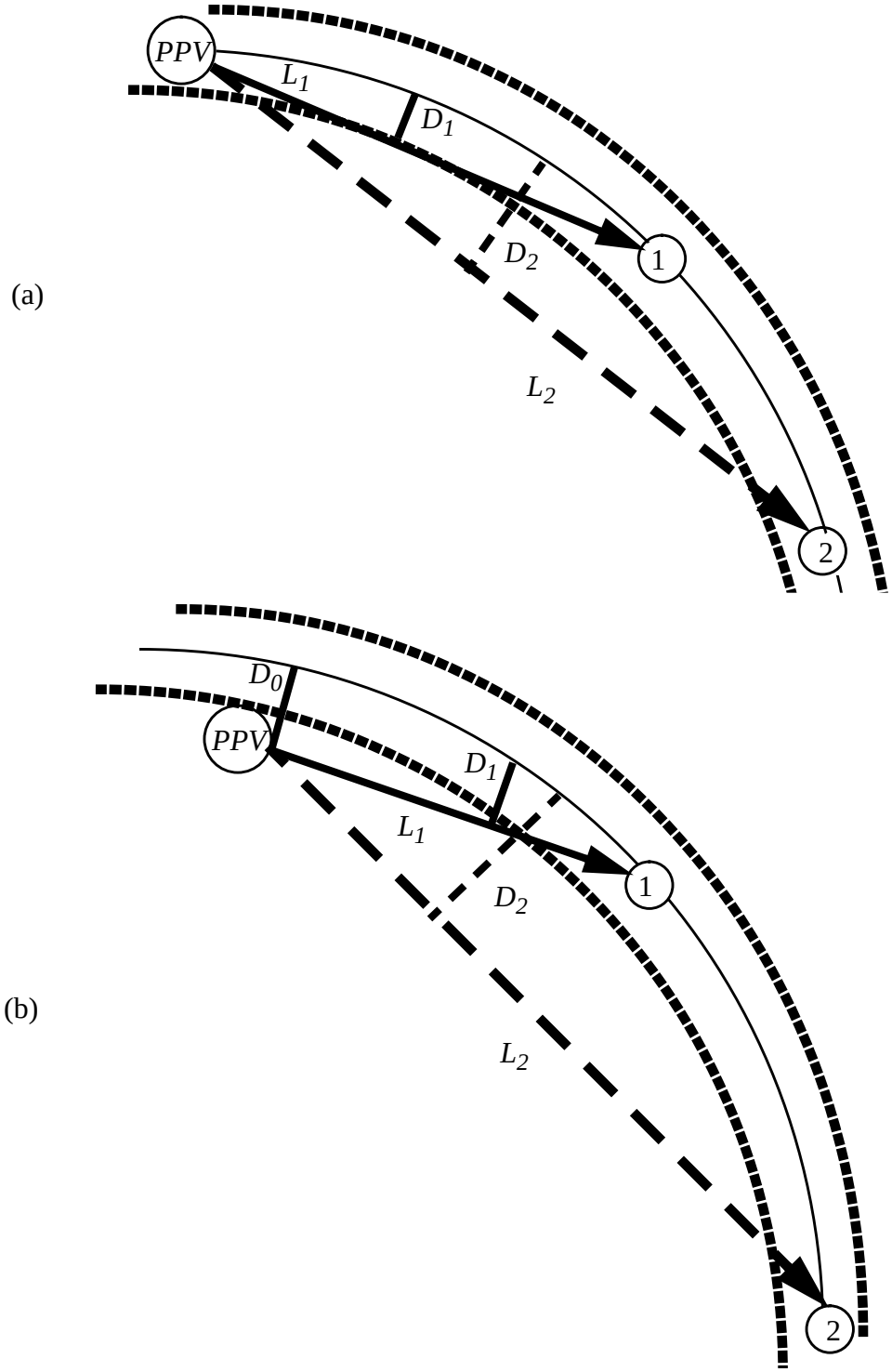

Figure 3.7. (a) Target selection when the *PPV* is within the attentional radius of the curve being traced; (b) Target selection when the *PPV* is outside the attentional radius of the curve being traced. See text for details.

the *PPV* within or else return it to within the attentional radius around the curve. For a given line segment (*L*) from the *PPV* to a potential target, the algorithm computes the distance (*D* in Figure 3.7a) from each point on the line segment to the closest point on the template curve. If this distance ever exceeds the threshold attentional distance *and* if the *PPV* is currently within that threshold distance to the template curve, then the target is rejected. Thus target 1 in Figure 3.7a is a viable target because distance D_1 between the template curve and the line segment L_1 never exceeds the attentional threshold distance from the curve being traced, whereas target 2 is rejected because distance D_2 exceeds the attentional threshold distance. If the *PPV* is currently beyond the attentional threshold distance, as in Figure 3.7b, then a target is rejected if the distance (*D*) from the line segment (*L*) to the template curve ever increases as one moves along the line segment toward the target.

In Figure 3.7b, target 1 is a viable target because the distance from the line segment L_1 to the template curve is always decreasing (distance D_1 is less than D_0) as one moves toward the target, whereas target 2 is rejected because distance D_2 is greater than D_0. Movement to any of the potential targets which survive this selection procedure would keep the trajectory within the attentional radius, or else return the trajectory to the attentional radius around the template curve while never moving away from it. Of the potential targets which survive the selection procedure, the algorithm then selects as *TPV* that position which is farthest from the *PPV.* This *TPV* is used in Equation (1). If the movement *PPV* passes the target, as when $PPVx > TPVx$ for a rightward horizontal movement,

then the input *TPV-PPV* (for both x and y synergies) to the DV_{vis} (Equation 1) and to the synaptic weights (Equation 3) is set to zero until a new target is chosen. A *TPV* is simply a point in cartesian coordinates, with *TPVx* serving the positive and negative x synergies and *TPVy* serving the positive and negative y synergies.

The difference vector to the target, DV_{vis}, is integrated toward the value of $TPV - PPV$, as in Equation (1):

Visual Difference Vector

$$\frac{dDV_{vis}}{dt} = [-\mu_1(DV_{vis}) + \mu_2(TPV - PPV)(1 - H(R \cdot H(tube) - \varepsilon))] . \qquad (1)$$

In (1), *R* is the learned cerebellar output. DV_{vis} is a two dimensional signal composed of DV_{visx} and DV_{visy}. For a given set of positive and negative opponent synergies, *R* in Equation (1) is the sum of the absolute values of the positive and negative synergy spectral outputs, *Rp* and *Rn*, respectively. For example, in the case of the x synergies, $Rx = |Rxp| + |Rxn|$. *H(tube)* equals 1 if the *PPV* is within the attentional radius of the template curve being traced, and it equals zero otherwise. $H(R \cdot H(tube) - \varepsilon)$ equals 1 if *PPV* is within the attentional radius of the template curve and the cerebellar output, *R*, is above some threshold value, ε. Otherwise, $H(R \cdot H(tube) - \varepsilon)$ equals zero and the visual difference vector, DV_{vis}, decays to zero. Thus, if memory is available ($R > \varepsilon$) and the prior movement was sufficiently accurate, remaining within the attentional "tube" around the curve so that *H*(*tube*) = 1, then memory directs the movement since

$H(R \cdot H(tube) - \varepsilon) = 1$ and Equation (1) reduces to $\frac{dDV_{vis}}{dt} = -\mu_1(DV_{vis})$. DV_{vis} decays to zero and memory alone then controls the movement. If the memory signal is too small ($R < \varepsilon$) or an error is made by deviating from the attentional radius around the template curve so that $H(tube) = 0$, then $H(R \cdot H(tube) - \varepsilon) = 0$. Equation (1) then reduces to the following:

$$\frac{dDV_{vis}}{dt} = [-\mu_1(DV_{vis}) + \mu_2(TPV - PPV)].$$

DV_{vis} grows towards the value of $TPV - PPV$ and vision controls the movement direction. In (1), $\mu_1 = 1$; $\mu_2 = 0.25$; and $\varepsilon = 0.001$.

Cerebellar learning is simulated as follows. A spectrum of Purkinje cell responses is created using Equation (2):

Cerebellar Spectral Component

$$g_{ij} = \gamma((t - (i-1) \cdot \Delta t)^2)(B - (t - (i-1) \cdot \Delta t)^{2.9}). \quad (2)$$

In (2), Δt is the time between the start of adjacent Purkinje cell spectra. It is varied between 0.25 and 0.05 to control spectral density (see Figure 3.19). Term g_{ij} models activation of Purkinje cell *i* for synergy *j* at time *t*. A total of four different synergies are used in the simplified view of the hand/arm muscle synergies adopted here: positive and negative x (j = 1, 2 respectively), and positive and negative y (j = 3, 4 respectively). AVITEWRITE uses these simplified representations of movement synergies and assumes that the movement direction generated by each synergy remains constant throughout letter writing. The model does not directly address the more complex issue of the variability of

the movement direction generated by a particular muscle synergy as the body posture or hand location in the workspace changes. One possible way of addressing the issue of variable synergy-specific directions would be to test whether the spectra learning the pattern of synergy activation during a typical writing movement could still learn the correct activation to complete the letter even if the direction associated with a particular synergy changed as the *PPV* traversed the workspace.

In Figure 3.15, a total of 80 spectral components (i = 80) are active in the positive x synergy (j = 1), and 33 are active in the negative x synergy. For a typical letter, a total of approximately 200 Purkinje cells are used in the spectra for the four synergies used in the model. Since a person may learn to write many different letters as well as other shapes, utilizing 200 or more Purkinje cells for each letter in the roman alphabet, or in the thousands of characters used in languages such as Chinese, would threaten to deplete the supply of Purkinje cells available for letter storage in the cerebellum, especially when one considers that the cerebellum is involved in more than just storing letters. A possible solution to this potential combinatorial explosion would be to utilize the same Purkinje cell spectra for multiple letters by assuming that multiple, independent weights exist between different parallel fibers and a given Purkinje cell. Also, the model could be modified to assume that only the muscle activations for a few basic curve segments are stored in the cerebellar spectra, and that they are somehow combined as needed to form different letters, just as different letters are combined to form words (Figures 3.26, 3.27).

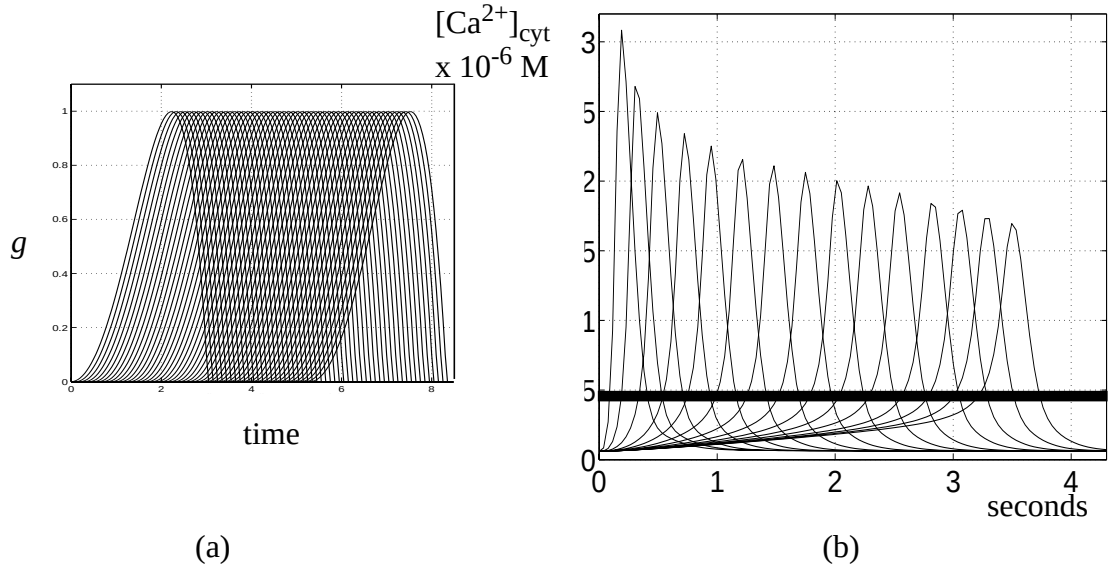

Figure 3.8. (a) Simulated Purkinje cell spectrum generated using Equation (2), $\Delta t = 0.1$; (b) Simulated Purkinje cell spectrum using Fiala et al. (1996) equations. AVITEWRITE uses simplified spectra with constant amplitude and duration, similar to the Fiala et al. spectrum with a long term depression activation threshold represented by the solid bar across (b).

In Equation (2), parameters $\gamma = 0.0136$ and $B = 25$. These parameters and the chosen exponents yield spectral components of constant maximum amplitude equal to 1 and a constant duration of 3 time units. This spectrum, depicted in Figure 3.8a, is a simplified version of that generated by the Fiala et al. (1996) model equations (Figure 3.8b). The two simplifications are (1) constant maximum amplitude responses of the Purkinje cells over time, and (2) constant durations of the Purkinje cell responses over time. For relatively short durations, these simplifications are valid if one assumes that Purkinje cell activity exceeds an activation threshold for long term depression to occur, as illustrated in Figure 3.8b. For learning of longer duration (slower) movements, decreasing spectral

density allows a given spectrum of Purkinje cell responses to span a longer period of time. A new Purkinje cell (PC) spectrum would need to be activated for movements which exceed the maximum spectral duration, estimated to be about 4 seconds in the Fiala et al. (1996) model. For most handwriting strokes or small groups of strokes, 4 seconds is sufficient time for a given PC spectrum to remain active.

The mossy fiber/parallel fiber inputs to the cerebellar spectra, analogous to the Conditioned Stimulus in the Fiala et al. (1996) model (Figure 2.8a), are represented by simple binary signals which gate the activities of particular spectra. Compare the binary glutamate input used in the Fiala et al. (1996) model equations (Figure 3.4) to the binary spectral activation gate, Glu, in Figure 3.15b.

The i^{th} synaptic weight z_{ij} between the parallel fibers and the Purkinje cells for synergy j is modified based on the teaching/error signal as described in Equation (3):

Cerebellar Synaptic Weights

$$\frac{dz_{ij}}{dt} = \alpha_z g_{ij}(-z_{ij} + \alpha(TPV_j - PPV_j)) \cdot H(TPV_j - PPV_j). \qquad (3)$$

Each synaptic weight is modified only if its spectral component g_{ij} is active and visual target information is available. Visual target information is defined by *TPV*. The teaching/error signal is assumed to be carried by climbing fibers, as in the spectral timing models of Fiala et al. (1996) and Grossberg & Merrill (1996; Figure 2.7). The basis for this assumption is discussed in section 4.5. Climbing fiber j's activity at each time step (Figure 3.14) is assumed to be proportional to the current size of jth component of the differ-

ence between the target position, *TPV,* and the present position, *PPV,* with synaptic weights increasing in proportion to the value of *TPV–PPV* in Equation (3). In particular, *H*(*TPV–PPV*) equals 1 if (*TPV–PPV*) > 0, and it equals 0 otherwise. Parameters $\alpha_z = 0.3$ and $\alpha = 0.08$ in (3).

For a discussion of AVITEWRITE's use of a continuously varying teaching signal as opposed to the discrete climbing fiber signals observed in vivo, please see section 4.6.

Note that the synaptic weight equation, in which the synaptic weight *increases* in proportion to the climbing fiber error signal, appears to describe long term *potentiation*, whereas earlier discussions of cerebellar spectral learning have referred to long term depression. In a real Purkinje cell, long term depression is associated with a pause in Purkinje cell firing which disinhibits the cerebellar nucleus. In the AVITEWRITE equations, only the net excitatory effect of parallel fiber inputs on subsequent cerebellar nucleus activation is modelled. The intermediate sign reversals that occur between the time of a parallel fiber input to a Purkinje cell and subsequent activation of the deep cerebellar nucleus are omitted for simplicity. This simplification was also made in Barto et al.'s (1999) cerebellar reaching model, which is discussed in section 4.11.2.

The synaptic weight z_{ij}, in turn, gates the PC spectral activity g_{ij} before an output signal is formed. The gated spectral activity $h_{ij} = g_{ij}z_{ij}$. Each term $g_{ij}z_{ij}$ provides a local view in time of the learned information. The sum of these terms provides a continuous sampling of the climbing fiber teaching signals. Thus, the population response of the Purkinje cells is summed to form the adaptively timed cerebellar output, R_j, for synergy *j*,

as in Equation (4):

Adaptively Timed Cerebellar Output

$$R_j = \sum_i h_{ij}. \tag{4}$$

The cerebellar output R_j is generated at a fixed rate in response to a given density of PC spectral components g_{ij} through time. The output rate of R can be altered by changing spectral density. Decreasing spectral density allows movement learning at variable speeds.

A cortical Working Memory buffer, whose dynamics are illustrated in Figure 3.9, is hypothesized to allow performance of learned movements at variable speeds while preserving movement and velocity profile shape. In the model, R is temporarily stored in a working memory buffer, simulated as a discretely sampled set of values from the continuous cerebellar output:

$$WM_x(t) = R_1(t_i) + R_2(t_i) \quad \text{for } t_i \le t < t_{i+1} . \tag{5a}$$

$$WM_y(t) = R_3(t_i) + R_4(t_i) \quad \text{for } t_i \le t < t_{i+1} . \tag{5b}$$

In (5), t_i is the i^{th} time that DV_{gate}, which is defined in (11) below, becomes zero from a positive value. At time $t = 0$, $WM(0) = R(0)$.

The dynamics of the spectral working memory are illustrated in Figure 3.9. For fast speeds, the working memory buffer effectively passes the motor command along to the trajectory generator without much delay. Since a command is read from the working memory very soon after it has been stored there, the memory "bin" (Figure 3.9c, d) which

had stored the command is quickly emptied of its contents and made available for the storage of another motor command. The size of the working memory therefore remains small. For slower movements, a given motor command must be stored in the working memory longer, and a backlog of motor commands accumulates while a current command is being executed. The size of the working memory is therefore inversely related to the movement speed. For very slow movements, a large working memory capacity is needed with up to almost 140 bins in Figure 3.9c for a *GO* signal size of $J = 7$.

As shown in Figure 3.1, the spectral working memory output, *WM*, is combined with the visual difference vector, DV_{vis}, and scaled by a size-controlling *GRO* signal, *S*, to form the size-scaled, memory-enhanced difference vector, DV_S:

$$DV_{Sx} = S \cdot (WM_x + DV_{visx}), \tag{6a}$$

$$DV_{Sy} = S \cdot (WM_y + DV_{visy}). \tag{6b}$$

In (6), $S = 0.3$ during learning and was chosen at variable values after learning; see Figures 3.24 and 3.25 below.

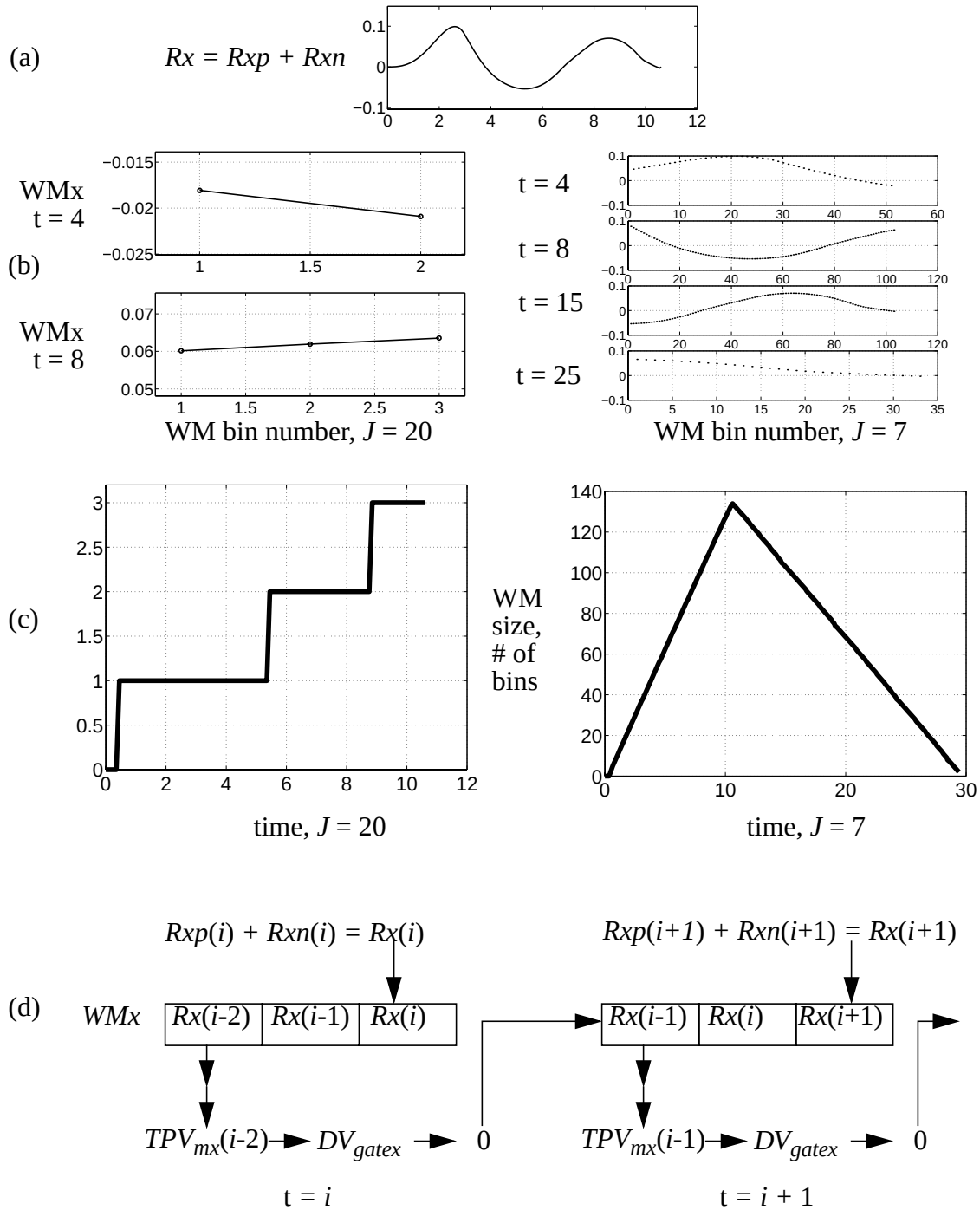

Figure 3.9. (a) Total cerebellar output for the x movement synergy for the letter *l* on trial 37 of Figure 3.13; (b) Snapshots of the signal stored in the working memory buffer for the x synergy, *WMx*, at times t = 4 and 8 for the letter *l* written with *GO* signal size *J* = 20

(left), and times t = 4, 8, 15, and 25 for *l* written with *GO* signal size *J* = 7 (right). Use of the working memory to store spectral output allowed slower movement (*J* = 7) whose duration exceeded the duration of spectral activity. (c) *Left*: Working memory size during the fast movement with *J* = 20. Note that the last three commands stored in working memory were not executed because the *GO* signal was shut off when the end of the letter was reached. See the *GO* reset discussion in the Equations section. *Right*: Working memory size during the slow movement with *J* = 7 (Right). (d) Conceptual diagram showing storage of the total cerebellar output for the x movement synergy at time t in a working memory buffer, *WMx*. When a memory modulated target, TPV_m, derived in Equation (10), has been reached and DV_{gate} (Equation 11) reaches a value less than or equal to zero, then the next motor command, *Rx*, is read from the working memory buffer. Note that the number of *Rx* values stored in the working memory may vary with the speed of the movement, as seen in (c). The data presented here were generated during the speed scaling simulations depicted in Figure 3.22.

The DV_S is multiplied by a speed-controlling, fast-rising *GO* signal to define the outflow movement velocity vector, which is integrated to form the Present Position Vector for the x and y synergies:

Present Position Vector

$$\frac{dPPV(t)}{dt} = DV_S \cdot GO \,. \tag{7}$$

The *GO* signal is defined as follows:

***GO* Signal**

$$\frac{dG}{dt} = \gamma_1(-G + J) \tag{8}$$

$$GO = G(t) \,. \tag{9}$$

The size of the input *J* determines the asymptote of the *GO* signal. *J* can be varied to alter the movement speed. *J* was varied between 19.25 and 20 during learning, and down to 7 after learning (see Figures 3.20, 3.21, 3.22). Parameter γ_1 = 8.

During learning, a narrower range of *GO* signal sizes was chosen to prevent excessively delayed error feedback to the spectra resulting from slow movement. Using sparser spectral densities can extend the time during which spectra are active and subject to error-feedback-based weight modification (Figure 3.20, Table 3.1), but if the feedback delay grows too large, then the spectra will have become inactive and no longer subject to weight modification when the error signal arrives. Learning would then be impaired. After a letter has been learned, a wider range of *GO* signals can be used since no errors are being committed and the weights are not modified.

Equation (7) is integrated to generate the movement trajectory. For simplicity, movement commands to the hand/arm system are represented by four cerebellar memory divisions. Each memory division controls one of the muscle synergies for either the positive or negative horizontal or vertical movement direction.

The *GO* signal is reset by setting $J = 0$ when DV_S equals zero at the beginning of a movement. Thus, when the letter *s* is written, as in Figure 3.10, the *GO* signal is reset at the beginning of the letter, and then at each of the two stopping points during execution of the letter. In order to shut the *GO* signal off when the end of the curve is reached, or when the end of a segment is reached in a letter with multiple stopping points (Figure 3.10), the following reset rule is used:

***GO* Reset Rule**

The *GO* signal is reset at the start of a given synergy's activation by setting $J = 0$. When opponent synergies switch control of a movement, then the *GO* signal is shut off for the prior synergy when the spectral component activations g_{ij} for that synergy have all

decayed to a value less than 0.01. The *GO* signal for the newly activated synergy is turned on when its spectral components become active at the time $DV_{vis} + R$ changes sign. During visually guided movements, when particular regions of the letter have been reached, such as intermediate stopping points at corners or points of x and y direction reversal, (see the cursive letter *s* in Figure 3.10) or the end of the letter, then the *GO* signal for all synergies is reset if the movement velocity is below a threshold value or a direction reversal occurs. *J* is set to 0 for all synergies if the *PPV* is in a region near a stopping point and both the x and y velocities are less than a threshold absolute value (chosen as 0.006), or if either the x or y velocity reverses sign near a stopping point, indicating that the stopping point has been passed and that the *GO* signal should be shut off, thereby stopping the movement. Specifically, movement is stopped if the above conditions are met and the *PPV* is within a square with sides of 0.2 units centered on the stopping point. The choice of the size of the square region is arbitrary and can be varied based on the scale of the letter without adversely affecting the model's performance.

If visual feedback is lacking and/or memory alone controls the movement, then a proprioceptive, velocity-dependent *GO* reset rule can be used. For example, the *GO* signal can be reset when the tangential velocity is below a threshold value and the acceleration is negative.

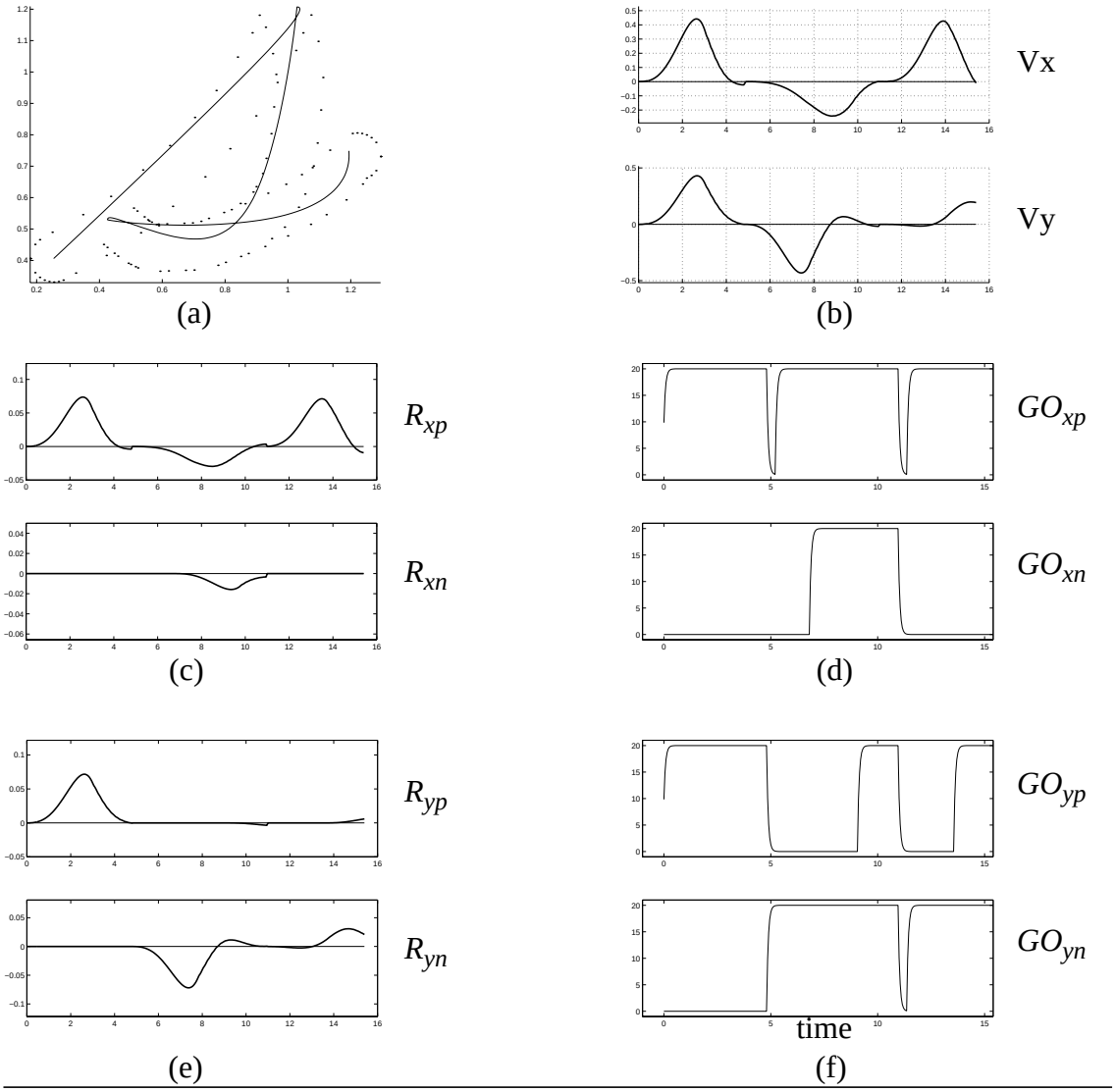

Figure 3.10. (a) Letter *s* written by AVITEWRITE after 56 learning trials with r_a = 0.075, Δt = 0.2, J = 20. The dotted tube represents attentional focus around the template curve. (b) x (top) and y (bottom) velocity profiles, Vx, Vy; (c) Learned cerebellar output R_{xp}, R_{xn}, for the positive (top) and negative (bottom) x direction movement synergies; (d) Volitional speed controlling *GO* signals for the positive (top) and negative (bottom) x direction movement synergies; (e) Learned cerebellar output R_{yp}, R_{yn}, for the positive (top) and negative (bottom) y direction movement synergies; (f) Volitional speed controlling *GO* signals for the positive (top) and negative (bottom) y direction movement synergies. In (c) and (e), note that *R* for the positive synergies may become negative, and *R* for the negative synergies may become positive. This situation arises because the weights in Equation (3) may be positive or negative. Since a positive value of *R* for the positive synergy

corresponds to disinhibition of the cerebellar nuclei, negative weights for the positive synergy could be interpreted as potentiation of Purkinje cell activity that would lead to further inhibition of cerebellar nuclei and of the given muscle synergy. The inverse relation would hold for the negative synergy, so that a negative value of *R* would represent disinhibition of the cerebellar nuclei.

Readout of the Working Memory buffer's discrete movement commands is controlled as follows. A memory-modulated target (TPV_m) is generated for the x and y synergies as follows:

Memory-Modulated Target

$$TPV_m(i+1) = TPV_m(i) + DV_S \,. \tag{10}$$

It tracks the cumulative DV_S through time. The *PPV* is subtracted from the TPV_m to form a

Gating Difference Vector

$$DV_{gate} = TPV_m - PPV \,. \tag{11}$$

DV_{gate} controls readout from the WM buffer. The next cerebellar command that has been stored in Working Memory is read from the WM buffer when DV_{gate} is less than or equal to zero; that is, when the current TPV_m has been reached or surpassed. By altering the size of the *GO* signal, the rate at which TPV_m is reached by the outflow *PPV* can be controlled. Thus, Working Memory readout is controlled by the speed of the movement, which is determined by *PPV* (see Figure 3.1). This gating rule ensures that the shapes of the movement and its velocity profile are preserved as performance speed is changed by a

different choice of the volitional *GO* signal.

The movement velocity profiles generated by the model represent outflow movement commands, not the actual performance of the arm/hand system. There is filtering of the movement signal downstream of the central command by the peripheral muscle apparatus (Contreras-Vidal et al., 1997). An assumption of low-pass filtering in the command pathway is commonly made in muscle models (Barto et al., 1999, p.567). Therefore, the

Acceleration Profile

$$A(t) = \frac{\frac{dPPV(t)}{dt} - \frac{dPPV(t-D)}{dt}}{D} \tag{12}$$

generated by the present model is filtered using a first order differential equation:

Muscle-Filtered Acceleration Profile

$$\frac{dA_f}{dt} = (-A_f(t) + A(t)) \, . \tag{13}$$

The step size in (12) is $D = 0.05$. Without such filtering, the acceleration profile is jagged, with sudden jumps (Figures 3.11b, 3.11e, and 3.12a) which occur due to the overlap of a finite number of spectra (Figure 3.12c) whose Purkinje cell output is summed to form the memory trace. For comparison, the acceleration can be filtered using standard signal processing techniques, such as a fourth order Butterworth filter with a 7 Hz cutoff frequency, as is often used in the processing of handwriting data (Figures 3.11d and 3.11g).

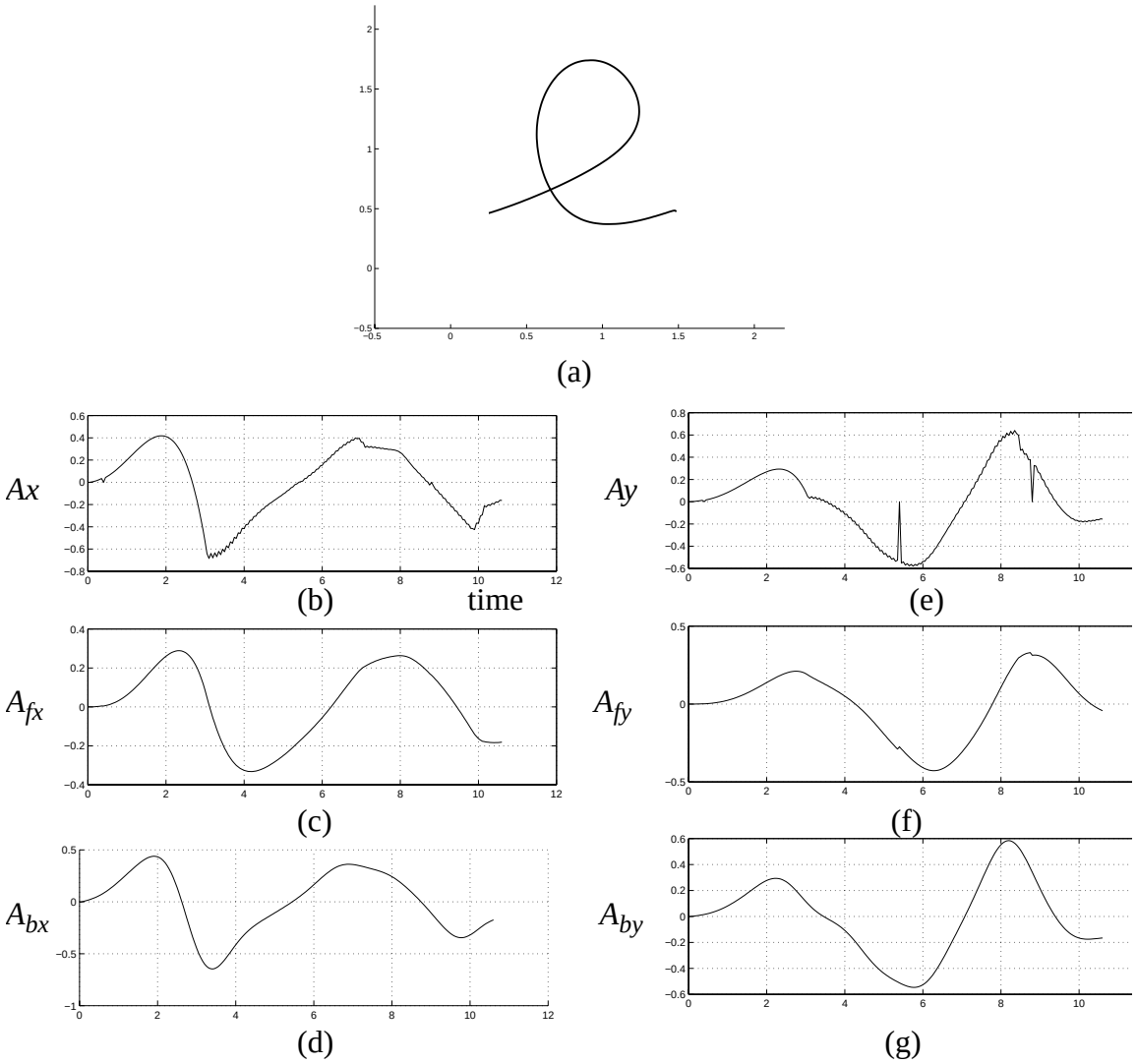

Figure 3.11. (a) Letter *l* learned in 37 trials with r_a = 0.055, Δt = 0.1, and J = 20; (b) actual x acceleration *Ax*; (c) x acceleration filtered (A_{fx}) using Equation (13); (d) x acceleration filtered (A_{bx}) using a Butterworth filter with a 7 Hz cutoff frequency; (e) actual y acceleration *Ay*; (f) y acceleration filtered (Af_y) using Equation (13); (g) y acceleration filtered (A_{by}) using a Butterworth filter with a 7 Hz cutoff frequency.

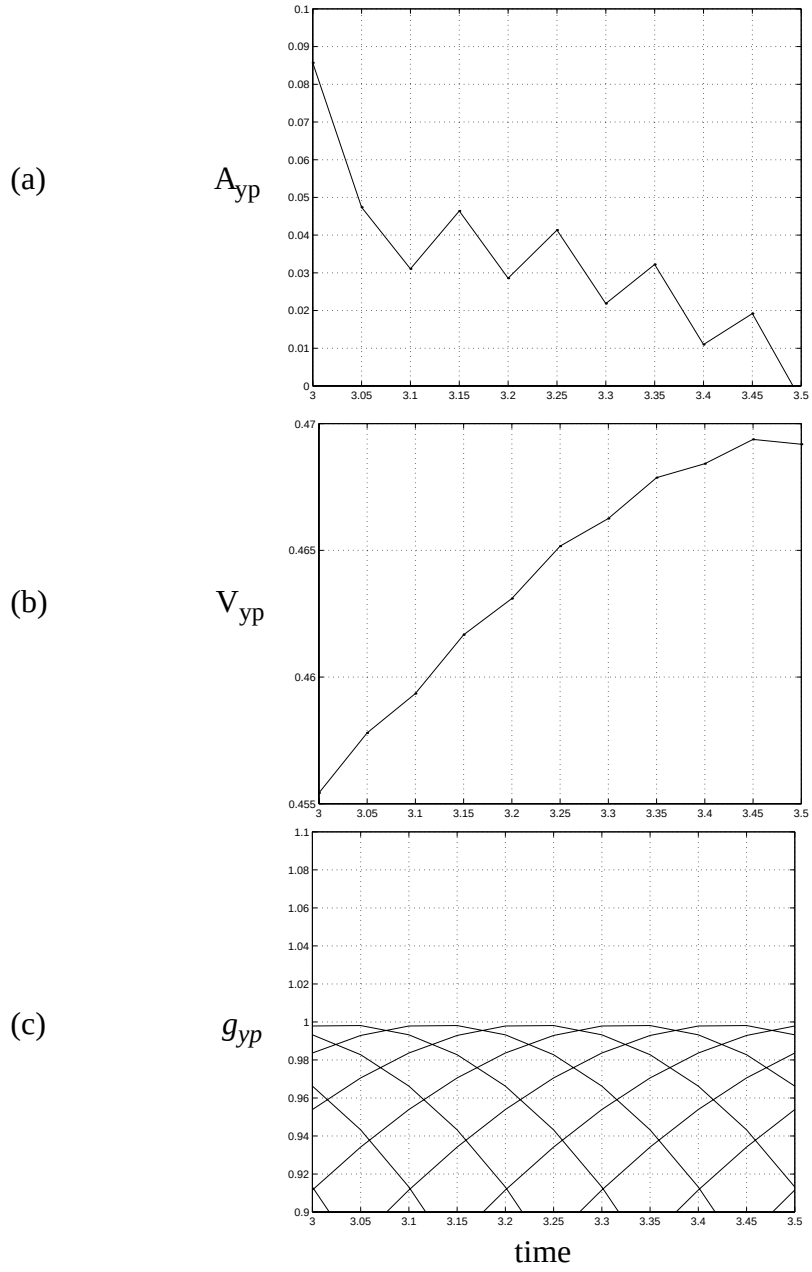

Figure 3.12. (a) Close-up view of the jagged, unfiltered acceleration profile (A_{yp}) of the positive y synergy for the letter *l* shown in Figure 3.11. (b) Close-up view of the velocity profile. (c) Close-up view of the finite number of overlapping spectral components whose weighted, summed output is integrated in Equation (7) to generate the movement velocity. Sparser spectral components would yield a more jagged acceleration profile, just as denser spectral components would yield a smoother acceleration profile. The model assumes that the acceleration is filtered by the peripheral muscle apparatus (Equation 13).

3.4 Simulations

Simulation results are now presented which demonstrate the following features of the spectral handwriting learning model: (1) the model's ability to learn to generate cursive letters with realistic velocity profiles; (2) generation of an inverse relation between curvature and tangential velocity; (3) generation of a Two-Thirds Power Law relation between curvature and velocity; (4) the ability to vary the movement speed during learning, with a gradual increase in speed as learning proceeds; (5) variable speed performance of learned movements with preservation of the movement shape and the shape of the velocity profile; (6) the ability to vary the size of movements while maintaining isochrony as well as the shape of the velocity profiles; and (7) the ability to yield coarticulatory context effects, such as variation of letter size and downstroke duration due to adjacent letters.

3.4.1 Learning a Letter

Figures 3.13 and 3.14 illustrate the learning process as AVITEWRITE learns to write the cursive letter l by tracing a template curve for thirty-seven trials. On early trials, mistakes are made as the newly forming memory competes for control of the movement with visually reactive movements to targets on the curve. Memory control is initially poor and requires corrective reactive movements which yield a segmented trajectory and a velocity profile that consists of several discrete peaks. As learning proceeds over multiple trials, performance gradually improves and the writing time decreases until, on trial thirty-seven in this case, the memory representation of the synergy activations is able to drive an accurate, fast writing movement which does not deviate from the attentional radius around the

template curve.

Figure 3.14 shows the dynamics of several model components during the learning process. The visual difference vector (DV_{vis}) from the present position (*PPV*) to a target (*TPV*) is integrated in Equation (1) and competes with memory, *R*, to control the movement. If *R* is less than a threshold value of $\varepsilon = 0.001$ or if movement exceeds a distance r_a from the template curve, then a target, *TPV,* is chosen and DV_{vis} grows toward the value of $TPV - PPV$. If $R > \varepsilon$ and the *PPV* is within a distance r_a of the template curve, then DV_{vis} decays toward zero. The Purkinje cell population response, *R*, which forms the cerebellar memory output, is shaped by learning as the parallel fiber/Purkinje cell synaptic weights are modified in Equation (3) based on the error signal $TPV - PPV$. Note that on trial 37 (right side of figure), memory alone controls movement and keeps it within the attentional radius r_a of the template curve. No errors are made and DV_{vis} and $TPV - PPV$ equal zero throughout the learned movement.

Figure 3.15 shows the corresponding spectral activations during trial 37. Figure 3.16 shows a sample of how the model can learn the letters of the alphabet. Strokes that require lifting of the pen from the page and hand repositioning, such as the cross of the letter *t* or the dots of the letters *i* and *j*, are omitted for simplicity.

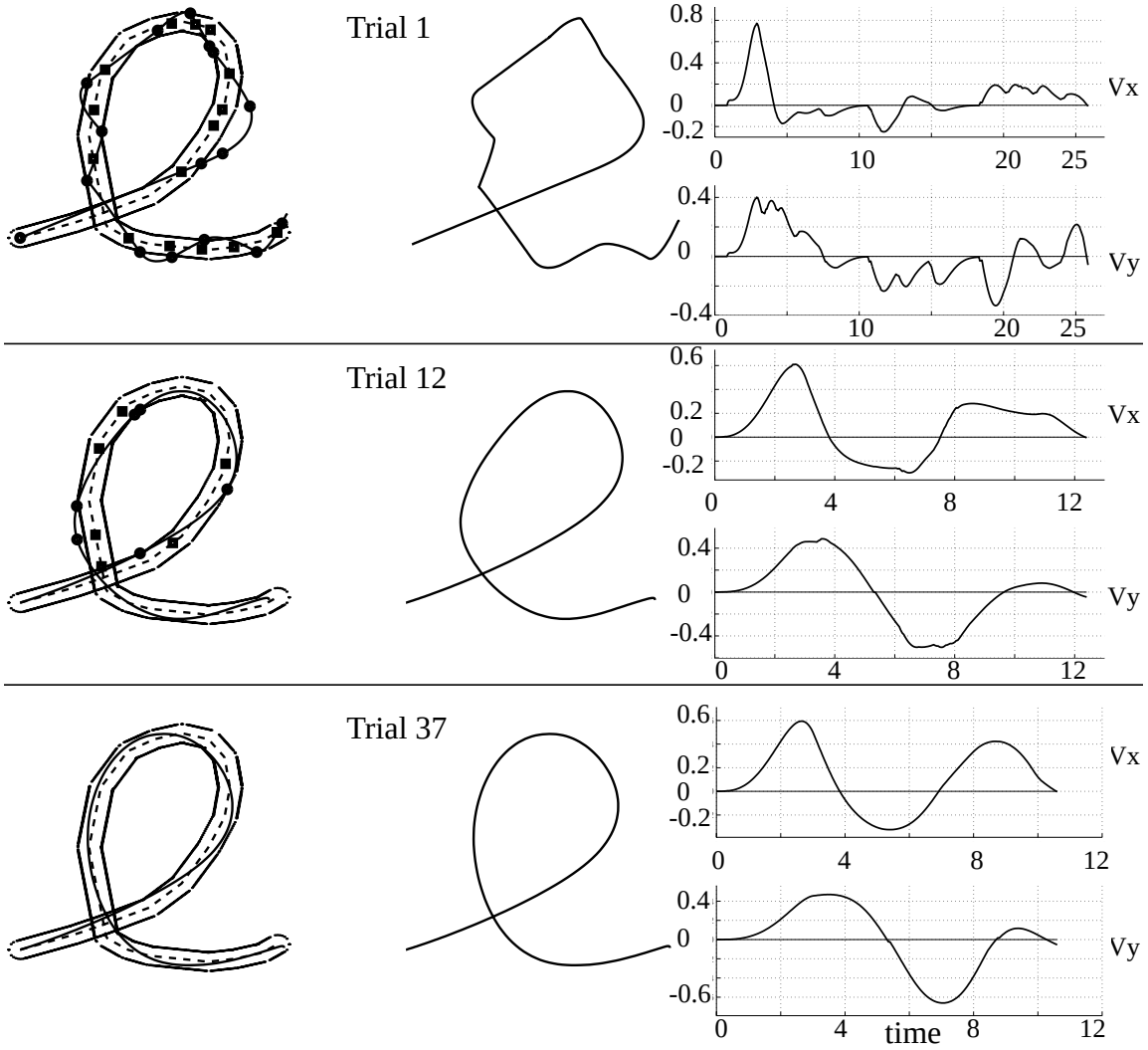

Figure 3.13. The progression of learning the letter *l* with r_a = 0.055, Δt = 0.1, and *J* = 20. *Left:* The attentional focus is illustrated by the tube around the dashed template curve. Circles indicate the *PPV* when a new target, marked by a square, is chosen, either because memory is too small or because the *PPV* has exceeded the distance, r_a, from the template curve. *Middle:* AVITEWRITE's *l* viewed in isolation. *Right:* x (top) and y (bottom) velocity profiles, Vx, Vy. (a) Learning trial 1; (b) Learning trial 12; (c) Final learning trial 37. The letter is now drawn without deviating from the attentional radius around the template curve. Note also that the writing time has decreased from over 25 to under 11 time units.

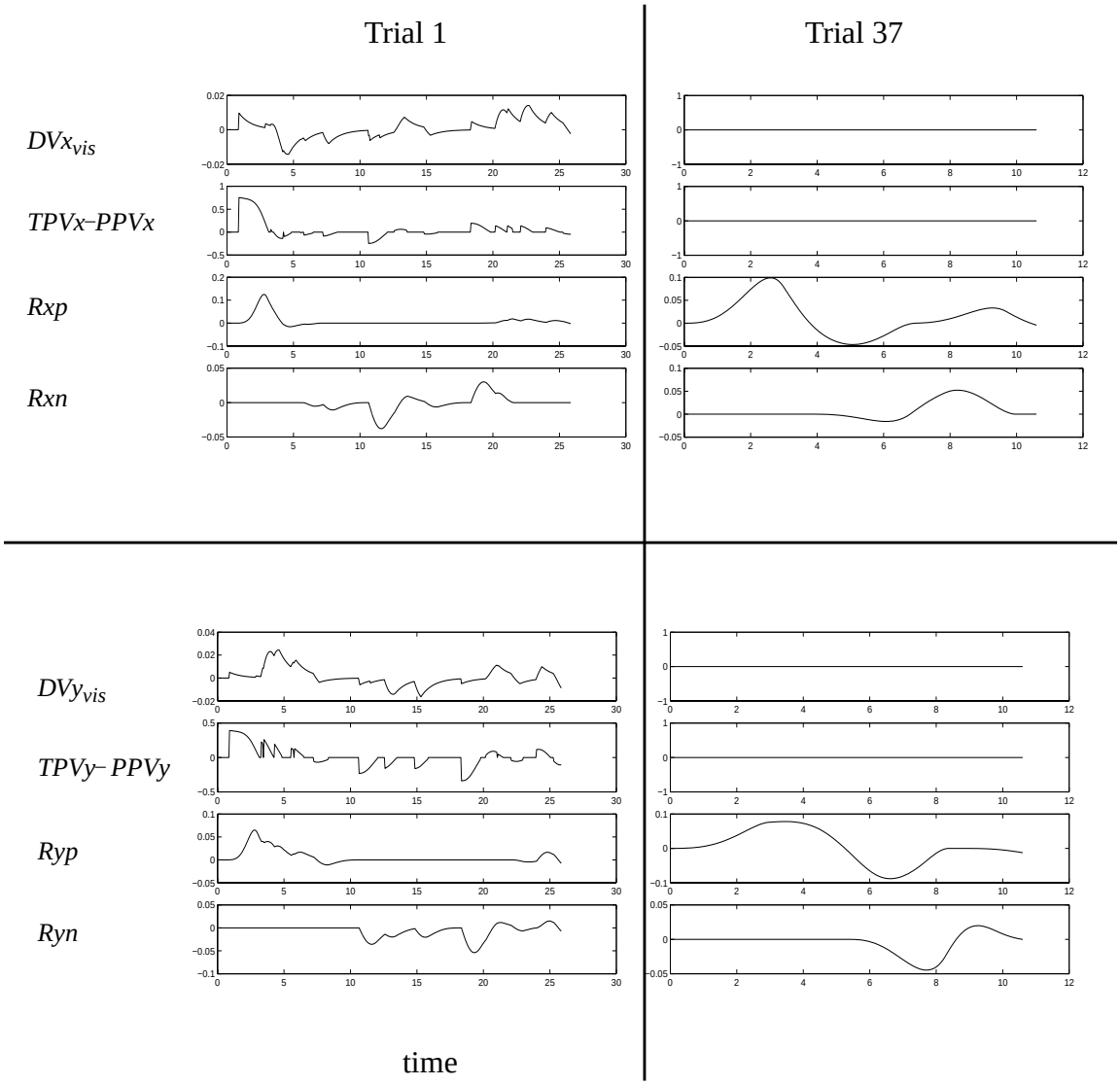

Figure 3.14. Model components during learning of the letter *l* of Figure 3.12. *Left:* trial 1; *Right:* trial 37; *Top:* Positive and negative x synergies; *Bottom:* Positive and negative y synergies. DV_{vis} is the visual difference vector which is integrated to drive reactive and corrective movements. $TPV - PPV$ is the signal used to form DV_{vis} in Equation (1) as well as the climbing fiber error signal which leads to synaptic weight modification at the parallel fiber/Purkinje cell synapse in Equation (3). *Rxp*, *Rxn*, *Ryp*, and *Ryn* are the learned cerebellar outputs for the positive and negative, x and y synergies.

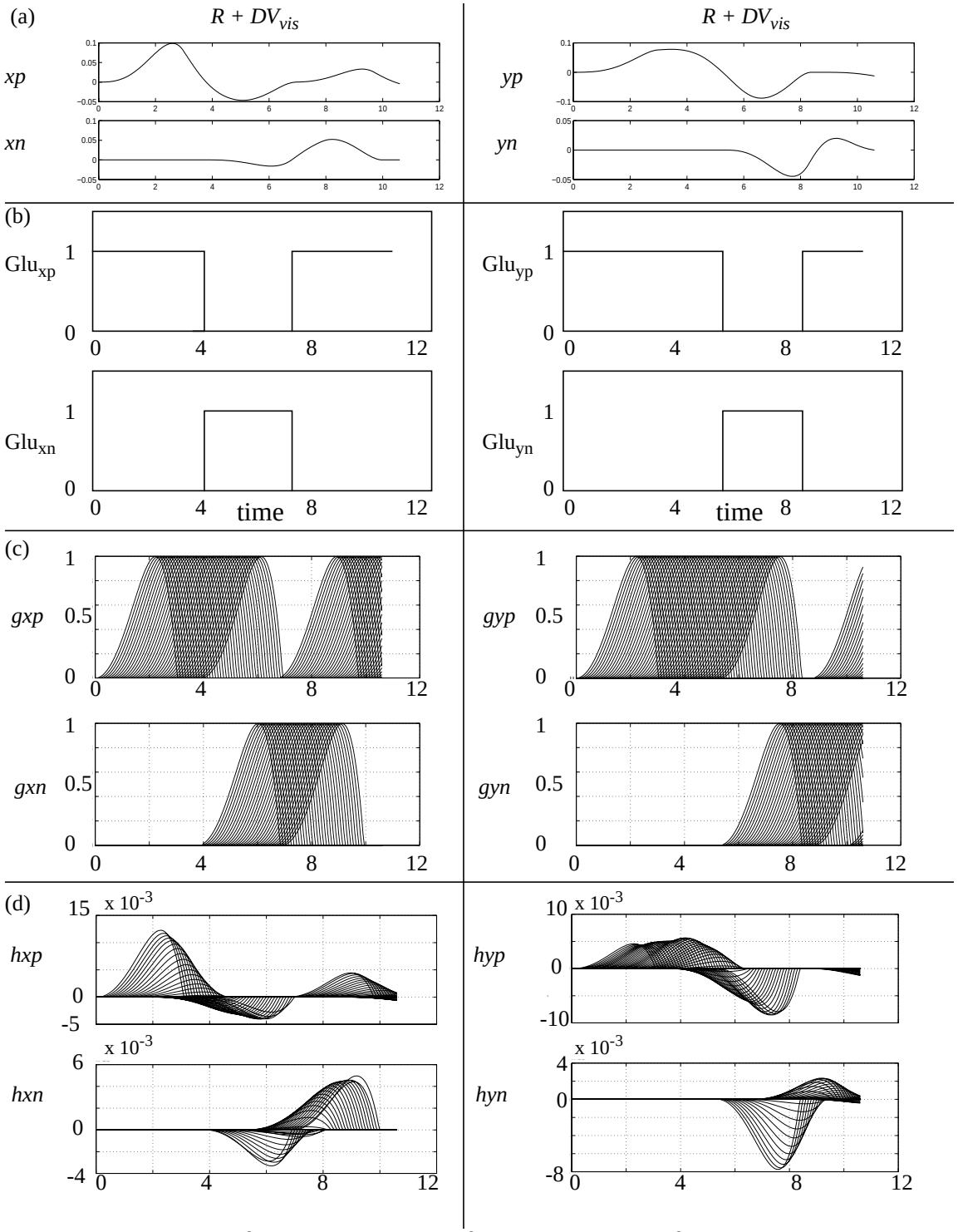

Figure 3.15. Figures of model components for the generation of spectra and spectral synergy switching. See the text below for details.

In Figure 3.15 above, (c) illustrates the response of the Purkinje cell spectra during trial 37 of learning the letter *l*. In (b), one sees the cerebellar step input which causes release of glutamate from parallel fibers that triggers spectral activation of the positive and negative, x and y synergies, xp, xn, yp, yn. Inputs to opponent synergies switch when the sum $R + DV_{vis}$ changes sign in (a). When $R + DV_{vis} \geq 0$, $Glu_p = 1$ and $Glu_n = 0$. The opposite relation, $Glu_p = 0$ and $Glu_n = 1$, holds when $R+DV_{vis}<0$. In (c) one sees the spectrum of Purkinje cell responses (*g*) generated using Equation (2). Note that input to the spectrum of one synergy is shut off when the net movement direction, given by $DV_{vis} + R$, changes sign. A new synergy and Purkinje cell spectrum are then activated. Such synergy switching occurs at approximately times t = 4 and 7 in the positive and negative x synergies (left: *gxp*, *gxn*) and t = 6 and 9 in the positive and negative y synergies (right: *gyp*, *gyn*). Figure 3.15d shows the pattern of learned Purkinje cell activations (*h*) formed when *g* is gated by the parallel fiber/Purkinje cell synaptic weights (*z* in Equation 3) formed during learning.

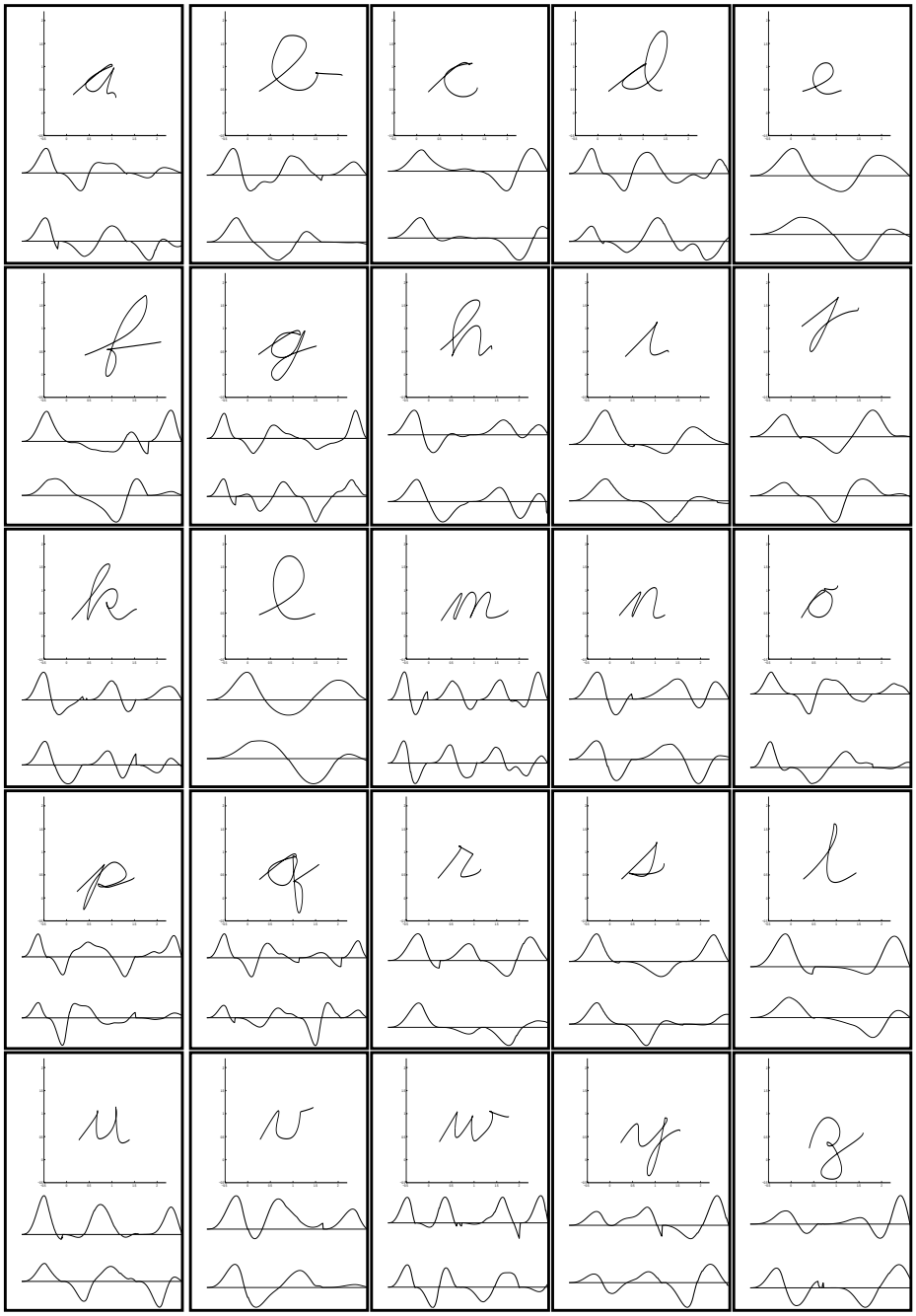

Figure 3.16. The alphabet as learned by AVITEWRITE; Each panel contains a letter at the top with the x velocity profile in the middle and the y velocity profile at the bottom. All letters were learned at the relative scale shown here. Note that the cross in the *t*, the letter *x*, and the dots on the *i* and *j* were omitted because they involved discontinuities in the movement, with lifting of the pen from the page and hand repositioning. See Appendix for parameter values and the number of learning trials required per letter.

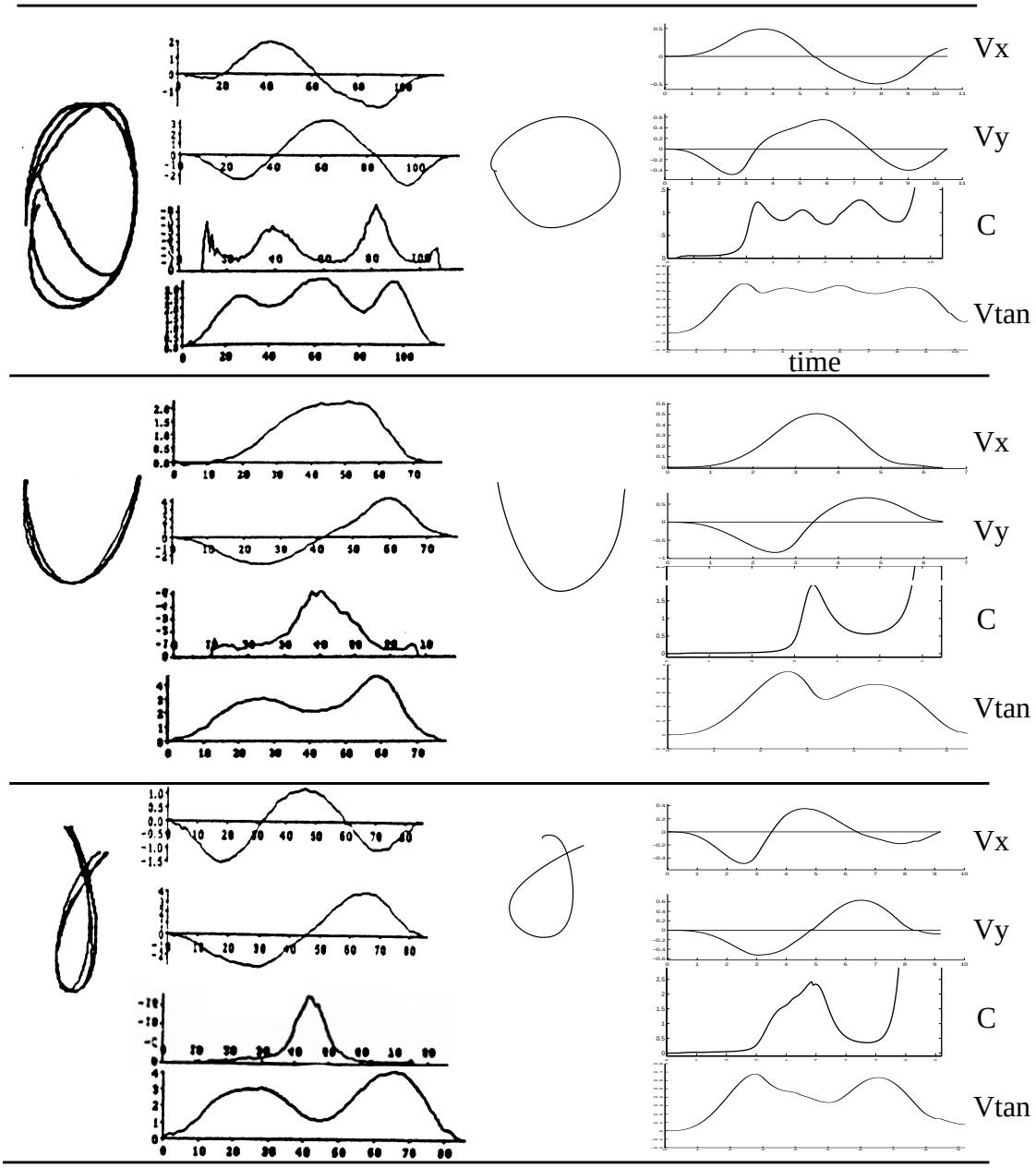

Figure 3.17. *Left:* Human writing with x and y velocity profiles (Vx,Vy), movement curvature (C), and tangential velocity (Vtan) (Reproduced with permission from Edelman & Flash, 1987). *Right:* Similar shapes learned by AVITEWRITE. The curvature was calculated using acceleration filtered with Equation (13). The peaks in curvature near the ends of the simulated trajectories are the result of the x and y velocities (Vx, Vy) getting very small and are not seen in the human data because the curvature has been truncated prior to the end of the velocity profile where velocity reaches zero. See Appendix for model parameters.

3.4.2 Inverse Relation between Curvature and Velocity

Figure 3.17 compares three letters learned by AVITEWRITE with similar letters written by adult human subjects (Edelman & Flash, 1987). Note the unimodal x and y velocity profiles generated for each synergy by both humans and AVITEWRITE. Also observe the inverse relation between tangential velocity and curvature. The peaks in curvature near the ends of the simulated trajectories are the result of the x and y velocities (Vx, Vy) getting very small, with Vx and Vy << 1. As seen in Equation (14):

$$C = \frac{(Vx \cdot Ay) - (Vy \cdot Ax)}{(Vx^2 + Vy^2)^{1.5}} \tag{14}$$

curvature C approaches infinity as the sum of Vx^2 and Vy^2 approaches zero. Note that this effect is not seen in the human data shown in Figure 3.17 since the curvature has been truncated prior to the end of the velocity profile where velocity reaches zero. Ax and Ay are the x and y acceleration, respectively.

3.4.3 The Two-Thirds Power Law

As curvature increases, the angular velocity required to move through the curve in a given amount of time also increases. Thus, angular velocity is a function of the curvature. This relation is quantified by the Two-Thirds Power Law, which states that the angular velocity is proportional to the curvature raised to the two-thirds power (Lacquaniti et al., 1983):

Two-Thirds Power Law

$$A = kC^{\frac{2}{3}}, \tag{15}$$

where A = angular velocity, C = curvature, and k is a proportionality constant. Equivalently,

$$V_{\tan} = kr^{\frac{1}{3}}, \tag{16}$$

where V_{tan} = tangential velocity, r = radius of curvature ($1/C$), and k is a proportionality constant. The law was originally reported to hold mainly for elliptical movements (Lacquaniti et al., 1983). Since then, others (Wann et al., 1988, p. 635) have reported that the law holds for handwriting movements at fast speeds. The law is violated when "size differences and translation are combined in a word" (Thomassen & Teulings, 1985, p. 260). Nevertheless, the law holds under many conditions in human handwriting movements. It is therefore of interest that the Two-Thirds Power Law relation emerges from the learning process described in the current model (Figure 3.18). Although it is not immediately clear why this relation should result from spectral learning of muscle synergy activations, one should note that AVITEWRITE learns through an error-correcting process that works to keep the hand within some minimum distance of the curve being traced. In other words, AVITEWRITE effectively places bounds on the variance of the hand position relative to the template curve being traced. Harris and Wolpert (1998) found that a curved movement trajectory which minimizes the positional variance of the hand will yield the Two-Thirds Power Law relation. The emergence of this law from AVITEWRITE may therefore be due to its approximation of a variance-minimizing movement learning strat-

egy.

The Two-Thirds Power Law prediction of tangential velocity becomes unrealistically large as the curvature of the movement becomes very small (C<<1), as may occur near the beginning and end of a movement (Figure 3.17), causing the large spikes in the power law predictions in Figure 3.18. Filtering the acceleration with Equation (13) reduces the number of these spikes by preventing sudden drops in curvature due to the jagged, unfiltered acceleration of Figures 3.11 and 3.12.

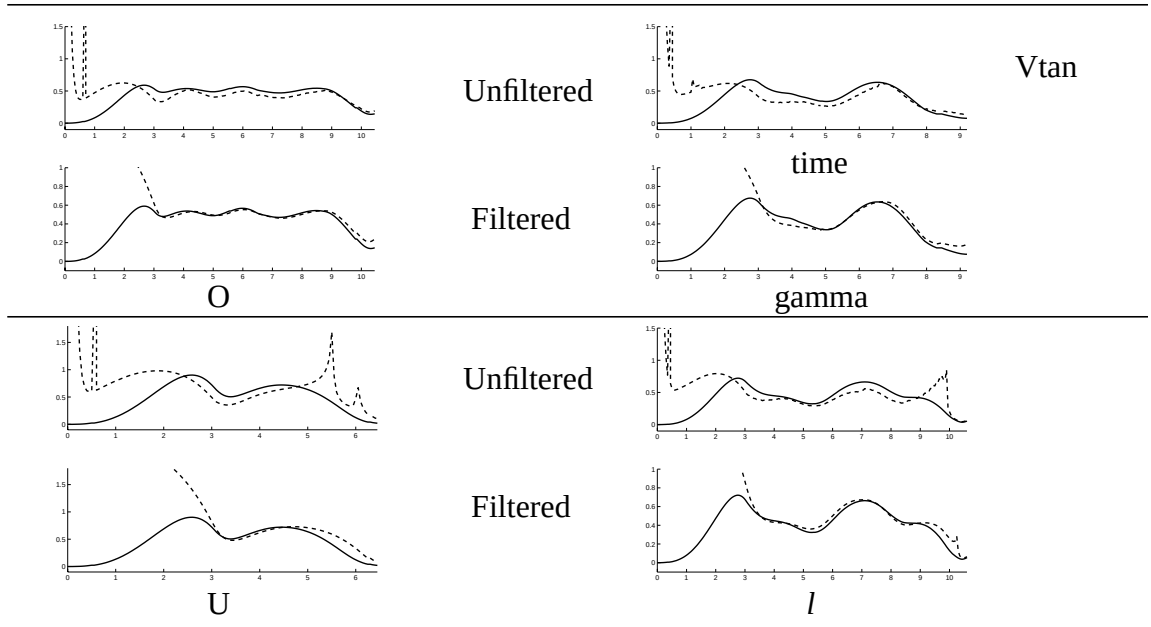

Figure 3.18. Two-Thirds Power Law predictions (dotted lines) of tangential velocity (Vtan) compared to the actual tangential velocity (solid lines) of AVITEWRITE for the letters O, U, gamma, and *l*. For each letter, the top panel shows the power law prediction calculated using the unfiltered model acceleration profile, and the bottom panel shows the prediction calculated using acceleration filtered with Equation (13). The values used for the constant of proportionality (*k*) in Equation (15) are as follows. O: 0.5; U: 0.6; gamma: 0.45; l: 0.5.

3.4.4 Variable Speeds During Learning

When a human learns a new task, the task must usually be performed more slowly during the early stages of learning than at later stages. An attempt to increase the speed of performance before the motor system has adequately learned the task results in increased numbers of errors. Common examples of this gradual speed increase during learning are learning to play musical instruments or learning a new language. A similar phenomenon occurs during the learning of handwriting movements (Alston & Taylor, 1987, p. 115; Burns, 1962, pp. 45-46; Freeman, 1914, pp. 83-84). Figures 3.13 and 3.20 show that this gradual decrease of movement duration over multiple learning trials is a feature of AVITEWRITE's learning as well. The decrease in movement duration over the course of learning in AVITEWRITE may occur for two reasons. (1) In the early trials, the memory is not yet fully developed. As a result, the movement repeatedly deviates from the attentional radius around the template curve being traced, and the total distance moved may exceed the length of the template curve (Figure 3.13a). As learning progresses, the movement remains within the attentional radius more and more, so the total movement distance may decrease (Figure 3.13b, and 3.13c). (2) Since fewer DV_{vis}'s have contributed to forming the memory at earlier trials (the memory forms a cumulative representation of all the DV_{vis}'s over all past learning trials), the size of the memory signal R may be smaller at a given time for earlier trials as compared to later trials. As can be seen from equations (5)-(7), the movement velocity is proportional to the size of the cerebellar memory output, R. Thus, the increase in the size of the memory signal over the course of learning can also lead to a speed increase and a decrease in movement duration as learning progresses.

In addition to a decrease of movement duration resulting from the learning mechanism described above, a person may also voluntarily alter the speed of a movement. The model allows for such speed scaling during learning by varying the volitional *GO* signal along with the density of the cerebellar spectra which are sampling the movement error signals. Note that altering spectral density also alters the size of the memory signal, *R*, generated at a given time. Since the movement velocity is proportional to the size of *R*, the speed is altered both by changes in the *GO* signal and by changes in the spectral density.

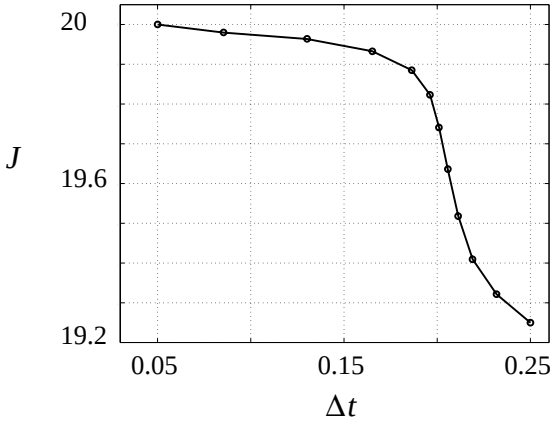

Figure 3.19. The functional relation between *GO* signal size (*J*) and spectral density, given by the time separation between adjacent cell responses, Δt. This relation was imposed algorithmically in order to define a range of spectral densities and *GO* signal sizes capable of learning a letter at a wide range of speeds across learning trials. Figure 3.20 and Table 3.1 show that the range of movement durations during learning is greater when the *GO* signal size and spectral density gradually increase during learning than when they are held constant.

If the execution rate of movement commands stored in the working memory is reduced by decreasing movement speed via the *GO* signal, error feedback to the cerebellum is delayed. Reducing spectral density during learning increases the time span over which spectra are active, thereby allowing synaptic weights to be modified by delayed error feedback. Reducing spectral density therefore allows learning to continue despite varia-

tions in movement speed.

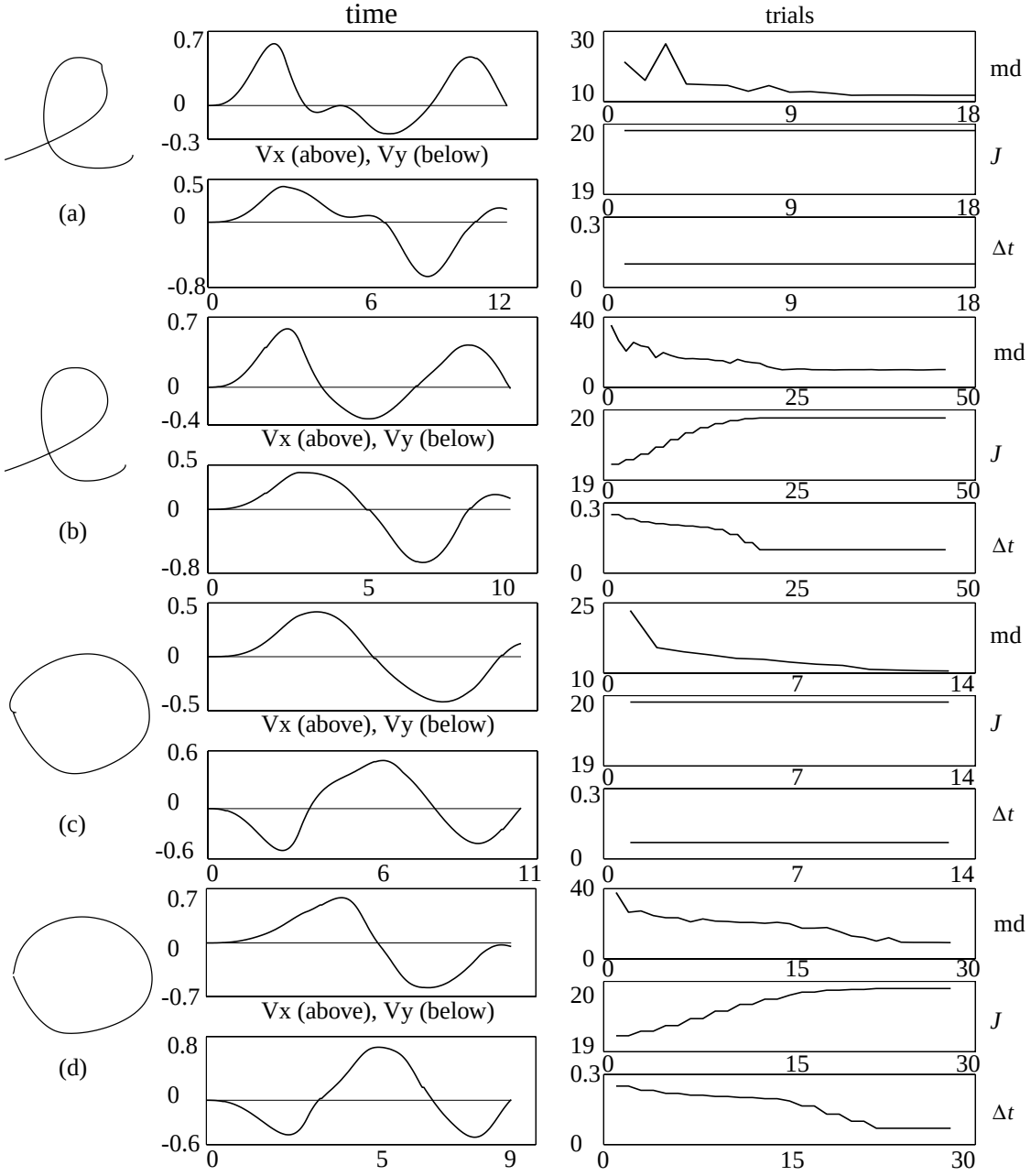

Figure 3.20. Letters learned with variable speed compared to learning at a constant, fast speed. In (a) and (c), the *GO* signal and spectral density were held constant (J = 20, Δt = 0.1). In (b) and (d), the *GO* signal and spectral density were incrementally increased every two trials according to the function in Figure 3.19 (starting at J = 19.25, Δt = 0.25; ending at J = 20, Δt = 0.1). The result was an increase in the range of movement durations, as seen in Table 3.1. (a) through (d): *Left:* Letter learned by AVITEWRITE; *Mid-*

dle: x and y velocity profiles, Vx, Vy; *Right:* (top) trials versus movement duration (md); (middle) J over the course of learning; (bottom) Δt over the course of learning.

(a)

Condition for letter *l*	Maximum Movement Duration (t_{max})	Minimum Movement Duration (t_{min})	t_{max}/t_{min}	Trials at Highest *GO* and Spectral Density	Total Trials
Constant *GO* and Δt	26.45	11.80	2.24	18	18
Increasing *GO* and Δt	35.40	9.90	3.58	26	46

(b)

Condition for letter O	Maximum Movement Duration (t_{max})	Minimum Movement Duration (t_{min})	t_{max}/t_{min}	Trials at Highest *GO* and Spectral Density	Total Trials
Constant *GO* and Δt	23.35	10.45	2.23	13	13
Increasing *GO* and Δt	37.80	9.25	4.09	7	28

Table 3.1. Comparison of the range of movement durations and the number of learning trials needed for error-free movement when the *GO* signal and spectral density are incrementally increased during learning (Figure 3.20) or held constant at the maximum speed. For both letters *l* and O in tables (a) and (b), respectively, note that the range of movement durations, and therefore speeds, is greater when the *GO* signal and spectral density are gradually increased as learning progresses. For the letter *l*, fewer trials are needed to learn the letter at a constant, high speed. However, the performance is slightly worse as reflected in the more segmented velocity profiles of Figure 3.20 (a) compared to (b), in which movement speed is volitionally increased during learning by increasing the *GO* signal and spectral density. For the letter O, performance is very similar when the *GO* signal and spectral density are held constant or increased during learning, but fewer trials are needed to learn the letter at the fastest speed when the *GO* signal and spectral density are gradually increased during learning.

The results of simulations in which speed is gradually increased over the course of learning by increasing the *GO* signal and the spectral density are shown in Figure 3.20 and Table 3.1. As learning progresses, the movement speed gradually increases as reflected by the general decrease in movement duration across the learning trials (Figure 3.20). Eventually, the movement reaches a maximum speed at which learning converges to error free performance with unimodal, bell-shaped velocity profiles for each synergy.

If the movement speed is kept constant at a low value with a sparser spectral density, then a slower, more segmented movement is learned (Figure 3.21).

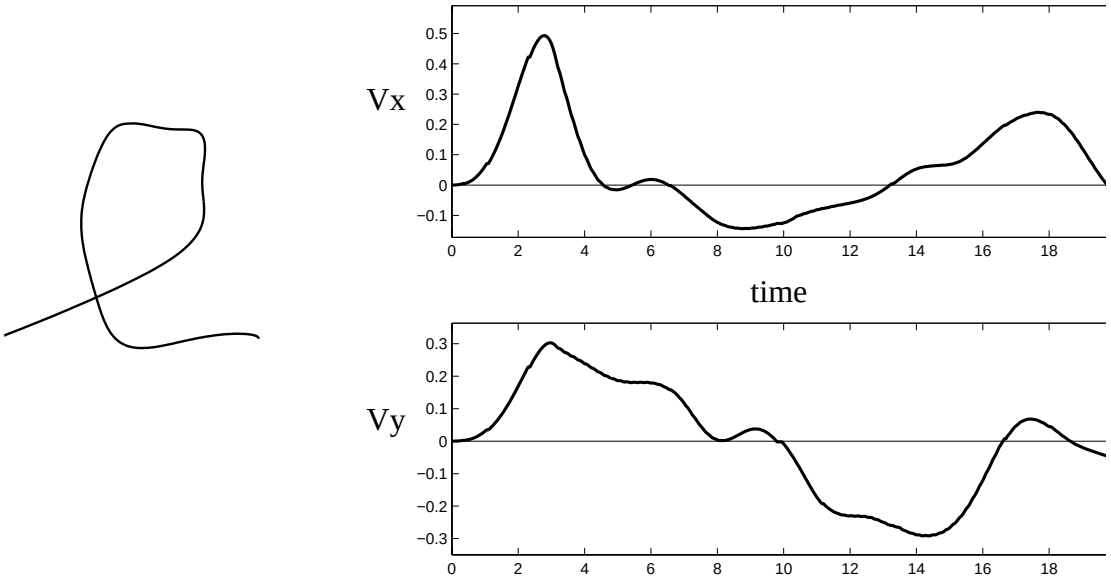

Figure 3.21. Letter *l* learned when the speed-controlling, volitional *GO* signal is kept low (J = 19.75) with a sparser spectral density (Δt = 0.2) throughout learning. r_a = 0.065.

3.4.5 Speed-Scaling of a Learned Movement

Previously learned movements can be written at a wide range of speeds with relatively little distortion of the shape of the movement or the velocity profiles. Wright (1993) has

shown that the speed of handwriting movements can be varied by a factor of about 2.8 (a range of 0.6 to 1.66 times the baseline speed) without significantly altering the letter shape. Presumably, there is no new learning taking place during such speed-scaling since the letters have been written by the subjects for years.

The model yields speed-scaling by a comparable factor without shape or velocity profile distortion, as shown in Figure 3.22. Speed is altered by varying the size of the *GO* signal by varying input *J* in Equation (8). These results are obtained through the use of a working memory buffer which transiently stores the outputs of the cerebellar long term memory and sends them on to the motor apparatus at a rate which can be decreased relative to the rate of cerebellar readout (Equations 5-7, Figure 3.1). Since the rate of readout from the working memory buffer is speed dependent, more motor command information will be stored in the buffer as speed is decreased and the time required to reach a given memory-modulated target (TPV_m) is increased. Figure 3.22c shows the variable number of elements stored in the working memory as the speed is varied. For the fast movement (Figure 3.22c, Left), each TPV_m is reached quickly, thereby triggering readout of the next command from the working memory before many additional commands have been received from the cerebellar long term memory. The number of elements stored in the working memory therefore remains small. For the slow movement (Figure 3.22c, Right), the cerebellar spectra responsible for the learned movement complete their activity at the same time as for the fast movement (at about time t = 11), but the rate at which the commands are read from the working memory is much slower because the *GO* signal is smaller. It therefore takes more time to reach a given TPV_m and trigger readout of the

next command from the working memory. A backlog of commands accumulates in the working memory. When the cerebellar spectra finish their activation response and stop sending additional commands to the working memory, the number of commands stored in working memory begins to diminish as they are read out from the working memory. Each time a command is read from the working memory, it is subsequently deleted from the memory in order to make space in memory for additional commands. When no new commands arrive, the size of the memory shrinks toward zero as each new command is executed.

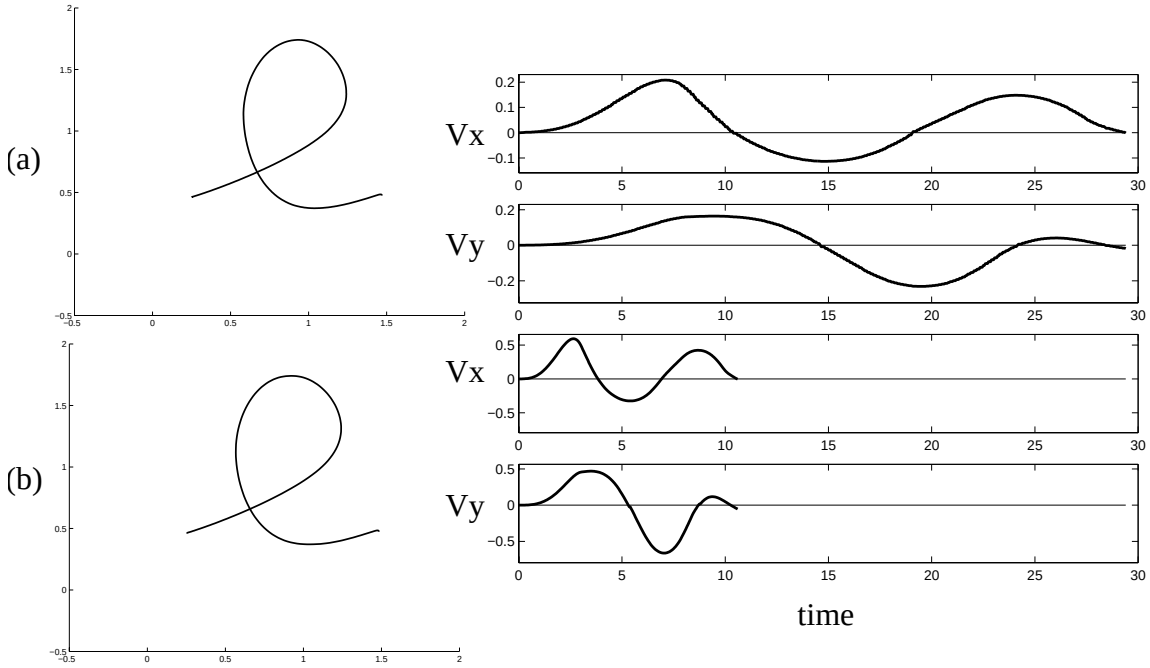

Figure 3.22. Speed scaling of the letter *l* with preservation of the letter shape and the shape of the x and y velocity profiles, Vx, Vy. (a)*:* Letter *l* with the *GO* signal input $J = 7$ in Equation (8). (b)*:* Letter *l* with the *GO* signal input $J = 20$.

If learning has been completed at some final spectral density, altering spectral density thereafter results in distortions of the movement and its velocity profile. Thus, attempting to control the speed of learned movements by altering spectral density alone may trigger new movement errors, as seen in Figure 3.23. Instead, AVITEWRITE uses the volitional *GO* signal in conjunction with the working memory system to yield speed scaling with shape invariance. Since no new learning is required, and hence no delayed error feedback, the spectral density is kept constant at the value reached on the last learning trial at which error-free movement was achieved. The model therefore assumes that an attentional gate couples the *GO* signal and spectral density during attentive imitation, but that they are decoupled during automatic performance of a previously learned letter.

Altering spectral density once error-free, memory-driven performance has been achieved alters the shape of the spectral population output, *R*, and can yield trajectory distortions and errors due to deviation from the attentional radius around the curve which would trigger new corrective movements and synaptic weight modification (Figure 3.23). Although changing spectral density after learning in conjunction with *GO* signal size changes (Figure 3.19) does alter movement duration as seen in Figures 3.23a and 3.23b, the letters and the velocity profiles are distorted relative to each other and to the original *l* from Figure 3.20b due to disproportionate scaling of the summed spectral population output as the degree of overlap of positively and negatively weighted spectral components is altered (Figure 3.15d). This effect is particularly pronounced in Figure 3.23a at the direction reversal at the top of the *l*, where the greater overlap of positively and negatively weighted spectral components cancels the net population output and results in the shorter

y direction movement amplitude seen in the letter.

Increasing the *GO* signal beyond the maximum value (the asymptote of $J = 20$ in Figure 3.19) causes the movement speed to exceed the rate of memory readout of upcoming synergy activation commands, also leading to errors in the movement trajectory. The rate at which memory output is sent from long-term storage in the cerebellum is therefore the speed-limiting component of the model.

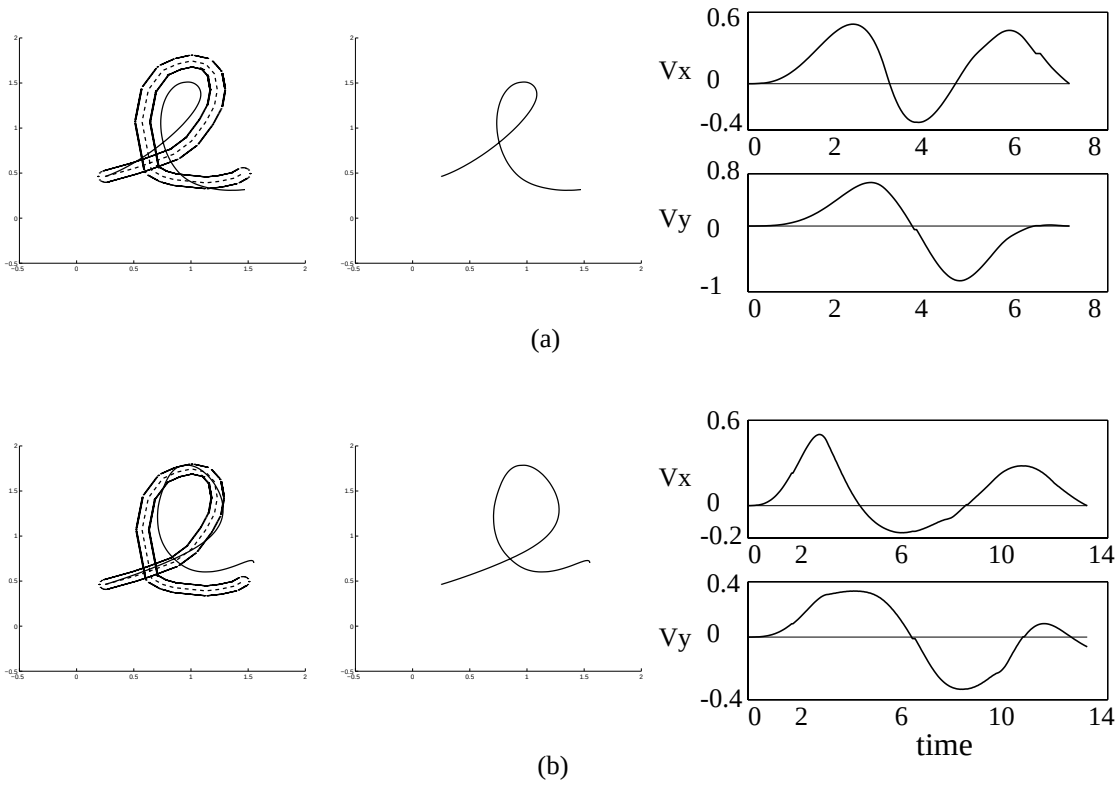

Figure 3.23. The effect of altering the spectral density of the letter *l* after learning with $\Delta t = 0.1$: (a) Spectral density is increased by decreasing the time separation Δt between adjacent spectral components to 0.05. (b) Spectral density is decreased by increasing Δt to 0.13.

3.4.6 Size Scaling and Isochrony

Size can be scaled in the model by varying the volitional *GRO* signal *S* in Equation (6). Using the same value of *S* for both horizontal and vertical directions will uniformly alter the size of a letter without altering the ratio of height to width (Figure 3.24). However, Wann & Nimmo-Smith (1990) have shown that humans do alter this ratio when scaling letter sizes; that is, vertical and horizontal sizes can be scaled independently. In their experiment of size scaling, subjects were found to increase the horizontal (x) component of movement by 46% and the vertical (y) component by 78% (p. 111). Figure 3.25 shows the result of a simulation in which different *GRO* values *S* are used for the horizontal and vertical directions, with the x synergies' *GRO* signal *Sx* increased 46% and *Sy* by 78%, relative to the value used during learning.

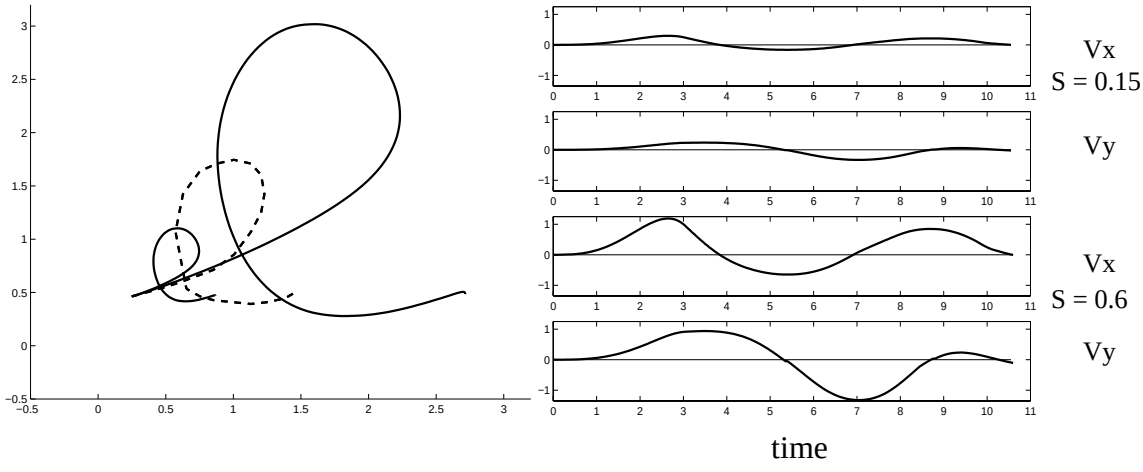

Figure 3.24. Size scaling with isochrony. The dashed letter *l* is the template curve traced during learning with a baseline, size-scaling *GRO* signal *S* = 0.3. *S* = 0.15 for the smaller, solid *l* written by AVITEWRITE, and *S* = 0.6 for the larger, solid *l*. Both the large and the small *l* are written in the same amount of time, as seen in the x and y velocity profiles, Vx, Vy.

One noteworthy feature of human handwriting is isochrony; namely, the tendency for shapes of different sizes to be drawn in the same amount of time. Isochrony is also a feature of the model's performance, as seen in Figures 3.24 and 3.25. Humans are capable of isochrony only for a limited range of sizes. Isochrony is observed at small sizes, but it fails at large sizes; that is, the isochrony principle is valid within the "neighborhood of normal letter heights (approx. 0.5 cm) [but the] writing time will increase at some point where force demands become too high" (Thomassen & Teulings, 1985, p. 255). "Writing time is not invariant across changes in writing size, but increases by a small amount" (Wright 1993, p. 49).

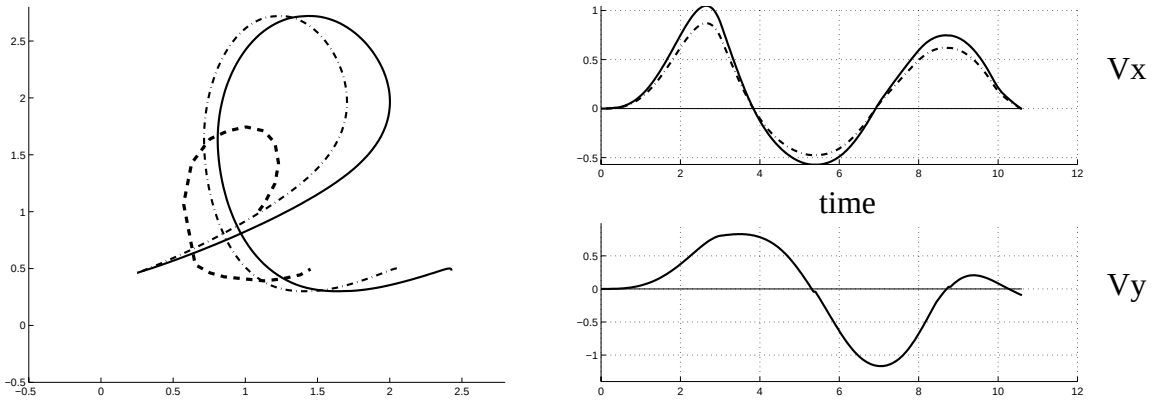

Figure 3.25. Independent scaling of horizontal and vertical components of size. The small, dashed letter *l* is the template curve traced during learning with a baseline, size-scaling *GRO* signal parameters $S_x = S_y = 0.3$. The two larger *l*'s both have a y *GRO* signal parameter $S_y = 0.53$. The large, dash-dotted *l* has an x *GRO* signal of $S_x = 0.44$ corresponding to the dotted x velocity profile, Vx, while the large, solid *l* has $S_x = 0.53$ with a solid x velocity profile.

The human limits to isochrony may be due to the physical limitations of the hand/arm system and/or to some limit of the central force-control mechanisms of the brain, as exemplified in the extreme case of Parkinson's disease patients who appear to have a

"reduced capability to maintain a given force level for the [prolonged] stroke time periods" required when letter size is greatly increased (Van Gemmert et al., 1999, p. 685).

Note that size is *not* altered in the simulations during learning, since the current model's error correction system assumes the template curve is being traced. In a tracing task, altering size would be interpreted as an error. Issues related to copying a shape from a page or from a chalkboard are treated in the Discussion section.

3.4.7 Coarticulatory Context Effects in Handwriting

The writing of a cursive letter may be affected by adjacent, connected letters. Thomassen & Schomaker (1986) demonstrate context effects which they assume are due to coarticulation; that is, "anticipatory and overlapping instructions to the motor system" (p. 257). Coarticulation is the concurrent activation of muscles working toward different goals. Different sets of muscles with separate goals can be working simultaneously, or the same set of muscles can be receiving motor commands to carry out separate goals. In the latter case, the muscles' movements may be a summation or averaging of the commands they receive. If conflicting commands are received, some muscles in a group which usually work together toward a common goal may carry out one command while other muscles in the group carry out other commands (Ohman 1965, pp. 166, 168; Fowler et al. 1993, p. 179).

Thomassen & Schomaker (1986) find that "more rapid writers... display stronger context effects than slower writers" (p. 257). This finding is consistent with the observed increase in speech *carryover coarticulation* with increases in speaking rate. "Carryover"

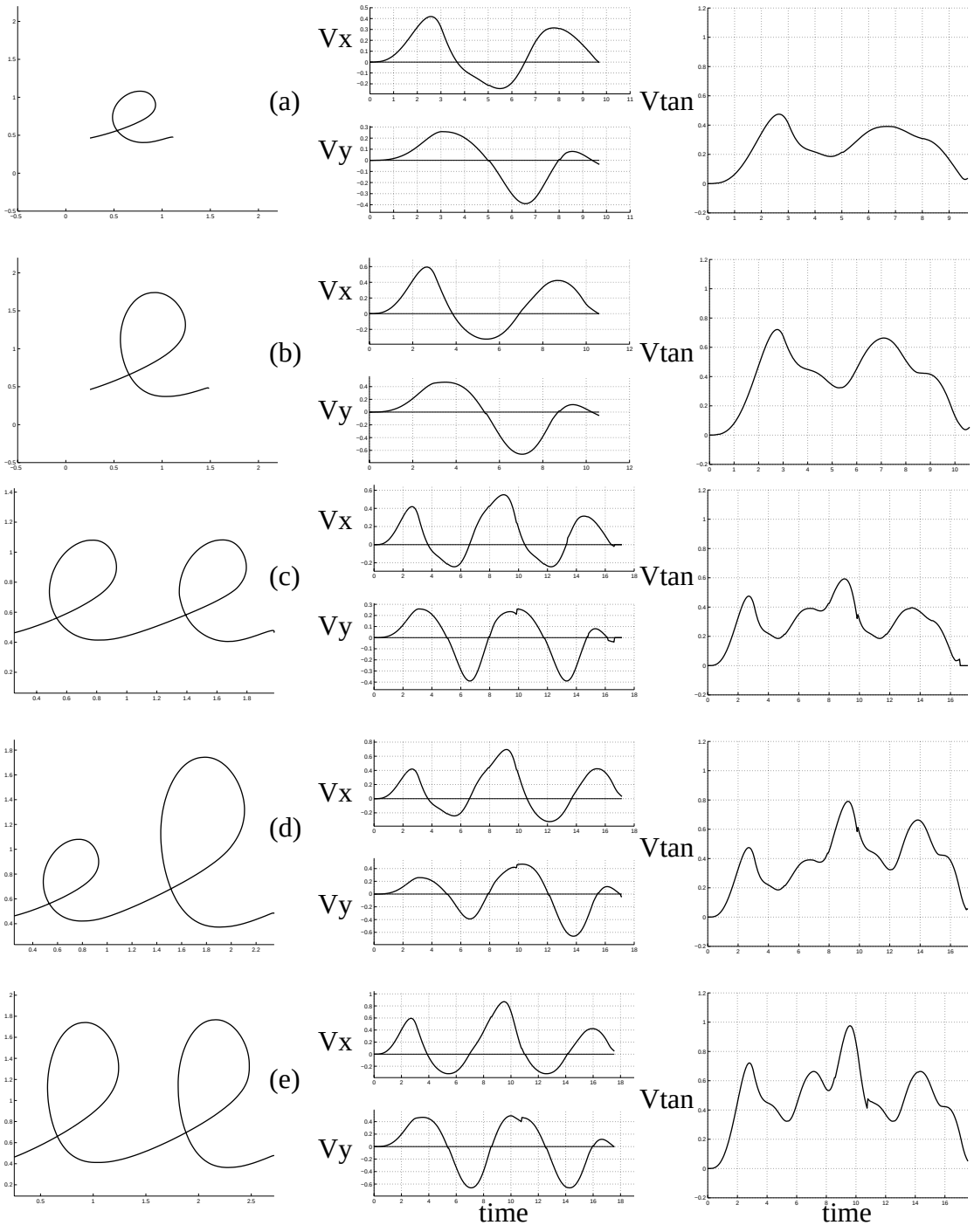

Figure 3.26. Simulated combinations of the letters *e* and *l*. *Left:* The letters; *Middle:* x and y velocity profiles, Vx, Vy; *Right:* Tangential velocity, Vtan. See Table 3.2 b for data derived from these figures and compared to human data from Greer & Green (1983) in Table 3.2a.

("perseverative", "left to right") coarticulation occurs when movement changes occur after different initial conditions (Ostry et al. 1996). For example, starting to write the letter *l* when the hand position is still at a higher vertical position on a preceding *e* downstroke would cause a carryover coarticulatory effect on the trajectory of the movement that would yield shape differences compared to an *l* that starts from an initial condition of zero velocity at a lower vertical position.

In order to test the idea that some of the observed context effects in handwriting are due to carryover coarticulation, connected letters were simulated with varying degrees of overlap of the corresponding spectral memories. In other words, the degree of superposition between adjacent letters was varied. The letters *e* and *l* were learned by the modelled system (Figures 3.26a, 3.26b). The learned memory traces were then read out successively with varying degrees of overlap. It was found that some of the downstroke duration and size effects observed by Thomassen & Schomaker (1986) could be replicated by varying the degree of superposition between adjacent letters. In the simulation of the string *eele*, shown in Figure 3.27, the relative timing of the loading of the previously learned letter memories was varied and the sizes of the letters were compared. The second *e* can be made smaller than the other *e*'s by increasing its superposition with the large vertical upstroke of the following l, thereby cancelling a large part of the *e* downstroke (Figures 3.27b, 3.27c). Increasing the time separation between letters can eliminate the coarticulatory size effects in the model, as seen in Figure 3.27a.

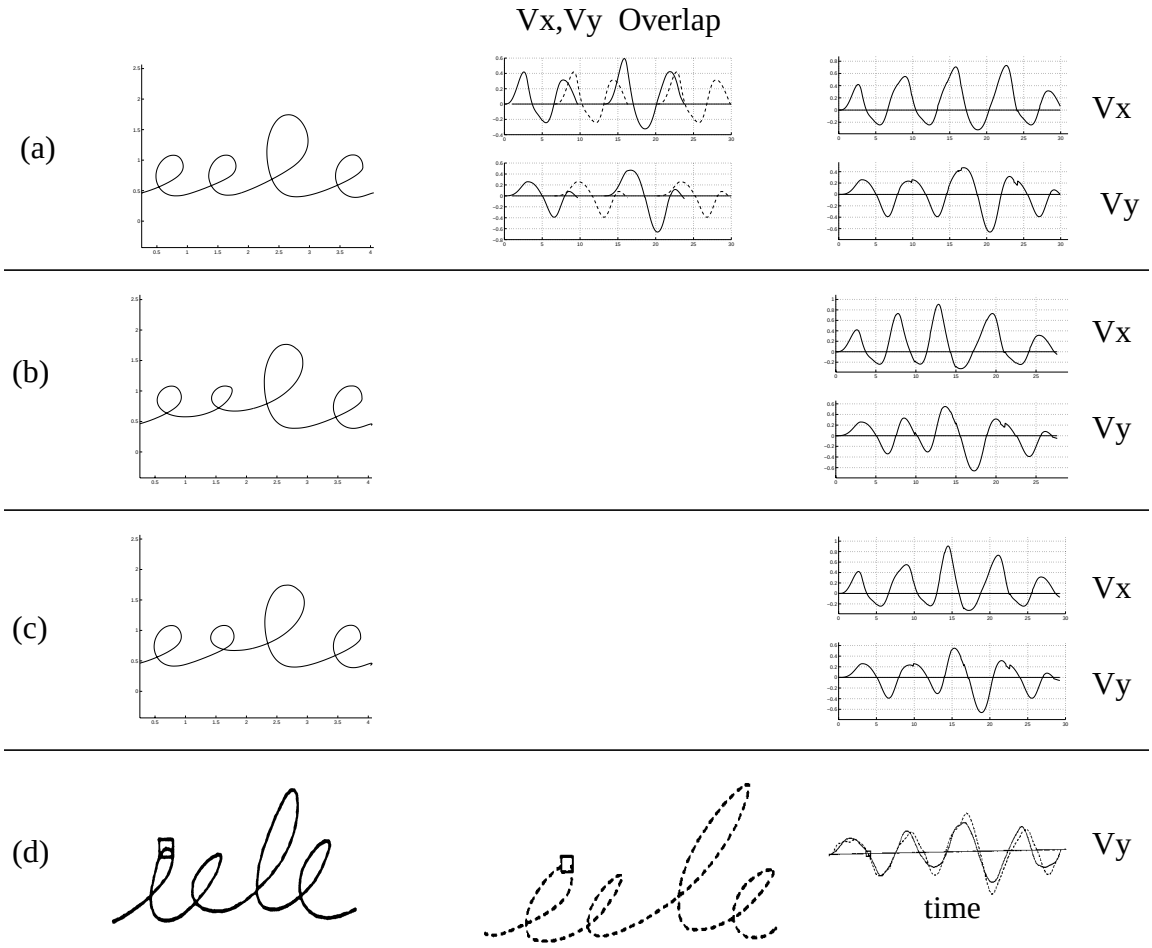

Figure 3.27. (a) through (c): Simulated *eele* with varying degrees of overlap between the letters. Timing relations are as follows. (a) 6.6, 6.6, 7 (The second letter begins 6.6 time units after the first; the third starts 6.6 after the second, and the fourth starts 7 time units after the third, corresponding to the second Vx zero crossings shown in Vx Overlap.) Vx,Vy Overlap show the overlapping velocity profiles of the individual letters. (b) 5, 5, 7; (c) 6.6, 5, 7; (d) Human writing of *eele* by two subjects (Figure (d) reproduced with permission from Thomassen & Schomaker, 1986). The dotted y velocity profile, Vy, corresponds to the dotted *eele*.

Greer & Green (1983) reported that each letter (e or l in their study) has its own characteristic upstroke Vmax (maximum velocity) for a particular size. A characteristic Vmax is a also a feature of AVITEWRITE performance, since the velocity profile for

each letter is the result of learning. Thus, each time AVITEWRITE writes a given learned letter, the same learned movement commands are used and the same velocity profile is generated. Different letters have different characteristic Vmax's because of the different sequences of error signals generated during their learning. As the size of a learned letter is varied by changing the *GRO* signal, the Vmax will also vary, and it will be characteristic of that letter for that particular size.

(a) Experimental Context Effects

Letter type	Upstroke Vmax (units/ sec)	Time to Vmax (sec)
single *e*	7.8	0.094
ee: first *e*	8.5	0.090
ee: second *e*	10.0	0.070
el: *e*	9.2	0.085
single *l*	17.2	0.116
ll: first *l*	20.0	0.100
ll: second *l*	21.6	0.080
el: *l*	19.8	0.090

(b) Simulated Context Effects

Letter type	Upstroke Vmax (units/ sec)	Time to Vmax (sec)
single *e*	7.8	0.094
ee: first *e*	7.8	0.094
ee: second *e*	9.6	0.038
el: *e*	7.8	0.094
single *l*	11.7	0.097
ll: first *l*	11.7	0.097
ll: second *l*	15.9	0.038
el: *l*	12.8	0.049

Table 3.2. (a) Context effects observed in human subjects (Adapted with permission from Greer & Green, 1983) compared to (b) those observed for the connected letters simulated by AVITEWRITE and shown in Figure 3.26. The AVITEWRITE data are scaled relative to the experimental data for ease of comparison. The actual AVITEWRITE data, with arbitrary units, can be obtained by dividing the simulated Vmax value by 16.25 and the Time to Vmax by 0.0348.

Greer & Green (1983) found that it takes less time to reach the Vmax of the second *l* in *ll* than in *el* (Table 3.2a). The AVITEWRITE simulations also yielded such a result (Figure 3.26; Table 3.2b). Greer & Green also report that upstroke Vmax is higher for a given letter if it is written in a pair than if it is written alone. This effect also emerges for connected letters in the present model, due to the superposition of the last stroke of one letter and the first stroke of the following letter. However, such superposition implies that the Vmax of the upstroke of the first letter is the same as if the letter were written alone (since there is no preceding letter with which it is superposed) (Figure 3.26; Table 3.2). Greer & Green state that there was no reliable effect of letter position on the size of the Vmax for two repeated letters (*ll* or *ee*). However, the data shown in their article and reproduced in Table (3.2a) consistently show the upstroke Vmax of the second letter to be larger than that of the first letter for both *ee* and *ll*, as was the case in the current model simulations (Table 3.2b).

The focus of the data in Table 3.2 is the qualitative effect of letter position on Vmax and the time to Vmax in both human subjects and model simulations. However, one may note that there are quantitative differences between the human data and the model data even when the model data are scaled relative to the human data. Most strikingly, the Vmax of the model *l* is consistently smaller than that of the human *l*. The quantitative differences between the model data and the human data are probably due to a variety of factors, such as the fact that AVITEWRITE does not have a detailed representation of a real arm and its muscle dynamics. Further, the relative scales of the *e* and *l* learned by AVITEWRITE may not be the same as those from the averaged *e* and *l* data from Greer &

Green's eight subjects. Greer & Green (1983) do not show the actual letters written by their subjects. One possible explanation for the difference in Vmax between AVITEWRITE's *l* and the *l* from the averaged human data, written in the same context, is that AVITEWRITE's *l* is not as large relative to the *e* as the *l* written by the human subjects. If the height of AVITEWRITE's *l* relative to the *e* were smaller than that of the human subjects' letters, then AVITEWRITE's Vmax for *l* might be smaller than that observed in the human data. Finally, the Vmax scaling discrepancy could also be attributed to the use of a step-function *GO* signal, unlike that used in all other versions of the VITE model (including VITEWRITE).

Although superposition of the strokes of adjacent letters, such that the initial conditions for starting a given letter vary depending on the identities of adjacent letters—that is, carryover coarticulation—is an appealingly simple explanation for the above context effects, there are some data which it may not explain. Greer & Green (1983) found that it takes less time to reach the upstroke Vmax for an *e* if it is followed by an *l* than if it is followed by an *e*. Carryover coarticulation in the present simulations does not predict this result (Figure 3.26; Table 3.2b). One possible reason for the failure of simulations of *carryover* coarticulation to generate all the observed context effects is that some may be due to *anticipatory* coarticulation. Anticipatory coarticulation, occurs when the current pattern of muscle activity is influenced by a future context.

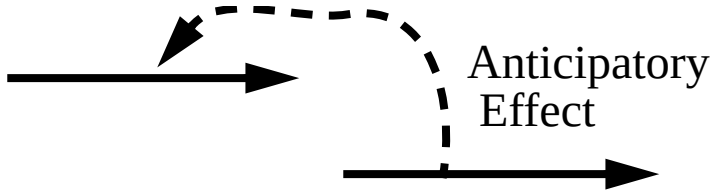

Figure 3.28. Conceptual diagram of anticipatory coarticulation. Preparation of a future movement may affect execution of a current one.

Some features of one written letter may be affected by the perception that another particular letter must be written following it:. “Anticipatory coarticulation is observed as a result of differences in the composition of the upcoming sequence... Anticipatory coarticulation is presumed to involve explicit adjustments to account for upcoming context, whereas carryover effects have been attributed to articulator mechanics” (Ostry et al., 1996, pp. 1570-71). Thus, it is possible that when Greer & Green (1983) found that it takes less time to reach the maximum upstroke velocity for an *e* if it is followed by an *l* than if it is followed by another *e*, they had found an example of anticipatory coarticulation in handwriting. Greer & Green (1983) hypothesized that this effect was due to the allocation of a limited amount of time for the writing of a letter pair, requiring the first letter to reach Vmax more quickly in order to allow time to change muscle force parameters for the writing of a different, second letter. Thus, the subject would have to anticipate the need for additional writing time for the second letter and increase the acceleration of the first letter.

Finally, note that several additional factors may play a role in handwriting context effects, such as: maintenance of a variable force level over time, as exemplified in Parkinson’s disease patients (Van Gemmert et al., 1999); processing demands of size and slant

variations which can decrease movement speed and fluency (van Den Heuvel et al., 1998); and memory loading effects, such as the longer reaction time for the first response in a learned sequence relative to later responses (Sternberg et al., 1980; Verwey, 1996).

CHAPTER IV

DISCUSSION

4.1 Data from Human Experiments

Much experimental research has been done on adult human handwriting in the last two decades. Among the reasons for this focus of interest are the following. Handwriting is a focal point, or confluence, for several motor control problems, such as temporal sequencing of stroke order, decomposition of movements into target-driven segments, characterization of mental movement coordinate systems, and the role of sensory feedback for motor planning. Handwriting studies allow these issues to be investigated in non-invasive, inexpensive, and easily executed experiments on human subjects.

Data about the nature of strokes (Teulings et al., 1986a; Viviani, 1986), motor planning of movements (Rosenbaum et al., 1995; Teulings et al. 1986b), size and speed control of movements (Plamondon & Alimi, 1997; Schillings et al., 1996; van Galen & Weber, 1998; Wann & Nimmo-Smith, 1990; Wright, 1993), and motor equivalence (the preservation of movement characteristics when done by different end effectors) (Wright, 1990)

are a small sample of the wealth of data available from adult humans. Since the focus of this research is the learning of human handwriting, data on adult generation of previously learned movements, such as letters, is necessary but not sufficient for the development of a model which describes how handwriting movements are learned. Much practice of novel movement patterns is required before children master handwriting. In addition, many handwriting studies have been done with children in order to improve the teaching of handwriting (see below). These studies reveal the progression of movement proficiency over years of practice. The fact that handwriting performance can improve over years of practice suggests that it is the result of cumulative learning from many individual writing trials. Unfortunately, few scientific studies of either adults or children address short-term changes in handwriting performance due to learning on individual movement trials.

4.2 Insights from the Pedagogy of Handwriting

"What a pupil can see (or visualize) he can make" (Burns, 1962, p. 14). One of the most important elements in the learning of handwriting is vision. Although adults can generate good handwriting even with the eyes closed, "the child... is largely dependent on his sense of sight for the correct formation of the letters..." (Freeman, 1914, p. 19). "In striving to copy the forms of the letters, he keeps their appearance in mind as well as he can and watches the letter which he is making in order to see when it deviates from the model and to bring back the stroke when it goes astray. He follows the stroke bit by bit with the eye, and it is his eye which seems mainly to "control" the stroke. After he has made the various letters over and over he gradually learns how it feels to make them... and

he finds it no longer necessary to follow the stroke minutely" (Freeman, p. 28). The above quotation concisely describes the abilities of both a child and of the AVITEWRITE model.

The learning of handwriting involves an ongoing comparison between the child's motor output and some desired output, which may be defined by a shape on a page or a blackboard, or by a shape "visualized" in the child's mind. Much classroom instruction is designed to highlight to the child the differences between his written output and a desired form. For example, Hendricks (1976) described an exercise in which a letter is projected on a chalkboard. The child must write the same letter on the board. By turning the projector on and off over the child's writing, the differences between the child's writing and the desired output can easily be seen.

Two issues immediately arise: The first issue concerns the distinction between continuous error correction during movement versus correction of future movements after past mistakes are brought to the child's attention. Whereas an error is corrected upon detection during tracing, a child told after movement completion that a particular feature needs to be changed in a particular way must try to remember this corrective information and apply it (with varying degrees of success) to future movements at the appropriate time during the course of the movement. Although one can envision a working memory linked to a timing mechanism which sends a stored error vector to the learning system at the appropriate time during a future trial, such a mechanism is not directly addressed by the AVITEWRITE model. The model does, however, introduce working memory and timing mechanisms which can form the foundation for such a competence.

The second issue concerns the visual-to-motor transformations required to make corrective movements during copying from a page, copying from a chalkboard, or imitation of another person's movements, as opposed to the tracing of a shape. The relevance of this issue is emphasized by Burns' observation that "copying from the board... is very difficult at the earliest stages of beginning work" in the teaching of children. "Children having their own copy of work to be done as "seatwork" would appear to be a more desirable practice" (Burns, 1962, p. 16). It therefore appears that the ability to visually remember a shape seen elsewhere and use it to guide movement is a non-trivial task which must develop in the child. The related task of comparing a writing trace to a template which is visible next to it requires a visual-to-motor transformation which allows the child to make, for example, a corrective movement to the right based on a template curve located to the left of the workspace. Similarly, movements can be guided by observing the movements of another person. "Imitation of a person [is] better than imitation of a copy merely" (Freeman, p. 74). Further, Hayes (1982) and Furner (1983) found that students' verbalization of stroke sequences is superior as a teaching aid to visual demonstration (imitation), copying, or tracing alone. There are therefore several sources of input which can be used to learn a handwriting movement. In the AVITEWRITE model, the mode of information input to the cortico-cerebellar system, be it from tracing, desktop copying, chalkboard copying, imitation (Iacoboni et al., 1999), verbal instruction, or even from sound error signals in the teaching of handwriting to the blind (Itoh & Yonezawa, 1990), is not the key focus of the modelling effort. Tracing a curve is one possible means of learning handwriting, but it is not the only one. The idea that continuous muscle syn-

ergy activations for curved movements can be learned through the use of appropriate error/teaching signals to cerebellar spectra can be used for learning with several modes of sensory information input, including those mentioned above. Studies addressing some of the sensory-to-motor transformation issues which would be required for AVITEWRITE to learn from different types of sensory information have previously been done by Guenther et al. (1994). For simplicity and convenience, the teaching/error vectors which drive the cortico-cerebellar movement learning in the model are generated by errors in tracing a template curve.

4.3 Applicability of the Target Selection Algorithm to other Learning Strategies

In view of the multiple possible modes of sensory input during handwriting learning, the target selection algorithm described in detail in the Equations section may not always be directly applicable to them all. Further, the details of the computer algorithm used to select targets are not intended to represent a brain process in detail. The computer algorithm can evaluate potentially hundreds of points as potential targets by sequentially calculating the changing distance from the line segment *L*, from the *PPV* to each possible target (Figure 3.7), to the template curve being traced. AVITEWRITE does not mean to suggest that the brain carries out such intensive serial calcuations each time a target must be selected. It is more likely that targets are chosen through a less computationally intensive algorithm, based on the attentional radius around the *PPV,* which keeps the *PPV* as close as possible to the template curve. Thus, the basic ideas which AVITEWRITE's target selection algorithm attempts to capture should be useful in describing handwriting

learning through tracing or through other means, such as imitation of a teacher's actual movements or copying of a letter from a page or chalkboard. In each of these different means of sensory input, AVITEWRITE leads one to expect an attentional focus around regions of the shape being imitated which shifts along the curve ahead of the hand position. Further, AVITEWRITE's target selection algorithm suggests that a person chooses targets for movement at the extreme of the attentional focus in order to learn the movement with fewer, less segmented strokes. The model also predicts that movements early during learning are more segmented than movements later during learning. Further, it predicts that movement duration over the course of learning decreases due to a combination of less segmented movements with shorter trajectories, as well as a larger amplitude memory trace.

4.4 Size Variation During Learning

As mentioned in the Simulations section, varying the size of either the template curve being traced or the trajectory generated by the model during learning would be perceived by the AVITEWRITE system as movement errors since such size variation would cause trajectory deviation from the attentional radius around the template curve. This problem highlights the limitations of a model of handwriting learning that is based solely on tracing. In the case of copying a letter from a page or chalkboard, there can be large size differences between the original letter and the curves drawn by the person. AVITEWRITE would require a size transformation from the visual difference vectors formed on the template curve to those used to drive reactive movements and form climbing fiber error sig-

nals in order to compare its own trajectory to a template curve of different size without triggering inappropriate error signals due to size differences as opposed to shape differences.

4.5 Evidence for a Cerebellar Role in Handwriting

It is known that there is cerebellar activity during drawing, and that the cerebellum is more active when lines are retraced than in new line generation because error detection (deviation from the lines) occurs during retracing but not new line generation (Jueptner & Weiller, 1998) (Figure 4.1). Since the cerebellum is more active during error corrections, it is likely that climbing fibers are signaling movement error, leading to LTD of Purkinje cell-parallel fiber synapses (Gellman et al., 1985; Ito, 1991; Ito & Karachot, 1992; Oscarsson, 1969; Simpson et al., 1996).

The cerebellum may also be involved in more complex tasks, such as sequential movements. It is known that there is a cerebellar role in procedural memory. In a sequential button press task, lesions to the dentate nucleus cause deficits in learning and memory (Lu et al., 1998). Further, Doyon et al. (1998) demonstrated through studies using a sequential finger movement task that the cerebellum and striatum are involved in the automatization and long-term retention of motor sequence behavior. The AVITEWRITE model shows how the cerebellum may be involved in learning a sequential handwriting task. AVITEWRITE also shows how the cerebellum may encode movement velocity. It is known that Purkinje cell simple spike discharge is direction- and speed-dependent (Coltz et al., 1999a; Ebner, 1998). Simple spikes result from summation of excitatory postsyn-

aptic potentials at parallel fiber-Purkinje cell synapses, across multiple Purkinje cell dendrites (Ghez, 1991, p. 631). AVITEWRITE assumes that movement context information, such as the movement direction and speed, is carried via the parallel fibers to the Purkinje cell populations controlling particular muscle synergies.

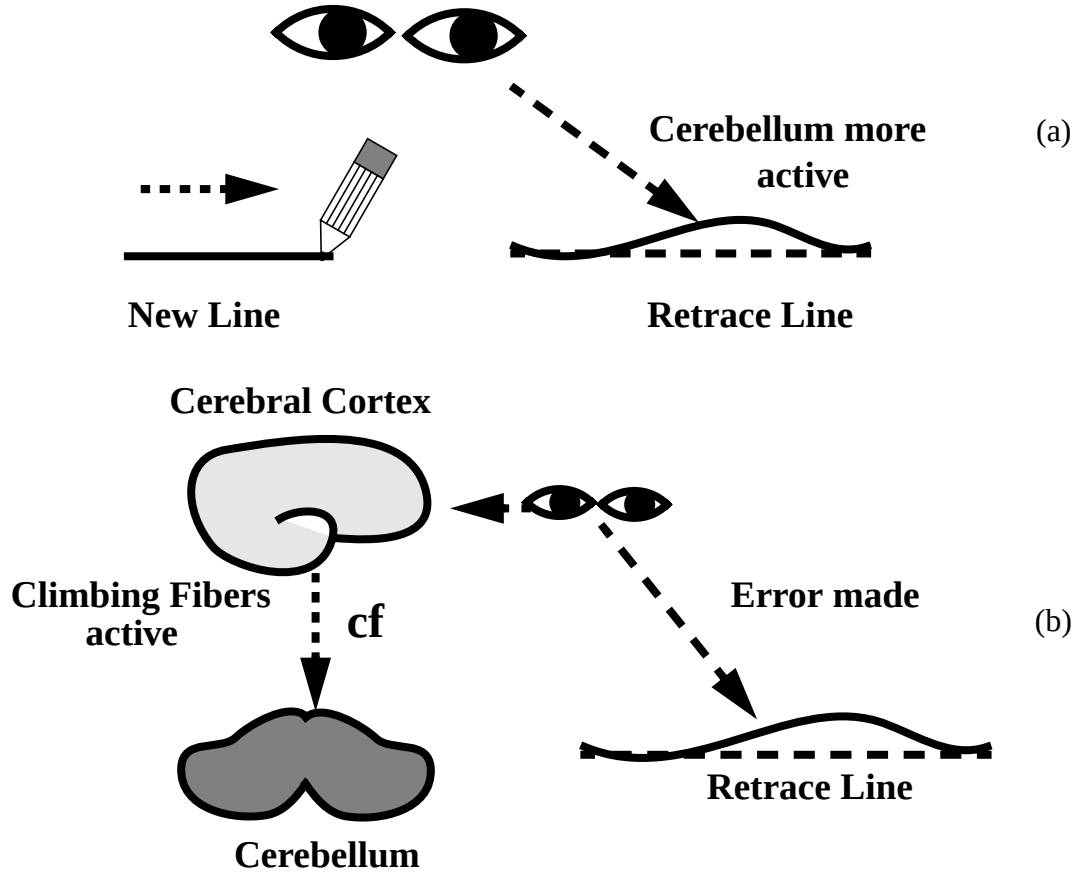

Figure 4.1. (a) Illustration of the findings of Jueptner & Weiller (1998); The cerebellum was found to be more active during line retracing than in new line generation. (b) AVITEWRITE hypothesizes that climbing fibers are carrying error signals generated during line tracing which are used to shape a cerebellar memory of the muscle synergy activations required to draw the line or curve.

Further, complex spike discharge of Purkinje cells is “spatially tuned and strongly related to movement kinematics” (Fu et al., 1997). A complex spike results when a single action potential is carried to a Purkinje cell via a climbing fiber, triggering a large Purkinje cell action potential followed by a high-frequency burst of smaller action potentials (Ghez, 1991, p. 631). In AVITEWRITE, the climbing fiber inputs act as error-correcting signals which train Purkinje cells that control particular muscle synergies to become hyperpolarized at the appropriate times during movement. AVITEWRITE therefore assumes that the climbing fiber signal is dependent on the direction and amplitude of a required corrective movement. The required corrective movement is different from, and possibly in the opposite direction to, the actual movement of that particular muscle synergy, which is reflected in simple spike activity. In fact, Coltz et al. (1999b) have found that complex spike discharge is direction- and speed-dependent, and that it is related to directions opposite those of the corresponding simple spikes, and to speeds different from those of the simple spikes. This appears to be further evidence that climbing fibers transmit a movement error signal. The model suggests how, using a spectrum of phase-delayed Purkinje cell activations based on adaptive timing mechanisms, learned cerebellar outputs may code movement gain and velocity.

4.6 Continuous versus Discrete Error Signals

The error/teaching signals sent to the cerebellar spectra in the AVITEWRITE model are continuously changing signals based on the time-varying value of the difference vector from the current hand position to the target. However, complex spikes triggered by

real climbing fiber signals have an average frequency of 1 Hz (Ghez, 1991, p. 632), with an increase to about 6 Hz which lasts approximately 500 msec when a monkey initially reaches toward a target or changes the direction of an ongoing movement from one target to a new target (Bloedel, 1994, pp. 71-72; Mano et al., 1986). In terms of the AVITEWRITE model, these observations suggest that the difference vector-based error signal should only be sent to the cerebellar spectra for a short time following the formation of the difference vector to a target. Although such simulations were not attempted for the current model, it should be possible to adjust the AVITEWRITE model to learn to write even with shorter lasting error signals. Two factors would allow such learning. First, the cerebellar spectral components span overlapping periods of time, so that an error signal arriving at time t and lasting until time $t + \Delta t$ would alter the weights of all spectral components that are active during that time interval. Since those spectral components may remain active beyond the time $t + \Delta t$ when the error signal is shut off, a short error signal may affect movement beyond the termination time of that error signal. Second, Equation (3) for the cerebellar synaptic weights contains a parameter, α, which scales the size of the climbing fiber error signal. Increasing the size of this parameter should allow an error signal of short duration to have an effect on the synaptic weights that is comparable to a prolonged error signal with a smaller value of α. In these ways, the AVITEWRITE model could be altered to utilize more realistic climbing fiber signals.

4.7 The Biochemistry of Spectral Timing

Fiala et al. (1996) hypothesized that the varying concentration of dendritic metabotropic glutamate receptors (subtype mGluR1) across the population of Purkinje cells allows adaptively timed LTD. They suggested that a spectrum, or series, of time-delayed calcium release patterns occurs across the Purkinje cell population in response to parallel fiber-induced activation of mGluR1. Since different cells may have different concentrations of mGluR1 just outside the synaptic junctions with parallel fiber terminals, the cells may have different temporal patterns of calcium release over time. Cells with greater concentrations of mGluR1 will exhibit faster calcium release than cells with smaller concentrations of mGluR1. In other words, they may have a "spectrum" of calcium release with a corresponding spectrum of potential changes (depolarizations).

The spectrum of calcium release over a time span of up to four seconds (Fiala et al., 1996, p. 3768) allows pairing of timed, Purkinje cell inhibition via long term depression with a conditioned stimulus. Timed inhibition of Purkinje cells disinhibits the cerebellar interpositus nucleus, allowing a movement response to be made at the appropriate time. The sequence of events posited by Fiala et al. (1996) to allow timed long term depression of Purkinje cells is outlined as follows. mGluR1 activation is responsible, via a chain of biochemical events (Figure 4.2) involving inositol 1,4,5-trisphosphate (IP_3), diacylglycerol (DAG), and release of intracellular calcium stores, for the phosphorylation and inactivation of AMPA receptors. Phosphorylation of a Ca^{2+} -dependent K^+ channel protein (g_K) increases the conductance of the associated K^+ channel (Fiala et al., 1996, p. 3765). If mGluR1 alone is activated, then protein phosphatase-1 (PP-1) competitively dephos-

phorylates, and reactivates, the AMPA receptors and reduces the g_K conductance. The AMPA receptor will therefore maintain an equilibrium level of activation allowing AMPA-mediated Excitatory Post-Synaptic Potentials (EPSPs) in response to parallel fiber inputs. The Ca^{2+}-dependent potassium channel will remain closed, thereby preventing hyperpolarization.

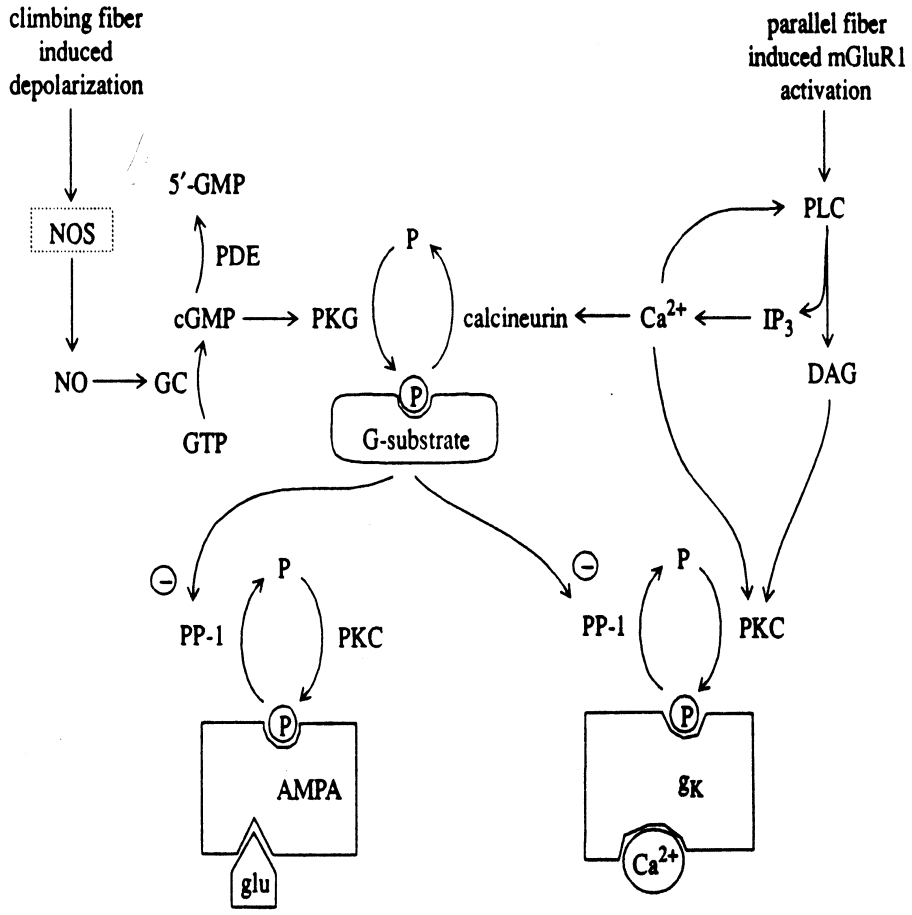

Figure 4.2. Biochemical processes mediating learning of a timed response in cerebellar Purkinje cells. (Reproduced with permission from Fiala et al., 1996.)

If a climbing fiber input arrives at the Purkinje cell, another chain of biochemical events occurs which inhibits PP-1. If the climbing fiber input arrives during the period of

heightened calcium concentration which follows parallel fiber-induced mGluR1 activation, then the AMPA receptors and g_K remain phosphorylated. The Purkinje cell is therefore hyperpolarized after a delay due to the transient Ca^{2+} release's effect on the Ca^{2+}-dependent K^+ channel and AMPA-mediated EPSPs are suppressed. This is how the model of Fiala et al. (1996) proposes that long term depression of the Purkinje cell occurs.

Assuming that there is a spectrum of mGluR1 concentrations across the Purkinje cell population, then calcium release following parallel fiber-induced mGluR1 activation will peak at different times in different Purkinje cells (PCs). Hyperpolarization (and LTD) will therefore occur to a varying degree in different PCs depending on the intracellular Ca^{2+} concentration at the time of climbing fiber activation (Figure 2.8a). In their model, Fiala et al. (1996) suggest that the intracellular Ca^{2+} concentration at the time of climbing fiber activation is a function of the PC's mGluR1 receptor concentration. PCs with higher calcium concentrations at the time of CF input arrival will have correspondingly higher degrees of hyperpolarization and LTD. PCs whose Ca^{2+} concentration has returned to baseline by the time the CF input arrives will not experience any LTD.

Key aspects of the metabolic cascade for Purkinje cell LTD that was predicted above have since been confirmed by Finch & Augustine (1998) and Takechi et al. (1998). In particular, Takechi et al. (1998) reported that parallel fiber-PC "synaptic Ca2+ transients are mediated by activation of metabotropic glutamate-responsive mGluR1-type receptors and require... [IP_3] -mediated Ca2+ release from intradendritic stores" (p. 757). Finch & Augustine (1998) found that "repetitive activation of the synapse between parallel fibres

and Purkinje cells causes InsP3 [IP_3] -mediated Ca2+ release in the Purkinje cells... [which is] restricted to individual postsynaptic spines, where both metabotropic glutamate receptors and InsP3 receptors are located, or to multiple spines and adjacent dendritic shafts" (p. 753). Further, they found that IP_3 causes prolonged depression of parallel fiber-PC signals which is "limited to synapses where the Ca2+ concentration is raised" (p. 753).

4.8 Motor Equivalence

The term "motor equivalence" refers to the observation that humans can perform tasks that were learned with one end effector using other end effectors. A common example of motor equivalence is signing one's name with a pen held in one's toes or even in one's mouth. In this example, the task of signing, learned using a hand, is performed strikingly well using a foot or the mouth. The style of the signature is often recognizable as belonging to a particular writer, even when it is written with the foot or mouth. In its simplest form, motor equivalence suggests that there is an abstract, effector-independent representation of the movement in the brain.

However, the matter becomes more complex when one considers the additional observation that movements learned using the dominant hand are *not* reproduced as accurately using the non-dominant hand or foot. Further, the style of the writing using a non-dominant hand or foot is not easily recognized as belonging to a given writer when compared to writing by the dominant hand or foot. A quantitative study of the writing of dominant versus non-dominant end-effectors was done by Wright (1990). He found that there were

significant differences between the writing of the dominant end-effector and the non-dominant one, implying the existence of separate motor programs for right and left limbs. Based on these findings, one hypothesis is that the motor program, learned over many years of practice for a given hand, must undergo a coordinate transformation in order for it to be used for the contralateral, anatomically "reversed" limb. The coordinate transformation is imperfect, and the imperfections result in the observed differences in the writing of left and right end-effectors. In the case of writing with the ipsilateral hand or foot, the coordinate transformation is less complex since the homologous muscles require no reversal of motor commands.

Evidence for either an abstract, effector independent representation of a movement, and/or a coordinate transformation from one effector to another was found by Rijntjes et al. (1999). The authors found that the regions of premotor cortex involved in a learned, hand movement task were also active when the ipsilateral foot carried out the learned movement, but not when the foot engaged in a spontaneous, unlearned movement. Thus, either an abstract set of learned motor commands or "movement parameters" is stored and used for the hand and foot, or else a hand-specific motor memory is undergoing a coordinate transformation in order to allow the foot to benefit from the learned hand-movement information.

How does AVITEWRITE deal with the issue of motor equivalence? Evidence supports a muscle/synergy specific cerebellar control system (Rispal-Padel, 1993; Thach et al., 1993; Welsh & Llinas, 1997). Thus, the cerebellar muscle control signals learned by the model would apply only to the muscle synergies involved in learning the handwriting

task. What happens to the control signals which are sent to the cortex from the cerebellar memory when a writing task must be accomplished by the foot? Do they undergo a coordinate transformation so that the foot can benefit from the movement learned by the hand? AVITEWRITE does not explicitly analyze the roles of cortical regions in sensory-motor coordinate transformations. However, artists who draw by holding a brush in a foot or in the mouth, possibly due to hand or spinal cord injury, may develop additional skill over years of practice. AVITEWRITE suggests that spectral learning specific to the muscle synergies required for mouth or foot-mediated drawing could allow such performance improvement over time.

The above discussion of motor equivalence also raises the issue of the coordinate scheme in which AVITEWRITE operates. The visual difference vectors DV_{vis} are in spatial/cartesian coordinates corresponding to planar hand movements. The cerebellar output to the muscle synergies should be in motor coordinates, but it appears to be in spatial coordinates in AVITEWRITE since it is combined, after temporary storage in the spectral working memory buffer, with DV_{vis} in the size-scaled, memory enhanced difference vector, DV_S. AVITEWRITE omits explicit modelling of the spatial-to-motor coordinate transformations that would be needed to convert both the DV_{vis} and the climbing fiber error/teaching signals to motor coordinates since such transformations have been addressed in previous work, such as the sector maps of saccade error correction in Grossberg and Kuperstein (1986, pp. 66-68), the DIRECT model of motor equivalent reaching and tool use of Bullock et al. (1993a), and the DIVA model of speech production (Guenther et al., 1998; Callan et al., 2000).

4.9 Teaching versus Correction

One potential source of confusion in the AVITEWRITE model is the use of climbing fiber "error" signals to learn movements when no errors have yet been committed. For example, on the first learning trial in the model simulations, there is no pre-existing cerebellar memory for a given shape. As the reactive movement is made toward a target, what triggers the climbing fiber activity even if the reactive movement generates no error? Although evidence exists for a role of climbing fiber signals in error correction (Gellman et al., 1985; Ito, 1991; Ito & Karachot, 1992; Oscarsson, 1969), no experiments have yet been done to differentiate climbing fiber "error" signals from possible climbing fiber "teaching" signals which may arise prior to error commission. The model assumes that the Difference Vector to a visual target acts like a teaching signal whenever it occurs.

4.10 VITEWRITE and AVITEWRITE: Some Differences

In order to avoid potential confusion among readers familiar with the VITEWRITE model of Bullock et al. (1993b), several of the key differences between AVITEWRITE and VITEWRITE are highlighted here. The first difference which should be apparent is that AVITEWRITE is adaptive. It can learn to generate the strokes for particular letters which needed to be predefined through Planning Vectors in VITEWRITE. If VITEWRITE had been capable of learning and remembering how to write letters, then the sequence of Planning Vectors would have constituted its memory.

AVITEWRITE's ability to learn came at the price of greater system complexity and the need for a large memory capacity relative to VITEWRITE. One advantage of VITE-

WRITE was that relatively few Planning Vectors were required to represent a letter. For example, VITEWRITE would require only five Planning Vectors (three for the x synergy and two for the y synergy) to represent the movement amplitudes and directions for the letter *l*. In contrast, AVITEWRITE's spectra use approximately 200 Purkinje cells to store the synergy activations to write the letter *l*. Further, the spectral working memory buffer used to transiently store spectral output and read it out at a speed-dependent rate may store up to about 135 values of the spectral output (Figure 3.9). AVITEWRITE's larger memory capacity is needed because it learns and stores continuous, time-varying information about muscle synergy activation which must be read from memory throughout a given movement. However, the pattern of synergy activation in VITEWRITE arises from the interaction of a discrete number of Planning Vectors and integrated Movement Vectors with a gradually increasing *GO* signal. Thus, VITEWRITE stores the pattern of muscle synergy activation implicitly as abstract Planning Vectors that are used to form a relatively small number of widely-spaced targets for movement. AVITEWRITE stores the pattern of muscle synergy activation explicitly as synaptic weights which yield a continuous, time-varying pattern of Purkinje cell potentials. It then uses this continuous memory signal to form many closely-spaced targets for the movement.

The nature of the *GO* signals used in the two models also differs. In AVITEWRITE, a fast rising, effectively binary *GO* signal is used which is reset at the start of a given synergy's activation. When opponent synergies switch control of a movement, then the *GO* signal is shut off for the prior synergy and turned on for the current synergy. During visually guided movements, when particular regions of the letter have been reached, such as

intermediate stopping points in segmented letters (*s* in Figure 3.10, *m*, *w*, etc.) or the end of the letter, then the *GO* signal for all synergies is reset if the movement velocity is below a threshold value or a direction reversal occurs. If visual feedback were lacking, then a proprioceptive, velocity-dependent *GO* reset rule could be used (such as resetting *GO* when the tangential velocity is below a threshold value and the acceleration is negative). In AVITEWRITE, *GO* reset does not explicitly cause memory readout either from the spectra or from the spectral working memory. It is the speed of movement, determined by the size of the *GO* signal, which affects the rate of readout from the spectral working memory by changing the rate at which the memory-modulated targets, TPV_m, are reached.

In contrast, VITEWRITE uses a gradually and indefinitely increasing *GO* signal which is reset for a given synergy when movement velocity returns to zero upon completion of a planned DV component. Further, *GO* reinitiation is linked to readout of the next Planning Vector. In VITEWRITE, movement ends and the *GO* signal is shut off when the last target, derived from the Planning Vector, has been reached.

In summary, what VITEWRITE lacks relative to AVITEWRITE is the ability to learn. What AVITEWRITE lacks relative to VITEWRITE is memory sparseness and architectural simplicity. Future directions for research include making AVITEWRITE more similar to its predecessor with regard to these two attributes. The cerebellar-cortical learning model of Rhodes and Bullock (Rhodes, 2000) is relevant here because it treats sequence learning while assuming only a small capacity motor working memory. However, it has not been applied to handwriting acquisition.

4.11 Handwriting Models: General Overview

As the human handwriting database has grown, so too has the number of models which attempt to replicate and/or explain the human data. Two general methodologies of handwriting modelling become apparent from a review of the literature. The first methodology focuses on computational models which attempt to replicate features of human handwriting, such as velocity and acceleration profiles, and relations between different aspects of the movement dynamics, such as curvature and angular velocity. Plamondon and Maarse (1989) refer to such models as exemplifying the "bottom-up" approach to handwriting modelling. Such bottom-up models include optimization models (Edelman & Flash, 1987; Flash & Hogan, 1985; Wada & Kawato, 1995) which minimize performance measures such as the third and fourth time derivatives of position or the change in torque, and oscillator models (Hollerbach, 1981; Saltzman & Kelso, 1987; Singer & Tishby, 1994) which combine various velocity sinusoids to yield different movement shapes. More recently, Plamondon and Guerfali (1998) describes a "delta-lognormal" model which defines movement velocity as a Gaussian, or normal, function of nine motor system parameters. Some bottom-up models adequately fit various constraints imposed upon them by the human movement data. Unfortunately, most bottom-up models make only passing reference to biological implementation of the computational system. The goal of bottom-up models is to "produce handwriting forms and not to simulate the psychomotor process" (Plamondon & Maarse, 1989, p. 1062). Little if any explanation is usually given of how the human brain may carry out often intensive calculations that require global knowledge of an entire planned movement trajectory, as in the optimization

models. Further, most bottom-up handwriting models describe static systems, with no ability to adapt to changes over time through learning.

The second methodology of handwriting modelling focuses on psychologically descriptive models (Ellis, 1982; Kellogg, 1996; van Galen, 1991; van Galen et al., 1986). These “top down” models usually summarize many of the requirements of a handwriting system by addressing as much data as possible. Thus, they do address such issues as learning, movement memory, planning, and sequencing, coarticulatory and task complexity effects of strokes, etc., which are often omitted from bottom-up models. However, most top-down models provide no mathematical description of their words and do not attempt computer simulations to verify that their proposed systems can actually perform the tasks they claim.

AVITEWRITE attempts to unify the two approaches to handwriting modelling described above by addressing both the psychological and neurobiological constraints on the task of learning to write.

4.11.1 Summary and Critique of Some Representative Models

Hollerbach (1981) described the handwriting process as a system of coupled, horizontal and vertical direction oscillators superimposed on a rightward horizontal movement of constant velocity. He used such a system to generate various cursive writing trajectories, and was able to modify size and slant of the shapes by modifying frequency and amplitude relations in the oscillatory system. Although Hollerbach did not explicitly address speed scaling, one could imagine that altering the “constant” velocity horizontal progres-

sion along with some frequency changes in the oscillators would allow speed scaling. Whether such speed scaling could be accomplished with relative shape invariance is an open question. His model assumed the existence of some baseline oscillations, reminiscent of shape primitives (Edelman & Flash, 1987; Morasso, 1986), upon which sequences of modulations are imposed to generate specific shapes. Hollerbach suggested that motor programs, stored movement commands resulting from learning, consist of stored sequences of phase and amplitude modulations of the fundamental oscillatory process.

Hollerbach's model is clearly a "bottom-up model", since it deals with trajectory formation while avoiding such issues as cognitive representations of allographs or the details of motor learning. Indeed, unless noted otherwise, none of the representative models discussed herein deal with the learning of handwriting. As attractive as Hollerbach's model is in its conceptual simplicity, it fails to provide a bridge between target-driven reaching movements and the different, yet related, hand movements of writing. Further objections to the idea of oscillatory motor control are raised by Schomaker et al. (1989) and include the observation that humans have difficulty generating simple repetitive letter patterns for longer than two seconds without errors, and that discrete stroke-to-stroke size and timing variations occur often in handwriting.

Edelman & Flash (1987) presented a bottom-up model of trajectory formation based on dynamic minimization of the square of the third (jerk) or fourth (snap) derivative of hand position. The version which minimizes snap is reported to yield better correlation with human experimental data. The model assumes that all letters are formed by a concatenation of shape primitives, such as "cup", similar to a letter U, and "oval", like a letter

O. Further, the model generates each stroke primitive by use of a viapoint, an intermediate target prior to the end of the stroke. The model output is compared to human experimental data, and strong correlations are reported between model-generated position, velocity, and acceleration traces and the human counterparts. The inverse relation between movement velocity and curvature seen in human writing is demonstrated by the model. The use of numerical estimations of the degree of fit to the data is emphasized and contrasted with the purely subjective fit estimates in some models.

Unfortunately, no discussion is given of how a human is expected to actually minimize the fourth, or even the third derivative of hand position across an entire movement trajectory. Golgi tendon organs measure muscle tension (Gordon & Ghez, 1991). Further, Matthews (1972) showed that muscle receptors sensitive both to the length of the muscle and to the velocity of stretching exist. Thus, the first derivative of hand position is probably available to higher motor control centers. However, evidence supporting neural computation of higher derivatives of hand position is lacking. Is jerk or snap minimization merely an epiphenomenon of human trajectory planning? Finally, the shape primitives and corresponding viapoints are chosen arbitrarily in this model.

Schomaker et al. (1989) presented a production system model of handwriting with both top-down and bottom-up elements. The top-down elements include internal abstract categories of allograph symbols, as well as punctuation and “blanks” to drive horizontal movement. The bottom-up portion generates planar target trajectories of the pen-tip. The model is based on stroke chaining, in contrast to the continuous movement generation of Hollerbach (1981). A stroke is defined as a “combined acceleration plus deceleration

movement unit for a spatial axis in Cartesian space" (p. 157) with a near sinusoidal velocity profile. Unfortunately, no explanation is given of the manner in which humans generate such velocity profiles. Further, the model assumes "locked" x and y velocity commands, in contrast to findings showing independent x and y velocity scaling (Wann & Nimmo-Smith, 1990; Burton et al., 1990). Finally, Schomaker et al.'s model is descriptive but not predictive for the following reason. The model requires that the stroke duration for generating a particular curve be specified in advance of the movement. The authors obtain the stroke duration by analyzing previous samples of that movement. Thus, their trajectory generation system is circular, in that a movement must already have been completed in order to obtain a key parameter required for the model to generate that movement.

Van Galen (1991) presented a top-down description of the handwriting task without attempting actual trajectory generation. Based on various psychophysical data, a hierarchical architecture consisting of processing modules, ranging from the intention to write through muscular adjustments, and memory storage buffers for each module was presented. Evidence suggesting concurrent long-term memory retrieval and short-term storage of multiple upcoming strokes (p. 180) led Van Galen to hypothesize that the "output from each [processing module] stage is transiently stored in working memories... [to] accommodate for time frictions between information processing activities in different modules... A processor lower in the hierarchy can read information from the buffer with a unit size which is appropriate for that stage" (p. 182). Van Galen further hypothesized that the letter forms are stored in long-term memory as spatial codes for guiding the writ-

ing movement, whereas handwriting size and speed are monitored in a separate stage. These hypotheses are relevant to the proposed AVITEWRITE model. The accommodation of "time frictions" mentioned above is consistent with the mechanism for speed scaling in the AVITEWRITE model.

The paper of Morasso and Sanguineti (1993) is a rare attempt to computationally explain some top-down cortical phenomena in handwriting, which also demonstrates how reaching and handwriting movements may be learned and generated by a common cortical mechanism. The authors developed SOBoS, a self-organizing body schema (a cortical feature map) which is capable of "learning, during exploratory movements, ...motor to sensory transformations" (p. 219). Motor planning is accomplished by minimizing the task constraints using a gradient descent search across the cortical neural field. Learning occurs through the application of a Hebbian learning rule to the "neighborhood of the resonant element" (p. 221); that is, to the group of cells most activated by a particular sensory input pattern.

Since reaching experiments have shown that intermediate positions of the end-effector "must be generated by the motor planner in addition to the final one" (p. 226), the authors assumed that motor programs consist of sequences of targets, or via-points. Via-points are smoothly joined by nonlinear movement integration to the target, reminiscent of the VITE model (Bullock & Grossberg, 1988a, 1988b, 1991) described earlier. As in the VITE model, realistic, asymmetric velocity profiles are generated using a speed-controlling *GO* signal, defined by Morasso and Sanguineti (1993) as a smoothly growing and decaying Difference of Sigmoids (DOS). The authors believe such a DOS to be "more

plausible for supporting the smooth chaining" of strokes than the "digital control that shuts off the *GO* signal ...in the VITE model" (p. 227).

The only trajectory simulations presented by these authors are a few curves with asymmetric velocity profiles. No mechanism of via-point selection or sequential learning was presented. Finally, the model is mainly a cortical model, with brief reference to the basal ganglia in regard to the *GO* signal. No use is made of cerebellar processing, although the authors claim that the model can "initiate actual movements by supplying the cerebral motor cortex and the cerebellar cortex with the necessary planning patterns" (p. 233).

A further development of the dynamic optimization and via-point approach to bottom-up handwriting modelling is presented by Wada and Kawato (1995). The two main innovations of their model relative to earlier optimization/via-point models are the use of torque minimization as a trajectory criterion as well as a system for choosing and optimizing the number of via-points needed to regenerate a given shape with a particular error threshold. Although the authors believe that either a minimum muscle-tension-change or a minimum motor-command change criterion for trajectory formation would be a "biologically more plausible model" (p. 4), they use the minimum torque-change criterion for simplicity and ease of simulation. They also note that a minimum jerk model in joint angle space (Flash & Hogan, 1985) is equivalent to the minimum torque-change model when arm dynamics are linearly approximated.

The first difference between Wada & Kawato's torque minimization approach and previous minimum jerk models is the use of a "biologically plausible neural network" to achieve torque minimization, as opposed to the "implausible" matrix inversion required

of the spline method of jerk minimization. The second difference is the use of a via-point selection algorithm which chooses via-points to minimize the sum of the square error between a template trajectory and the model's output. Via-points are iteratively added to the movement path by defining the points at which maximum deviation from the template trajectory occurs as via-points. The error-threshold at which a point is added to the list of via-points can be modified to alter the accuracy of the model's trajectory.

Such a flexible error-threshold is reminiscent of the type of attentional mechanism which determines the accuracy of a movement in the AVITEWRITE model. The via-point selection algorithm is suggestive of a possible learning mechanism which iteratively stores an increasing number of via-points until a shape representation of desired accuracy is obtained. However, Wada & Kawato's model must complete an entire trajectory to a final target before the global trajectory information is available for their algorithm to choose a via-point. For example, their algorithm would make a straight line from the starting point of a letter "U" to the last point of the letter on the first trial of via-point selection. Thus their system is designed to make gross errors, approximating a U with a straight line, on its early trials. In other words, their via-point selection algorithm maximizes error in order to choose via-points. A more biologically reasonable approach would be to choose via-points so as to minimize error, just as targets are chosen by AVITEWRITE. Wada & Kawato demonstrated that their model can reproduce a given series of letters. However, no discussion was given of the model's ability to match other human performance data, such as velocity profiles or an inverse relation between curvature and tangential velocity.

Plamondon & Guerfali (1998) presented a bottom-up handwriting model using "delta-lognormal synergies". This name refers to the authors' definition of the velocity of a muscle synergy as a Gaussian function of the movement parameters that varies logarithmically with time. It is therefore not surprising to find that the model generates Gaussian, bell-shaped velocity profiles similar to human bell-shaped velocity profiles. The model uses superposition of strokes toward "virtual" via-points to generate continuous curves. As in Schomaker et al. (1989), Plamondon & Guerfali (1998) suggest that stroke timing is crucial in determining trajectory shape. However, as in Schomaker et al. (1989), no mechanism to learn and store such timing relations is described. One noteworthy feature of the Plamondon & Guerfali model is that the via-points are not necessarily ever reached. A new stroke may be launched toward a via-point in a different direction and superimposed on the prior stroke so that the first "virtual" via-point is not reached. The authors suggest that the subject is able to predict the amount of time it would take to reach a via-point. "The next stroke can thus be initiated before the completion of the current one, as though this latter stroke had been completed and its target had been reached" (p. 121). But how does the subject know when to launch the next stroke in order to generate a particular shape? Instead of choosing a via-point which is far away and does not need to be reached in order to generate a particular shape, why not choose a closer via-point and reach it?

The authors demonstrate an impressive fit between the model output and human data. Shape and tangential and angular velocities generated by the model are very close to those of human subjects. Further, the Two-Thirds Power Law relation between angular

velocity and curvature is demonstrated for the limited range of elliptical movements for which the law accurately describes human handwriting. Size changes are simulated by increasing the values of muscle synergy agonist and antagonist activation proportionally so that movement duration is kept constant. Writing slant can be modified by uniformly translating virtual via-point positions. Movement duration can be altered by changing agonist and antagonist activations while keeping individual stroke length constant. The authors state that there will be a loss in spatial precision as stroke duration is reduced. However, human handwriting speed can be varied by a factor of about 2.8 with only small shape changes (Wright, 1993). Plamondon et al. do not address this relative shape constancy over such a wide range of speeds. Finally, it should be noted that the excellent performance of the delta-lognormal model resulted after optimizing the model parameters and timing for each stroke to fit the curvilinear velocity and angular velocity traces of the human data.

It would be of interest to determine whether the trajectories and velocity profiles generated by AVITEWRITE could be accurately described by the delta-lognormal model which has yielded such good empirical fits to human curved trajectories. However, as noted previously in section 3.4.7 when describing the quantitative differences between the maximum letter upstroke velocity of Greer and Green's (1983) human subjects and the corresponding maximum velocity for AVITEWRITE's letter *l*, AVITEWRITE lacks a detailed description of an arm and uses a simplified central representation of arm muscle synergies, thereby raising doubt about its ability to accurately predict features of muscle dynamics during movement. Since it is not clear what features of human curved move-

ments allow for the delta-lognormal description's accuracy, it is difficult to predict whether AVITEWRITE's performance could be described by the delta-lognormal rule. Testing this possibility is one area for future research.

4.11.2 The Cerebellar Reaching Model of Barto et al. (1999)

A model similar in several respects to the current handwriting model was described by Barto et al. (1999). In their model, the authors describe a simplified cerebellar system for learning to reach to a target, utilizing climbing fiber error feedback to train the system to avoid target overshoots or undershoots. Barto et al. state that "the central control problem... is to terminate the... command sent to the agonist muscle at an appropriate time during the movement" (p.566). However, they also believe that "the dynamics of the stretch reflex [in the antagonist muscle] should then bring the movement to a halt at a desired endpoint" (p. 566). Although the stretch reflex may be sufficient to stop the movement for a simple reaching task (Ghez & Martin, 1982), it is insufficient to learn the direction reversals required for curved writing movements. Thus, not only must the agonist muscle command be terminated at the appropriate time, but the antagonist muscle command must be started at the appropriate time for curved writing movements. Such appropriately timed synergy switching is an important part of the AVITEWRITE handwriting learning model, and is detailed in the Model Description section.

Whereas AVITEWRITE attempts to unify features of an attentive cortico-cerebellar-basal ganglia system whose patterns of synergy activations may be modified through learning by populations of Purkinje cells (PCs), Barto et al.'s reaching model joins

together a spring-mass system to represent the limb motor plant with a single Purkinje cell. Thus, the Barto et al. model has more bottom-up components than the present model. It also has a greater focus on the synaptic connections of the single Purkinje cell modelled, including 2000 mossy fibers which are recoded into 40,000 binary parallel fibers that synapse on the modelled Purkinje cell. Since AVITEWRITE uses populations of Purkinje cells to represent complex movement sequences, it simplifies the representation of the synaptic connections to individual Purkinje cells. The 40,000 parallel fiber-Purkinje cell (pf-PC) synapses are represented by a single synaptic weight for each of the 200 to 400 Purkinje cells involved in the writing of a typical letter by the model.

One assumption common to both Barto et al.'s reaching model and the present handwriting model is that the pattern of long term depression learned by the Purkinje cell(s) causes a pattern of disinhibition of the cerebellar nuclei. The cortico-rubro-cerebellar network is represented in the reaching model as "simply an inverting mechanism that converts the inhibitory output of PCs into a positive command signal" (Barto et al., 1999, p.570). Such a representation is equally applicable to the AVITEWRITE model and the earlier spectral timing model of Fiala et al. (1996). Thus, the bell-shaped patterns of cerebellar memory activity shown in Figures 3.10 and 3.14 represent patterns of Purkinje cell long term depression summed across the Purkinje cell population. The pattern of PC activity inhibition leads to a pattern of disinhibition at the cerebellar nuclei.

Barto et al. also address the problem of delayed error feedback. "The training information in the form of CF activity is significantly delayed with respect to the relevant DZ [Purkinje cell Dendritic Zone] activity due to the combined effects of movement duration

and conduction latencies" (p. 11). To cope with this problem, they adopt Klopf's (1972, 1982) hypothesis of synaptic eligibility traces. "Appropriate activity at a synapse is hypothesized to set up a synaptically-local memory trace that makes the synapse "eligible" for modification if, and when, the appropriate training information arrives within a short time period" (p. 574). They compute the eligibility by simulating a second-order linear filter, with binary inputs whose impulse response rises quickly and then decays slowly after a "triggering event" (analogous to the conditioned stimulus in Fiala et al., 1996). "A synapse is therefore maximally eligible 255 ms after the triggering event and becomes effectively ineligible approximately 2 sec later, assuming no additional triggering events occur" (p. 575). The parallel fiber/PC synaptic weights are then modified in a manner proportional to the synapse's eligibility trace.

The idea of an "eligibility trace", allowing synaptic modification over a relatively prolonged period of time after a parallel fiber input, is strikingly similar to the spectrum of delayed Purkinje cell activations after a conditioned stimulus (CS) hypothesized in Fiala et al. (1996), and incorporated into the AVITEWRITE model. As seen in Figure 4.3, even the shape of the eligibility trace is qualitatively similar to a Purkinje cell activation response as simulated using the Fiala et al. (1996) model equations. The key difference is that Barto et al.'s eligibility trace occurs at the level of an individual synapse, whereas Fiala et al.'s spectral timing occurs at the level of an entire Purkinje cell. Barto et al.'s eligibility trace achieves selective modification of particular pf-PC synaptic strengths when a cf input arrives within 2 seconds of a triggering event. Fiala et al.'s simulations of a spectrum of phase delayed PC activations extend the period of time during which a cf

input may alter synaptic weights to about 4 seconds.

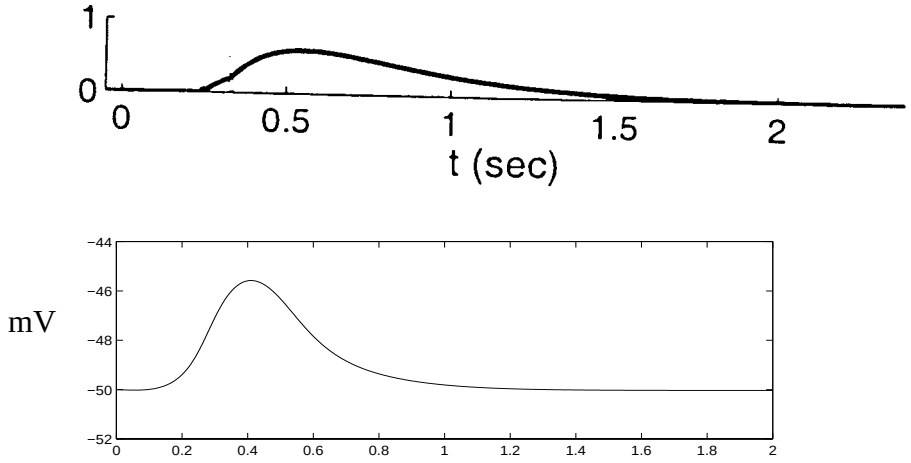

Figure 4.3. Two time spanning signals which allow synaptic modification following delayed stimulus input. *Top:* Eligibility trace of Barto et al. (1999) (Reproduced with permission); *Bottom:* A depolarization response of a single Purkinje cell generated from the Fiala et al. (1996) model equations.

4.12 Conclusion

The AVITEWRITE model describes how a person may learn to make curved handwriting movements. This model incorporates aspects of two previous groups of models: the spectral timing models of Fiala, Grossberg, & Bullock (1996), Grossberg & Merrill (1992), and Grossberg & Schmajuk (1989); and the VITE and VITEWRITE models of Bullock & Grossberg (1988a, 1988b, 1991) and Bullock, Grossberg, and Mannes (1993), respectively.

The AVITEWRITE model clarifies how the cerebral cortex, the cerebellum, and basal ganglia may interact during complex learned movements. There is both cooperation and competition between reactive vision-based imitation and planned memory readout. The cooperation includes interactions between cortical difference vectors and cerebellar,

adaptively timed spectral learning. The competition arises between cerebellar control of learned movements and error-driven, cortical control of reactive movements to attentionally chosen visual targets. The model suggests that there is an automatic shift in the balance of movement control between these cortical and cerebellar processes during the course of learning. Reactive movements are made to attentionally chosen targets on a curve at the same time as movement error signals are generated which allow the cortico-cerebellar system to learn how to draw the curve. Memory-based movements gradually supersede visually-driven movements as learning progresses. Finally, the model shows how challenging psychophysical properties of planar hand movements may emerge from this cortico-cerebellar-basal ganglia interaction.

Appendix: Parameter Values

The parameter values for the system equations are given in the text describing the equations. The variable parameters used during learning of the alphabet in Figure 3.16 are listed in Table A.1. The variable parameters used during learning of the O, U, and gamma in Figure 3.17 are listed in Table A.2.

Table A.1. Parameter values for the alphabet shown in Figure 3.16. $J = 20$.

Letter	Attentional radius (r_a)	Spectral density (Δt)	Number of Trials
a	0.080	0.10	16
b	0.150	0.10	11
c	0.060	0.10	77
d	0.080	0.15	10
e	0.035	0.08	74
f	0.100	0.15	15
g	0.0800	0.15	65
h	0.0900	0.10	8
i	0.0800	0.20	14
j	0.1000	0.15	27
k	0.0900	0.10	14
l	0.0550	0.10	37
m	0.0700	0.10	15
n	0.0750	0.08	14
o	0.0500	0.20	12
p	0.0825	0.15	7
q	0.1000	0.15	10
r	0.0650	0.10	9
s	0.0750	0.20	56
t	0.0800	0.15	8
u	0.0650	0.20	15
v	0.0700	0.10	10
w	0.0700	0.10	18
y	0.0875	0.10	31
z	0.1200	0.10	15

Letter	Attentional radius (r_a)	Spectral density (Δt)	Number of Trials
O	0.050	0.07	13
U	0.050	0.05	18
γ	0.055	0.10	49

Table A.2. Parameter values for the letters O, U, and gamma shown in Figure 3.17. J = 20.

References

Abend, W., Bizzi, E., Morasso, P. (1982). Human Arm Trajectory Formation. *Brain*, **105**, 331-348.

Alston, J., Taylor, J. (1987). *Handwriting: Theory, Research, and Practice*. New York: Nichols.

Andersen, R., Essick, G., Siegel, R. (1985). Encoding of spatial location by posterior parietal neurons. *Science*, **230**, 456-458.

Andersen, R. (1995). Encoding of intention and spatial location in the posterior parietal cortex. *Cerebral Cortex*, **5**, 457-469.

Arroyo-Anllo, E. M., Botez-Marquard, T. (1998). Neurobehavioral dimensions of olivopontocerebellar atrophy. *Journal of Clinical and Experimental Neuropsychology*, **20**, 52-59.

Atkeson, C. G., Hollerbach, J. M. (1985). Kinematic Features of Unrestrained Vertical Arm Movements. *The Journal of Neuroscience*, **5**, 2318-2330.

Bannerman, D. M., Yee, B. K., Good, M. A., Heupel, M. J., Iversen, S. D., Rawlins, J. N. (1999). Double dissociation of function within the hippocampus: a comparison of dorsal, ventral, and complete hippocampal cytotoxic lesions. *Behavioral Neuroscience,* **113**, 1170-1188.

Bartha, G. T., Thompson, R. F., Gluck, M. A. (1991). Sensorimotor learning and the cerebellum. In M. Arbib, J. Ewert (Eds.). *Visual structures and integrated functions*. Berlin: Springer.

Barto, A. G., Fagg, A. H., Sitkoff, N., Houk, J. C. (1999). A Cerebellar Model of Timing and Prediction in the Control of Reaching. *Neural Computation*, **11**, 565-594.

Berardelli, A., Hallet, M., Rothwell, J. C., Agostino, R., Manfredi, M., Thompson, M., Thompson, P. D., Marsden, C. D. (1996). Single-joint rapid arm movements in normal subjects and in patients with motor disorders. *Brain*, **119**, 661-674.

Bernstein, N. (1967). *The coordination and regulation of movements.* London: Pergamon Press.

Bizzi, E., Saltiel, P., Tresch, M. (1998). Modular organization of motor behavior. *Zeitschrift fur Naturforschung* [C], **53**, 510-517.

Bloedel, J. R. (1994). Functional heterogeneity with structural homogeneity: How does the cerebellum operate? In P. Cordo, S. Harnad (Eds.). *Movement control* (pp. 64-76). Cambridge: Cambridge University Press.

Buchanan, T. S., Almdale, D. P. J., Lewis, J. L., Rymer, W. Z. (1986). Characteristics of synergic relations during isometric contractions of human elbow muscles. *Journal of Neurophysiology*, **56**, 1225-1241.

Bullock, D., Cisek, P., Grossberg, S. (1998). Cortical Networks for Control of Voluntary Arm Movements Under Variable Force Conditions. *Cerebral Cortex*, **8**, 48-62.

Bullock, D., Fiala, J. C., Grossberg, S. (1994). A neural model of timed response learning in the cerebellum. *Neural Networks*, **7**, 1101-1114.

Bullock, D., Grossberg, S. (1988a). The VITE model: a neural command circuit for generating arm and articulator trajectories. In J. Kelso, A. Mandell, M. Shlesinger (Eds.). *Dynamic patterns in complex systems*. Singapore: World Scientific.

Bullock, D., Grossberg, S. (1988b). Neural Dynamics of Planned Arm Movements: Emergent Invariants and Speed-Accuracy Properties During Trajectory Formation. *Psychological Review,* **95**, 49-90.

Bullock, D., Grossberg, S. (1991). Adaptive neural networks for control of movement trajectories invariant under speed and force rescaling. *Human Movement Science,* **10**, 3-53.

Bullock, D., Grossberg, S., Guenther, F. H. (1993a). A Self-Organizing Neural Model of

Motor Equivalent Reaching and Tool Use by a Multijoint Arm. *Journal of Cognitive Neuroscience*, **5**, 408-435.

Bullock, D., Grossberg, S., Mannes, C. (1993b). A neural network model for cursive script production. *Biological Cybernetics*, **70**, 15-28.

Buonomano, D. V., Mauk, M. D. (1994). Neural network model of the cerebellum: temporal discrimination and the timing of motor responses. *Neural Computation*, **6**, 38-55.

Burns, P.C. (1962). *Improving handwriting instruction in elementary schools.* Minneapolis (pp. 45-46). Minneapolis, MN: Burgess Publishing Co..

Burton, A.W., Pick Jr., H.L., Holmes, C., Teulings, H. (1990). The Independence of Horizontal and Vertical Dimensions in Handwriting with and without Vision. *Acta Psychologica*, **75**, 201-212.

Callan, D. E., Kent, R. D., Guenther, F. H., Vorperian, H. K. (2000). An auditory-feedback-based neural network model of speech production that is robust to developmental changes in the size and shape of the articulatory system. *Journal of Speech, Language, and Hearing Research*, **43**, 721-736.

Caminiti, R., Genovesio, A., Marconi, B., Mayer, A. B., Onorati, P., Ferraina, S., Mitsuda, T., Giannetti, S., Squatrito, S., Maioli, M. G., Molinari, M. (1999). Early coding of reaching: frontal and parietal association connections of parieto-occipital cortex. *European Journal of Neuroscience*, **11**, 3339-3345.

Chapeau-Blondeau, F., Chauvet, G. (1991). A neural network model of the cerebellar cortex performing dynamic associations. *Biological Cybernetics*, **65**, 267-279.

Chieffi, S., Allport, D. A. (1997). Independent coding of target distance and direction in visuo-spatial working memory. *Psychological Research*, **60**, 244-250.

Coltz, J. D., Johnson, M. T. V., Ebner, T. J. (1999a). Cerebellar Purkinje cell simple spike discharge encodes movement velocity in primates during visuomotor arm tracking. *The Journal of Neuroscience*, **19**, 1782-1803.

Coltz, J. D., Johnson, M. T. V., Ebner, T. J. (1999b). Cerebellar Purkinje cell complex spike discharge during visuomotor arm tracking in primates: Relationships to movement parameters and comparisons to simple spike discharge. *Society for Neuroscience Abstracts*, **25**, 372.

Contreras-Vidal J.L., Grossberg, S., Bullock, D. (1997). A Neural Model of Cerebellar Learning for Arm Movement Control: Cortico-Spino-Cerebellar Dynamics. *Learning and*

Memory, **3**, 475-502.

Dagher, A., Owen, A. M., Boecker, H., Brooks, D. J. (1999). Mapping the network for planning: a correlational PET activation study with the Tower of London task. *Brain*, 122, 1973-1987.

Doyon, J., LaForce Jr., R., Bouchard, G., Gaudreau, D., Roy, J., Poirier, M., Bedard, P., Bedard, F., Bouchard, J. (1998). Role of the striatum, cerebellum and frontal lobes in the automatization of a repeated visuomotor sequence of movements. *Neuropsychologia*, **36**, 625-641.

Ebner, T. J. (1998). A role for the cerebellum in the control of limb movement velocity. *Current Opinion in Neurobiology*, **8**, 762-769.

Edelman, S., Flash, T. (1987). A model of handwriting. *Biological Cybernetics*, **57**, 25-36.

Ellis, A. (1982). Spelling and Writing (and Reading and Speaking). In A. Ellis (Ed.). *Normality and Pathology in Cognitive Functions*. London: Academic Press.

Feldman, A. G., Levin, M. F. (1995). The origin and use of positional frames of reference in motor control. *Behavioral Brain Science*, **18**, 723-806.

Fiala, J., Grossberg, S., Bullock, D. (1996). Metabotropic glutamate receptor activation in cerebellar Purkinje cells as substrate for adaptive timing of the classically conditioned eye-blink response. *The Journal of Neuroscience*, **16**, 3760-3774.

Finch, E.A., Augustine, G.J. (1998). Local calcium signalling by inositol-1,4,5-trisphosphate in Purkinje cell dendrites. *Nature*, **396**, 753-756.

Flash, T., Hogan, N. (1985). The Coordination of Arm Movements: An Experimentally Confirmed Mathematical Model. *The Journal of Neuroscience*, **5**, 1688-1703.

Fowler, C., Saltzman, E. (1993). Coordination and coarticulation in speech production. *Language and Speech*, **36**, 171-195.

Freeman, F. N. (1914). *The Teaching of Handwriting* (pp. 83-84). Boston, MA: Houghton-Mifflin, The Riverside Press Cambridge.

Freeman, J. A. (1969). The cerebellum as a timing device: an experimental study in the frog. In R. Llinas (Ed.). *Neurobiology of cerebellar evolution and development*, pp. 397-420. Chicago: American Medical Association.

Fu, Q.G., Mason, C.R., Flament, D., Coltz, J.D., Ebner, T.J. (1997). Movement kinematics encoded in complex spike discharge of primate cerebellar Purkinje cells. *Neuroreport*, **8**, 523-529.

Furner, B. (1983). Developing handwriting ability: A perceptual learning process. *Topics in Learning and Learning Disabilities*, **3**, 41-54.

Gellman, R., Gibson, A.R., Houk, J.C. (1985). Inferior olivary neurons in the awake cat: detection of contact and passive body displacement. *Journal of Neurophysiology*, **54**, 40-60.

Georgopoulos, A. P., DeLong, M. R., Crutcher, M. D. (1983). Relations between parameters of step-tracking movements and single cell discharge in the globus pallidus and subthalamic nucleus of the behaving monkey. *The Journal of Neuroscience*, **3**, 1586-1598.

Georgopoulos, A. P., Kalaska, J. F., Caminiti, R., Massey, J. T. (1982). On the relations between the direction of two-dimensional arm movements and cell discharge in primate motor cortex. *The Journal of Neuroscience*, **2**, 1527-1537.

Georgopoulos, A. P., Kalaska, J. F., Massey, J. T. (1981). Spatial trajectories and reaction times of aimed movements: Effects of practice, uncertainty, and change in target location. *Journal of Neurophysiology*, **46**, 725-743.

Georgopoulos, A. P., Lurito, J. T., Petrides, M., Schwartz, A. B., Massey, J. T. (1989). Mental rotation of the neuronal population vector. *Science*, **243**, 234-236.

Georgopoulos, A. P., Taira, M., Lukashin, A. (1993). Cognitive neurophysiology of the motor cortex. *Science*, **260**, 47-52.

Ghez, C. (1991). The Cerebellum. In E.R. Kandel, J.H. Schwartz, T.M. Jessel (Eds.). *Principles of Neural Science*, pp. 626-646. New York: Elsevier Science Publishers.

Ghez, C., Martin, J. H. (1982). The control of rapid limb movement in the cat. III. Agonist-antagonist coupling. *Experimental Brain Research*, 45, 115-125.

Goldman-Rakic, P. (1990). Parallel systems in the cerebral cortex: the topography of cognition. In M. Arbib, J. Robinson (Eds.). *Natural and artificial parallel computation, pp. 155-176*. Cambridge, MA: MIT.

Goldman-Rakic, P. (1995). Cellular basis of working memory. *Neuron*, **14**, 477-485.

Gordon, J., Ghez, C. (1991). Muscle Receptors and Spinal Reflexes: The Stretch Reflex. In E.R. Kandel, J.H. Schwartz, T.M. Jessel (Eds.). *Principles of Neural Science*, pp. 564-

580. New York: Elsevier Science Publishers.

Greer, K., Green, D. (1983). Context and motor control in handwriting. *Acta Psychologica*, **54**, 205-215.

Grossberg, S., Kuperstein, M. (1986). *Neural Dynamics of Adaptive Sensory-Motor Control* (pp. 66-68). Amsterdam: North-Holland.

Grossberg, S., Merrill, J. (1992). A neural network model of adaptively timed reinforcement learning and hippocampal dynamics. *Cognitive Brain Research*, **1**, 3-38.

Grossberg, S., Merrill, J. (1996). The hippocampus and cerebellum in adaptively timed learning, recognition, and movement. *Journal of Cognitive Neuroscience*, **8**, 257-277.

Grossberg, S., Schmajuk, N. (1989). Neural Dynamics of Adaptive Timing and Temporal Discrimination During Associative Learning. *Neural Networks*, **2**, 79-102.

Guenther, F., Bullock, D., Greve, D., Grossberg, S. (1994). Neural Representations for Sensory-Motor Control, III: Learning a Body-Centered Representation of a Three-Dimensional Target Position. *Journal of Cognitive Neuroscience*, **6**, 341-358.

Guenther, F. H., Hampson, M., Johnson, D. (1998). A theoretical investigation of reference frames for the planning of speech movements. *Psychological Review*, **105**, 611-633.

Hallett, M., Khoshbin, S. (1980). A physiological mechanism of bradykinesia. *Brain*, **103**, 301-314.

Harris, C. M., Wolpert, D. M. (1998). Signal-dependent noise determines motor planning. *Nature*, **394**, 780-784.

Hayes, D. (1982). Handwriting practices: The effects of perceptual prompts. *The Journal of Educational Research*, **75**, 169-172.

Hendricks, W. (1976). *SCRIBE: Suggested Activities to Motivate the Teaching of Elementary Handwriting* (p. 113). Stevensville, Michigan: Educational Service.

Hertrich, I., Ackermann, H. (1995). Coarticulation in slow speech: durational and spectral analysis. *Language and Speech*, **38**, 159-187.

Hollerbach, J. M. (1981). An Oscillation Theory of Handwriting. *Biological Cybernetics*, **39**, 139-156.

Hollerbach, J. M., Atkeson, C. G. (1987). Inferring limb coordination strategies from tra-

jectory kinematics. *Journal of Neuroscience Methods*, **21**, 181-194.

Hollerbach, J. M., Flash, T. (1982). Dynamic interactions between limb segments during planar arm movement. *Biological Cybernetics*, **44**, 67-77.

Hopfinger, J. B., Buonocore, M. H., Mangun, G. R. (2000). The neural mechanisms of top-down attentional control. *Nature Neuroscience*, **3**, 284-291.

Horak, F. B., Anderson, M. E. (1984a). Influence of globus pallidus on arm movements in monkeys, I. Effects of kainic acid-induced lesions. *Journal of Neurophysiology*, **52**, 290-304.

Horak, F. B., Anderson, M. E. (1984b). Influence of globus pallidus on arm movements in monkeys, II. Effects of stimulation. *Journal of Neurophysiology*, **52**, 305-322.

Iacoboni, M., Woods, R.P., Brass, M., Bekkering, H., Mazziotta, J.C., Rizzolatti, G. (1999). Cortical Mechanisms of Human Imitation. *Science*, **286**, 2526-2528.

Ito, M. (1984). *The cerebellum and neural control* (pp. 325-349). New York: Raven.

Ito, M. (1991). The cellular basis of cerebellar plasticity. *Current Opinion in Neurobiology*, **1**, 616-620.

Ito, M., Karachot, L. (1992). Protein kinases and phosphatase inhibitors mediating long-term desensitization of glutamate receptors in cerebellar Purkinje cells. *Neurosciences Research*, **14**, 27-38.

Itoh, K., Yonezawa, Y. (1990). Support System for Handwriting Characters and Drawing Figures for the Blind Using Feedback of Sound Imaging Signals. *Journal of Microcomputer Applications*, **13**, 177-183.

Jaffe, S. (1992). A neuronal model for variable latency response. In F. H. Eeckman (Ed.). *Analysis and modeling of neural systems*. Boston: Kluwer Academic Publishers.

Jueptner, M., Frith, C. D., Brooks, D. J., Frackowiak, R. S., Passingham, R. E. (1997a). Anatomy of motor learning. II. Subcortical structures and learning by trial and error. *Journal of Neurophysiology*, **77**, 1325-1337.

Jueptner, M., Stephan, K. M., Frith, C. D., Brooks, D. J., Frackowiak, R. S., Passingham, R. E. (1997b). Anatomy of motor learning. I. Frontal cortex and attention to action. *Journal of Neurophysiology*, **77**, 1313-1324.

Jueptner, M., Weiller, C. (1998). A review of differences between basal ganglia and cere-

bellar control of movements as revealed by functional imaging studies. *Brain*, **121**, 1437-1449.

Kalaska, J. F., Cohen, D. A. D., Hyde, M. L., Prud'homme, M. J. (1989). A comparison of movement direction-related versus load direction-related activity in primate motor cortex, using a two-dimensional reaching task. *The Journal of Neuroscience*, **9**, 2080-2102.

Kalaska, J. F., Cohen, D. A. D., Prud'homme, M. J., Hyde, M. L. (1990). Parietal area 5 neuronal activity encodes movement kinematics, not movement dynamics. *Experimental Brain Research*, **80**, 351-364.

Kawashima, R., Okuda, J., Umetsu, A., Sugiura, M., Inoue, K., Suzuki, K., Tabuchi, M, Tsukiura, T., Narayan, S. L., Nagasaka, T., Yanagawa, I., Fujii, T., Takahashi, S., Fukuda, H., Yamadori, A. (2000). Human cerebellum plays an important role in memory-timed finger movement: an fMRI study. *Journal of Neurophysiology*, **83**, 1079-1087.

Kellogg, R. (1996). A Model of Working Memory in Writing. In C. Levy, S. Ransdell (Eds.). *The Science of Writing*, pp. 57-71. Hillsdale, N.J.: Lawrence Erlbaum.

Kelso, J. A. S. (Ed.) (1982). *Human motor behavior.* Hillsdale, NJ: Lawrence Erlbaum.

Klopf, A. H. (1972). Brain function and adaptive systems- A heterostatic theory. Technical Report AFCRL-72-0164, Air Force Cambridge Research Laboratories, Bedfored, MA. A summary appears in *Proceedings of the International Conference on Systems, Man, and Cybernetics*, 1974, IEEE Systems, Man, and Cybernetics Society, Dallas, TX.

Klopf, A. H. (1982). *The Hedonistic Neuron: A Theory of Memory, Learning, and Intelligence*. Hemisphere, Washington, D.C.

Kretschmer, B. D., Fink, S. (1999). Spatial learning deficit after NMDA receptor blockade and state-dependency. *Behavioural Pharmacology*, **10**, 423-428.

Lacquaniti, F., Terzuolo, C., Viviani, P. (1983). The law relating the kinematic and figural aspects of drawing movements. *Acta Psychologica*, **54**, 115-130.

Lu, X., Hikosaka, O., Miyachi, S. (1998). Role of monkey cerebellar nuclei in skill for sequential movement. *Journal of Neurophysiology*, **79**, 2245-2254.

Mano, N. I., Kanazawa, I., Yamamoto, K. I. (1986). Complex spike activity of cerebellar Purkinje cells related to wrist-tracking movement in monkey. *Journal of Neurophysiology*, **56**, 137-158.

Matthews, P.B.C. (1972). *Mammalian muscle receptors and their central actions*. Balti-

more, MD: Williams and Wilkins.

Moore, J. W., Desmond, J. E., Berthier, N. E. (1989). Adaptively timed conditioned responses and the cerebellum: a neural network approach. *Biological Cybernetics*, **62**, 17-28.

Morasso, P. (1981). Spatial control of arm movements. *Experimental Brain Research*, **42**, 223-227.

Morasso, P. (1986). Understanding Cursive Script as a Trajectory Formation Paradigm. In H. Kao, G. van Galen, R. Hoosain (Eds.). *Graphonomics: Contemporary Research in Handwriting*, pp. 137-167. New York: Elsevier Science Publishers.

Morasso, P., Mussa Ivaldi, F. A., Ruggiero, C. (1983). How a discontinuous mechanism can produce continuous patterns in trajectory formation and handwriting. *Acta Psychologica*, **54**, 83-98.

Morasso, P., Sanguineti, V. (1993). Neurocomputing aspects in modelling cursive handwriting. *Acta Psychologica*, **82**, 213-235.

Mussa-Ivaldi, F. (1988). Do neurons in the motor cortex encode movement direction? An alternative hypothesis. *Neuroscience Letters*, **91**, 106-111.

Ohman, S. (1965). Coarticulation in VCV utterances: spectrographic measurements. *Journal of the Acoustical Society of America*, **39**, 151-168.

Oscarsson, O. (1969). Termination and functional organization of the dorsal spino-olivocerebellar path. *The Journal of Physiology (London)*, **200,** 129-149.

Ostry, D., Gribble, P., Gracco, V. (1996). Coarticulation of jaw movements in speech production: is context sensitivity in speech kinematics centrally planned? *The Journal of Neuroscience* **16**, 1570-1579.

Perrett, S.P., Ruiz, B.P., Mauk, M.D. (1993). Cerebellar cortex lesions disrupt learning-dependent timing of conditioned eyelid responses. *The Journal of Neuroscience*, **13**, 1708-1718.

Plamondon, R., Alimi, A. (1997). Speed/accuracy trade-offs in target-directed movements. *Behavioral and Brain Sciences*, **20**, 279-349.

Plamondon, R., Guerfali, W. (1998). The generation of handwriting with delta-lognormal synergies. *Biological Cybernetics*, **78**, 119-132.

Plamondon, R., Maarse, F. (1989). An evaluation of motor models of handwriting. *IEEE Transactions on systems, man, and cybernetics*, **19**, 1060-1072.

Pleskacheva, M. G., Wolfer, D. P., Kupriyanova, I. F., Nikolenko, D. L., Scheffrahn, H., Dell'Omo, G., Lipp, H. P. (2000). Hippocampal mossy fibers and swimming navigation learning in two vole species occupying different habitats. *Hippocampus*, **10**, 17-30.

Posner, M. I., Walker, J. A., Friedrich, F. A., Rafal, R. D. (1987). How do the parietal lobes direct covert attention? *Neuropsychologia*, **25**, 135-145.

Rhodes, B. J. (2000). *Learning-Driven Changes in the Temporal Characteristics of Serial Movement Performance: A Model Based on Cortico-Cerebellar Cooperation*. Dissertation, Boston University Graduate School of Arts and Sciences. Boston, MA..

Richer, F., Chouinard, M. J., Rouleau, I. (1999). Frontal lesions impair the attentional control of movements during motor learning. *Neuropsychologia*, **37**, 1427-1435.

Rijntjes, M., Dettmers, C., Buchel, C., Kiebel, S., Frackowiak, R.S.J., Weiller, C. (1999). A blueprint for movement: Functional and anatomical representations in the human motor system. *Journal of Neuroscience*, **19**, 8043-8048.

Rispal-Padel, L. (1993). Contribution of cerebellar efferents to the organization of motor synergy. *Revue Neurologique*, **149**, 716-727.

Rosenbaum, D.A., Loukopoulos, L.D., Meulenbroek, R.G., Vaughan, J., Engelbrecht, S.E.A. (1995). Planning reaches by evaluating stored postures. *Psychological Review*, **102**, 28-67.

Sadato, N., Ibanez, V., Deiber, M. P., Campbell, G., Leonardo, M., Hallett, M. (1996). Frequency-dependent changes of regional cerebral blood flow during finger movements. *Journal of Cerebral Blood Flow and Metabolism*, **16**, 23-33.

Saltzman, E., Kelso, J.A. (1987). Skilled actions: a task-dynamic approach. *Psychological Review*, **94**, 84-106.

Schillings, J., Meulenbroek, R., Thomassen, A. (1996). Limb Segment Recruitment as a Function of Movement Direction, Amplitude, and Speed. *Journal of Motor Behavior*, **28**, 241-254.

Schomaker, L., Thomassen, A., Teulings, H. (1989). A Computational Model of Cursive Handwriting. In R. Plamondon, C.Y. Suen, M.L. Simner, (Eds.). *Computer Recognition and Human Production of Handwriting*, pp. 153-177. Singapore: World Scientific.

Schwartz, A. B., Moran, D. W. (1999). Motor cortical activity during drawing movements: population representation during lemniscate tracing. *Journal of Neurophysiology*, **82**, 2705-2718.

Simpson, J.I., Wylie, D.R., De Zeeuw, C.I. (1996). On Climbing Fiber Signals and Their Consequence(s). *Behavioral and Brain Sciences*, **19**, 384-398.

Singer, Y., Tishby, N. (1994). Dynamical encoding of cursive handwriting. *Biological Cybernetics*, **71**, 227-237.

Soechting, J., Terzuolo, C. (1987). Organization of arm movements. Motion is segmented. *Neuroscience*, **23**, 39-51.

Stelmach, G., Mullins, P., Teulings, H. (1984). Motor programming and temporal patterns in handwriting. In J. Gibbon, L. Allan (Eds.). *Timing and Time Perception, Annals of the New York Academy of Sciences*, **423**, 144-157.

Sternberg, S., Monsell, S., Knoll, R.L., Wright, C.E. (1980). The latency and duration of rapid movement sequences: Comparisons of speech and typewriting. In R.A. Cole (Ed.). *Perception and production of fluent speech*, pp. 469-505. Hillsdale, N.J.: Erlbaum. (Reprinted from *Information Processing in Motor Control and Learning*, pp. 117-152, by G. Stelmach, Ed., 1978, New York: Academic Press)

St-Onge, N., Adamovich, S. V., Feldman, A. G. (1997). Control processes underlying elbow flexion movements may be independent of kinematic and electromyographic patterns: Experimental study and modeling. *Neuroscience*, **79**, 295-316.

Stuphorn, V., Bauswein, E., Hoffmann, K. P. (2000). Neurons in the primate superior colliculus coding for arm movements in gaze-related coordinates. *Journal of Neurophysiology*, **83**, 1283-1299.

Takechi, H., Eilers, J., Konnerth, A. (1998). A new class of synaptic response involving calcium release in dendritic spines. *Nature*, **396**, 757-760.

Teulings, H., Mullins, P., Stelmach, G. (1986a). The elementary units of programming in handwriting. In H. Kao, G. van Galen, R. Hoosain (Eds.). *Graphonomics: contemporary research in handwriting*, pp. 21-32. New York: North-Holland: Elsevier Science Publishers.

Teulings, H., Thomassen, A., van Galen, G. (1986b). Invariants in Handwriting: The Information Contained in a Motor Program. In H. Kao, G. van Galen, R. Hoosain (Eds.). *Graphonomics: Contemporary Research in Handwriting*, pp. 306-315. New York: North-

Holland: Elsevier Science Publishers.

Thach, W. T., Perry, J. G., Kane, S. A, Goodkin, H. P. (1993). Cerebellar nuclei: rapid alternating movement, motor somatotopy, and a mechanism for the control of muscle synergy. *Revue Neurologique*, **149**, 607-628.

Thomassen, A., Schomaker, L. (1986). Between-Letter Context Effects in Handwriting Trajectories. In H. Kao, G. van Galen, R. Hoosain (Eds.). *Graphonomics: Contemporary Research in Handwriting*, pp. 253-272. New York: North-Holland: Elsevier Science Publishers.

Thomassen, A., Teulings, H. (1985). Time, size and shape in handwriting: exploring spatio-temporal relationships at different levels. In J. Michon, J. Jackson, (Eds.). *Time, Mind, and Behavior,* pp. 253-263. Berlin: Springer-Verlag.

Turner, R. S., Anderson, M. E. (1997). Pallidal discharge related to the kinematics of reaching movements in two dimensions. *Journal of Neurophysiology,* **77**, 1051-1074.

Turner, R. S., Grafton, S. T., Votaw, J. R., Delong, M. R., Hoffman, J. M. (1998). Motor subcircuits mediating the control of movement velocity: A PET study. *Journal of Neurophysiology*, **80**, 2162-2176.

Turvey, M. T. (1990). Coordination. *American Psychologist*, **45**, 938-953.

van Den Heuvel, C.E., van Galen, G.P., Teulings, H.L., van Gemmert, A.W. (1998). Axial pen force increases with processing demands in handwriting. *Acta Psychologica (Amst)*, **100**,145-159.

van Galen, G.P., Meulenbroek, R., Hylkema, H. (1986). On the simultaneous processing of words, letters and strokes in handwriting: evidence for a mixed linear and parallel model. In H. Kao, G. van Galen, R. Hoosain (Eds.). *Graphonomics: Contemporary Research in Handwriting*, pp. 5-20. New York: North-Holland: Elsevier Science Publishers.

van Galen, G.P. (1991). Handwriting: Issues for a psychomotor theory. *Human Movement Science*, **10**, 165-191.

van Galen, G.P., Weber, J. (1998). On-line size control in handwriting demonstrates the continuous nature of motor programs. *Acta Psychologica*, **100**, 195-216.

Van Gemmert, A.W., Teulings, H.L., Contreras-Vidal, J.L., Stelmach, G.E. (1999). Parkinson's disease and the control of size and speed in handwriting. *Neuropsychologia*, **37**, 685-694.

Verwey, W.B. (1996). Buffer loading and chunking in sequential keypressing. *Journal of Experimental Psychology: Human Perception and Performance*, **22**,544-562.

Vindras, P., Viviani, P. (1998). Frames of reference and control parameters in visuomanual pointing. *Journal of Experimental Psychology-Human Perception and Performance*, **24**, 569-591.

Viviani, P. (1986). Do units of motor action really exist? In Heuer & Fromm (Eds.). *Experimental Brain Research Series 15*, pp. 201-216. Berlin: Springer-Verlag.

Wada, Y., Kawato, M. (1995). A theory for cursive handwriting based on the minimization principle. *Biological Cybernetics*, **73**, 3-13.

Waite, J. J., Chen, A. D., Wardlow, M. L., Wiley, R. G., Lappi, D. A., Thal, L. J. (1995). 192 immunoglobulin G-saporin produces graded behavioral and biochemical changes accompanying the loss of cholinergic neurons of the basal forebrain and cerebellar Purkinje cells. *Neuroscience*, **65**, 463-476.

Wann, J., Nimmo-Smith, I., Wing, A. (1988). Relation between velocity and curvature in movement: equivalence and divergence between a power law and a minimum-jerk model. *Journal of Experimental Psychology: Human Perception and Performance*, **14**, 622-637.

Wann, J. P., Nimmo-Smith, I. (1990). Evidence Against the Relative Invariance of Timing in Handwriting. *The Quarterly Journal of Experimental Psychology*, **42A**, 105-119.

Welsh, J. P., Llinas, R. (1997). Some organizing principles for the control of movement based on olivocerebellar physiology. *Progress in Brain Research*, **114**, 449-461.

Whalen, D. H. (1990). Coarticulation is largely planned. *Journal of Phonetics*, **18**, 3-35.

Wilson, F. A., O Scalaidhe, S. P., Goldman-Rakic, P. S. (1993). Dissociation of object and spatial processing domains in primate prefrontal cortex. *Science*, **260**, 1955-1958.

Wright, C. E. (1990). Generalized motor programs: reexamining claims of effector independence in writing. In M. Jeannerod (Ed.). *Attention and Performance 13: Motor representation and control*, pp. 294-320. Hillsdale, N.J.: Lawrence Erlbaum.

Wright, C.E. (1993). Evaluating the special role of time in the control of handwriting. *Acta Psychologica*, **82**, 5-52.

Zhou, T. L., Tamura, R., Kuriwaki, J., Ono, T. (1999). Comparison of medial and lateral septal neuron activity during performance of spatial tasks in rats. *Hippocampus*, **9**, 220-

234.

Zipser, D. (1986). A model of hippocampal learning during classical conditioning. *Behavioral Neuroscience*, **100**, 764-776.

CURRICULUM VITAE

Rainer Paine graduated in 1991 as a Benjamin Franklin Medal recipient from Boston Latin School, the nation's oldest public high school. He then entered the Seven-Year Liberal Arts/Medical Education Program at Boston University as a Trustee Scholar. Already interested in the study of the brain, he worked for a summer during his undergraduate years in the neurology research laboratory of Dr. Gregory Holmes at Children's Hospital of Boston. Upon commencement of his studies at Boston University School of Medicine in 1994, he was accepted into the combined MD-PhD program, through which he hoped to pursue his interest in the function of the brain. This hope was realized in 1996 when Rainer was accepted into the Department of Cognitive and Neural Systems at Boston University and awarded a departmental fellowship for research and teaching. There his interests became focused on the neural mechanisms of movement control. Upon completion of his doctoral studies, Rainer plans to complete his remaining medical training and then seek research opportunities aimed at further elucidating the mechanisms of human movement control and repairing them in patients in whom they fail.